UNIVERSITY OF PAVIA

PhD course in Translational Medicine

XXXIV cycle

Department of Molecular Medicine

Amyloidosis Research and Treatment Center

Foundation IRCCS Policlinico San Matteo

PhD Thesis on:

Harnessing proteotoxicity: Exploring the therapeutic potential of small molecule DUBs inhibitors in AL amyloidosis

Tutor:

Dr. Mario Ulisse Nuvolone

Candidate:

Dr. Alice Nevone

Academic year 2020/2021

Index

Abstract

Background and rationale

Systemic immunoglobulin light chain amyloidosis (AL) is a rare hematological disorder, closely related to multiple myeloma (MM), caused by a small bone marrow plasma cell (or B cell) clone secreting an unstable, patient-specific, amyloidogenic immunoglobulin light chain which misfolds, aggregate and forms amyloid deposits in target organs, leading to tissue damage and progressive organ dysfunction.

Recent observations suggested that the expression of unstable, amyloidogenic light chains induces ER stress and renders AL plasma cells critically dependent on the proteo-catabolic activity of the ubiquitin proteasome system (UPS). The proteasome inhibitor bortezomib has revolutionized the treatment of plasma cell disorders, and it is now part of the gold standard of treatment of AL amyloidosis. Unfortunately, a significant proportion of AL patients do not satisfactorily respond to bortezomib-based combinations, especially those cases carrying the t(11;14) translocation, which is seen in 50-60% of AL patients. Considering the possible clinical significance of targeting the proteasome for destabilizing AL amyloidosis plasma cells, a great interest rose for recent works testing deubiquitinating enzymes (DUBs), acting upstream of the proteasome and modulating proteasomal degradation of polyubiquitinated proteins, as novel promising targets in cancer, including MM. Whether this pathway is a valid therapeutic target in AL is presently unknown.

In the present study, we aimed at investigating the therapeutic potential of novel small molecule drugs (b-AP15, RA190, OPA, SJB3-019 and P5091) inhibiting selected deubiquitinating enzymes or ubiquitin receptors (UCHL5 and USP14, RA190, PSMD14, USP1 and USP7, respectively) in preclinical models of AL amyloidosis.

Materials and methods

We combined global and targeted transcriptional analyses of ubiquitin receptors and deubiquitinating enzymes in bone marrow plasma cells from control subjects or patients with plasma cell dyscrasias, including AL amyloidosis and MM, with pharmacologic and mechanistic studies in human AL and MM plasma cell lines and primary, patient-derived plasma cells and control cells from AL and MM patients and healthy donors. *Ad hoc* molecular assays and preclinical cellular models were established.

Results

Global transcriptomic analyses revealed a ubiquitous expression of DUBs inhibitors molecular targets in all the bone-marrow cellular compartments of healthy subjects and modestly deregulated expression of the investigated genes in AL amyloidosis or MM clonal plasma cells compared to healthy controls. Targeted transcriptional analyses of the six genes of interest in primary bone marrow-derived $CD138^+$ cells showed a trend toward higher expression levels in patients affected by AL amyloidosis compared to the MM patients, with only *USP7* upregulation reaching a statistical significance.

Exposure of ALMC-2 cells to b-AP15, RA190, OPA, SJB3-019 and P5091 led to a dose-dependent reduction of both cellular metabolic activity and viability and the induction of apoptosis. b-AP15 and RA190 drugs were prioritized for further investigations based on sensitivity and drug availability.

Treatment of ALMC-2 cells with b-AP15 or RA190 caused a progressive accumulation of polyubiquitinated proteins and an early transcription of *HMOX-1* and *HSPA6*, two genes associated with oxidative and proteotoxic stress, respectively, followed by a rapid induction of apoptosis of ALMC-2 cells. Anti-plasma cell activity was confirmed also in MM cell lines expressing the t(11;14) translocation, as well as in a 2D co-culture system with ALMC-2 and primary, bone marrow derived mesenchymal stromal cells.

Finally, nanomolar concentrations of b-AP15 or RA190 significantly reduced metabolic activity of primary, bone marrow derived $CD138^+$ cells from both newly diagnosed and relapsed/refractory AL amyloidosis patients and led to an upregulation in *HMOX-1* and *HSPA6* mRNA expression levels, while only marginally affecting matched $CD138^-$ or control peripheral blood mononuclear cells.

Conclusions

Collectively, our results confirmed anti-tumor activity of b-AP15 and RA190 both in AL amyloidosis cell lines and primary patient-derived plasma cells, independently on their translocational status, showing a specific anti-AL activity and a favorable therapeutic index. These data validate inhibition of DUBs upstream of the proteasome as a novel pharmacologic approach to overcome the proteasome inhibitor resistance in AL amyloidosis.

Introduction

Systemic immunoglobulin light chain (AL) amyloidosis is at the same time the prototype of what has been initially referred to as "small dangerous B cell clones" and is now termed "monoclonal gammopathies of clinical significance" (MGCS) and the archetype of protein misfolding and deposition diseases[1-4].

Monoclonal gammopathies of clinical significance are a group of conditions in which a small, quiescent B cell clone, not requiring any treatment *per se*, is associated with potentially severe organ damage due to the toxicity of the monoclonal immunoglobulin or to other mechanisms[1,2].

Protein misfolding and deposition diseases or amyloidoses are characterized by a usually soluble protein or peptide that fails to acquire or maintain its native, functional fold, while assuming a misfolded insoluble form that undergoes aggregation and extracellular deposition in forms of so-called amyloid fibrils[3,5].

Indeed, systemic AL amyloidosis is a rare hematological disorder, caused by a small bone marrow plasma cell (or B cell) clone secreting a highly unstable, patient-specific, amyloidogenic immunoglobulin light chain[6]. Misfolding and aggregation of the monoclonal light chain lead to the formation of amyloid fibrils which deposit in different target organs, ending with cell death, tissue damage and progressive organ dysfunction[1,3]. If not rapidly responding to therapy, AL amyloidosis is quickly and invariably fatal, mainly due to cardiac dysfunction.

Epidemiology and survival

AL amyloidosis is the most common form of systemic amyloidosis in the United States and the European Union, with an annual incidence of approximatively 12 cases per million per year, as assessed both by population-based and non-population-based studies[7-9]. In the past few years, the incidence and prevalence of this disease have increased probably as a consequence of earlier diagnosis, improved treatment strategies and longer life expectancy and this trend seems likely to rise in future[6,9-11]. The reported mean age of AL amyloidosis patients at diagnosis is 63 years, with less than 10% of patients under 50 years, and the disease affects males slightly more frequently than females[6,11,12].

Once AL amyloidosis becomes symptomatic, it can rapidly progress and lead to death. A recent Swedish study based on almost 1500 AL amyloidosis patients diagnosed between 1995 and 2013 assessed the median overall survival at 1.72 years (20.6 months), with a median overall survival significantly improved over time: from 0.77 years (9.2 months) observed in the period 1995-99 to

3.48 years (41.8 months) observed in the period 2010-13[ref.11]. Moreover, improvement in early mortality was also observed, with the 1-year survival significantly increasing from 43% (1995-99) to 70% (2010-13)[ref.11]. Similar data were reported by the Mayo Clinic group on 1551 patients with AL amyloidosis diagnosed at their institution from 2000 to 2014[ref.13]. Patients from the last reporting group (2010-2014) were less likely to have more than 2 involved organs, showed higher rates of deep hematologic response to therapies (very good partial response or better) and improved overall survival[13]. These observations are in line with what has been observed in recent clinical studies and are the results of early recognition of this disease and the availability of new highly effective anti-plasma cell drugs and supportive treatments, all factors that have contributed to change the natural history of this life-threatening disease[14-16].

Susceptibility

Little is known on the genetic predisposition to develop AL amyloidosis. Recently, a genome wide association study (GWAS) has been performed in a cohort of 1229 AL amyloidosis patients and results have been compared to data obtained in patients affected by multiple myeloma, a malignant plasma cell dyscrasia closely related to AL amyloidosis. This study identified 10 SNPs that are significantly associated with a genetic susceptibility to AL amyloidosis, 5 of which were AL amyloidosis specific[17]. The most significant association identified was relative to variant rs9344 (G/A870) that maps to chromosome 11q13.3 in a splice site in cyclin D1, and that appeared to be a more prominent driver in AL amyloidosis than in multiple myeloma[17].

The only known risk factor for developing systemic AL amyloidosis besides aging is the presence of a pre-existing monoclonal gammopathy of undetermined significance (MGUS), a pre-malignant condition characterized by a quiescent and indolent plasma cell (or B cell) clone[18]. Indeed, subjects with an MGUS have a relative risk of developing AL amyloidosis which is 8.8 higher compared with individuals without MGUS matched for age and sex[19]. Overall, about 1% of MGUS patients with long follow up eventually develop AL amyloidosis, and of all MGUS patients experiencing a hematologic progression, about one tenth progresses towards AL amyloidosis[19,20].

Even if the presence of an MGUS (or a monoclonal gammopathy more in general) is a well-established risk factor for the development of AL amyloidosis, this disease is diagnosed late also in patients with a known monoclonal gammopathy in hematological follow up[21].

Overall, the median time to diagnose AL amyloidosis from clinical onset range from 180 to 441 days according to different studies, with many patients having to consult different physicians before achieving a final diagnosis[22-25].

The amyloidogenic clone

Clonal type

Systemic AL amyloidosis is more commonly caused by a plasma cell clone residing within the bone marrow. Exceptionally, AL amyloidosis can occur in the context of other lymphoproliferative diseases, including Waldenström macroglobulinemia[26-29], non-Hodgkin lymphoma[30-33], chronic lymphocytic leukemia[34,35], POEMS syndrome[36,37] and light chain deposition disease[38-42].

Clonal size

The amyloidogenic clone is usually modest in size, with a median bone marrow plasma cell infiltration of about 10%[43]. Among 1255 patients with systemic AL amyloidosis evaluated at the Mayo Clinic between 2000 and 2010, 8% of patients had more than 10% bone marrow plasma cells + hypercalcemia, renal failure, anemia, and/or lytic bone lesions attributable to clonal expansion of plasma cells (CRAB criteria), thus showing a co-existent, symptomatic multiple myeloma, while 38% of patients showed more than 10% bone marrow plasma cells with no CRAB signs[44]. The presence of more than 10% bone marrow plasma cells or the co-existence of a symptomatic multiple myeloma with CRAB signs define equally high-risk populations of patients with AL amyloidosis[44].

Beside mature plasma cells constituting the main elements, there are indications that other cells can be part of and sustain the amyloidogenic clone, as demonstrated through the use of anti-idiotypic antibodies raised against the patients' specific M protein produced by the respective clones[45]. These additional elements include undifferentiated bone marrow progenitors, very late-stage B cells, as well as circulating plasma cells and B lymphocytes within the peripheral blood[45-49]. Clonotypic cells have also been documented within the apheretic stem cell harvest used for autologous stem cell transplantation after high dose chemotherapy, raising the possibility that these elements may play a role in disease relapse after the transplantation procedure[47,50]. Also, the percentage of circulating peripheral blood plasma cells harbors a negative prognostic impact[51,52]. Of note, a study demonstrated that, at least in a subset of patients with AL amyloidosis, light chain isotype-restricted plasma cells expressing the same type of V_L gene as the light chains found within the amyloid deposits can be found also in the spleen, suggesting that this organ may act as another source of amyloidogenic light chains[53].

Proliferation

The amyloidogenic plasma cell clone has a minimal but measurable kinetics of proliferation, with replicating elements being represented mainly by lymphoplasmacytic cells within the bone

marrow[45]. The percentage of bone marrow plasma cells duplicating their DNA can be assessed through microscopic (plasma cell labelling index) or flow cytometric studies (plasma cell proliferating index) and correlates with a poorer prognosis in AL patients[54,55].

The low proliferation rate of the amyloidogenic clone explains why less than 1% of patients with AL amyloidosis not displaying a coexisting myeloma already at diagnosis eventually progress towards myeloma during the course of their disease[56].

Low clonal proliferation, along with the rarity of the disease, hampers experimental work with primary plasma cells from patients with AL amyloidosis. There are only few studies on the biology of AL plasma cells (discussed in the section on molecular profiling) and even less so are pharmacologic investigations employing primary, patient-derived primary cells[57,58].

Derivation of immortalized, plasma cell lines, is also problematic, as witnessed by the availability of only two sister cell lines derived from an individual patient affected by multiple myeloma and associated AL amyloidosis[59]. This is remarkably different with respect to multiple myeloma, for which more than 60 cell lines have been successfully established and are largely employed for mechanistic and pharmacologic studies worldwide[60,61].

Such considerations also apply to the possibility of transferring primary, patients' derived tumoral plasma cells in mice and maintaining them *in vivo* for biologic and pharmacologic studies. Indeed, there are several, well established xenograft mouse models of multiple myeloma, including immune-deficient mice implanted with fetal human bone (SCID-hu) or synthetic bone scaffolds (SCID-synth-hu), or immunodeficient mice highly engineered to express multiple permissive factors through transgenesis[62-64]. Conversely, no xenoengraftment model has been thus far applied to the study of AL amyloidosis thus far.

Cytogenetic abnormalities

The amyloidogenic plasma cell clone is characterized by different cytogenetic alterations. Translocations affecting the 14q32 locus of immunoglobulin heavy chains (*IGH*) are seen in more than 75% of cases[65]. The most frequent alteration occurring at this locus is the translocation t(11;14), which is present in 50-60% of AL amyloidosis patients, a percentage that is significantly higher than the one observed in patients affected by multiple myeloma[66]. Other translocations insisting on the 14q32 *locus* are the t(4;14), present in 2-14% of patients, followed by t(14;16), t(6;14) and t(14;20) present in 3%, 2% and 1% of patients, respectively[49,67]. Gain 1q21 can be found in 20% of cases, while hyperdiploidy is rather infrequent in AL amyloidosis, being present in only 11% of patients, in contrast to what is observed in other plasma cell disorders[68,69]. Of note, hyperdiploidy and translocation t(11;14) are mutually exclusive[68]. Intraclonal heterogeneity as defined in terms of cytogenetic aberrations is less frequent in amyloidogenic plasma cell clones

compared to other, non-AL plasma cell dyscrasias, possibly reflecting the higher rates of t(11;14) translocation and lower rates of hyperdiploidy[70]. Importantly, some of these cytogenetic abnormalities show a predictive relevance in terms of hematologic response towards specific anti-plasma cell regimens, whose mechanistic bases remain not completely defined[69,71,72].

Molecular profiling

From a molecular point of view, considering copy number variations, somatic mutations, immunophenotypic and gene expression profiles, AL plasma cells show an intermediate profile between MGUS and multiple myeloma.

Copy number alterations can be identified in virtually all cases, with a pattern and a magnitude reminiscent of what is observed in patients with myeloma[73-75]. Knowledge of the mutational landscape in AL amyloidosis is still limited. However, based on the results of the few studies reported so far, it has emerged that: 1) there is no unifying mutation in amyloidogenic plasma cells; 2) gene frequently mutated in patients with multiple myeloma are mutated seldomly in AL amyloidosis; 3) there is a minimal overlap in terms of mutated genes across different patients and different studies, pointing towards a high heterogeneity in terms of somatic mutations in AL amyloidosis[73,75-78].

Simultaneous assessment of the clonal plasma cells immunophenotypic protein expression profile and the bone marrow cellular composition through multiparametric flow cytometry in patients with AL amyloidosis (n=99), MGUS (n=20) or multiple myeloma (n=52) and healthy control subjects (n=30) mapped AL amyloidosis in the crossroad between MGUS and multiple myeloma[79]. Interestingly, this study also showed lack of homogenously-positive CD56 expression, reduction of B-cell precursors and a predominantly-clonal plasma cell compartment in the absence of a myeloma like tumor plasma cell expansion as distinctive hallmarks of AL amyloidosis[79].

The transcriptome of amyloidogenic plasma cell clone is only marginally perturbed with respect to normal plasma cells, with only 38 deregulated genes being identified in AL plasma cells (n=9) compared to normal plasma cells from control subjects (n=6)[ref.73]. Yet, gene expression analysis conducted on plasma cells of a cohort of AL amyloidosis (n=24), multiple myeloma (n=28) and healthy control subjects (n=6) has identified a subset of 12 genes (including *CCND1*, encoding cyclin D1) that distinguish AL amyloidosis and multiple myeloma with an accuracy of 92%[80]. Another study employing gene expression profiling on bone marrow plasma cells from 16 patients with AL amyloidosis has identified a subgroup of cases with overexpression of *CCND1*[81]. This feature possibly reflected the presence of the t(11;14) translocation, as *CCND1* is located at the 11q13 *locus* and it is often overexpressed in the presence of this translocation, under the influence of the *IGH* promoter on chromosome 14. Noteworthy, *CCND1* overexpression was associated with

the production of light chain only M protein, and to a lower response rate to initial therapy and poorer survival[81]. Interestingly, in a recent study combining bulk and single-cell RNA sequencing, amyloidogenic and multiple myeloma clonal plasma cells showed divergent transcriptional profiles, with the former being closer to plasma cells from secondary lymphoid organs and the latter being more similar to peripheral blood plasma cells and newborn bone marrow plasma cells[82].

Amyloidogenic immunoglobulin light chains

In AL amyloidosis, the plasma cell or B cell clone secretes a patient-specific amyloidogenic immunoglobulin light chain, which can deposit in virtually any organ, with the only exception being the brain. The organs more frequently affected by amyloid deposits are heart (82%), kidney (68%), soft tissues (17%), liver (14%), peripheral and autonomic nervous system (12% and 10%, respectively)[17]. Clinical manifestations depend on the type and number of affected organ(s) and on the extent of amyloid deposits and can be highly polymorphic[6].

In 75% of cases with systemic AL amyloidosis the monoclonal immunoglobulin light chain is of the λ isotype. Germline gene usage in AL amyloidosis is significantly different with respect to the germline gene usage observed in the normal polyclonal bone marrow cells or in other monoclonal gammopathies, due to the preferential use of a small set of *IGLV* or *IGKV* germline genes in AL amyloidosis. In particular, three germline genes, i.e. *IGLV6-57*, *IGLV2-14* and *IGLV3-01*, alone account for the 60% of Vλ amyloid regions, while *IGKV1* and *IGKV4* are most recurrent Vκ families in AL amyloidosis[83,84]. Of note, different studies have pointed towards an association of germline gene usage and amyloid organ tropism, with *IGLV6-57* being associated with renal involvement[83,85], *IGKV1* with soft tissues and bone involvement[86] and *IGLV1-44* and *IGLV3* with cardiac involvement[87].

Only a small fraction of the amyloidogenic light chain (estimated to be <5%) tends to form amyloid fibrils *in vivo*, probably due to specific structural features of the immunoglobulin light chain itself[84]. Mutations in immunoglobulin light chains can lead to a destabilization on their structure, increasing the chance of misfolding and aggregation[88-93].

Sequence comparison of amyloidogenic and control immunoglobulin light chains suggests a higher number of non-conservative mutations in AL light chains[94,95]. Very recently, machine learning has been employed to develop predictive algorithms to identify potentially amyloidogenic immunoglobulin light chains, with LICTOR being applicable to λ light chain sequences and VL-AmYPred being applicable to both κ and λ light chain sequences[95,96]. As sequence-based identification of amyloidogenic light chains may promote early diagnosis, an external validation of

these predictive algorithms is needed and studies evaluating the potential clinical utility of such an approach will be of interest.

Furthermore, post-translational modifications such as glycosylation, cysteinylation, tryptophan oxidation and truncation, may be contributing factors in amyloidogenicity of light chains, although this field deserves further investigations[4].

AL amyloid formation

The development of a plasma cell disorder predates the onset of amyloid related organ dysfunction by many years. A retrospective study based on prediagnostic sera from 20 cases with AL amyloidosis and 20 healthy controls matched for age, sex, race, and age of serum sample showed that a monoclonal immunoglobulin was detected in 100% of cases and none of controls, with the M protein being present in 100%, 80%, and 42% of cases at less than 4 years, 4 to 11 years, and more than 11 years before diagnosis, respectively[97]. Also, increased levels of serum immunoglobulin free light chains precede the development of AL amyloidosis for many years[97].

This important clinical observation is in line with the notion that amyloidogenesis is a slow process occurring through a "nucleated growth" mechanism consisting of three phases:

1) A nucleation phase (or lag phase): monomeric precursors start to assembly in oligomers, possibly originating a critical nucleus (often called "seed");

2) an elongation phase: as soon as a critical nucleus has been generated, fibrils formation proceeds with a very fast kinetics, with an exponential growth by incorporating any monomer in aggregation-prone conformation;

3) a stationary phase: fibrils can release oligomers (that may or may not be toxic) or can further assembly with other proteins or factors forming amyloid deposits[98].

This type of transition is thermodynamically possible, since the difference in energetic level associated with the aggregation-prone unfolded state of the protein and the most stable native conformation is very low and easily surmountable by naturally occurring thermal fluctuations[99].

Emerging data from recent structural studies employing cryo-electron microscopy on AL amyloid extracts from affected patients are clearly indicating a high three-dimensional heterogeneity and the presence of patients' specific features, including the exact fibril fold, which differs across different patients[100-103]. On the other hand, some commonalities have been identified based on the comparison of the few AL fibrils characterized so far: 1) *Ex vivo* amyloid fibrils contain a dominant fibril morphology consisting of a single, polar protofilament; 2) the fibril core is composed of the variable domain of the precursor light chain, while the constant domain is either structurally

disordered or proteolytically removed; 3) the disulfide bond within the native variable domain is retained; 4) the antiparallel N-to-C orientation of the fibril protein implies a 180° rotation around the disulfide bond with respect to the native fold; 5) the substantial difference between the fibril protein conformations and their respective, natively folded light chain precursors implies a global structural rearrangement and/or unfolding process taking place during fibrillogenesis; 6) extracted amyloid fibrils are decorated with blurry density of uncertain origin, possibly arising from fibril protein segments outside the ordered fibril core, or from additional components adhering to the fibril surface[102].

Anti-clonal therapy to treat systemic AL amyloidosis

As mentioned above, in AL amyloidosis the underlying plasma cell tumor is usually small and poorly proliferating but secretes a highly unstable immunoglobulin light chain which misfolds and progressively deposits extracellularly leading to life-threatening organ dysfunction. The disease course and prognosis of AL amyloidosis are determined by the light chain intrinsic toxicity rather than by the malignancy of tumoral plasma cell clone[104-106]. Thus, even if the plasma cell clone *per se* is not very proliferating and aggressive, eradication of the amyloidogenic clone is crucial to block the production of the light chains and ameliorate organ function[104,105].

Indeed, the only substantial therapeutic success has been so far achieved by interventions aimed at eliminating or substantially reducing the supply of the amyloidogenic precursor[107]. This holds true also for other types of systemic amyloidoses, including AA amyloidosis, a form of systemic amyloidosis complicating longstanding chronic inflammation, with amyloid deposits deriving from the proteolytic processing of the liver-derived acute phase reactant SAA, and ATTR amyloidosis, caused by misfolding and deposition of transthyretin, either in its wild-type form in elderly subjects, or in the presence of destabilizing mutations (**Fig. 1**, **Fig. 2**). Using the evocative analogy of the source of the amyloidogenic precursor being the tap, and the water on the floor damaging the flat being the amyloid deposits, this strategy has been effectively described with the motto “turn off the tap”[105] (**Fig. 1**, **Fig. 2**).

In the case of systemic AL amyloidosis, reduction or elimination of the underlying plasma cell disorder has been pursued by exploiting therapeutic interventions originally developed against the more prevalent multiple myeloma, even though these diseases are characterized by a distinctive biology of the underlying plasma cell clone and its secreted M protein[108].

Anti-plasma cell therapy currently available in the clinics to treat AL amyloidosis include alkylating agents, steroids, proteasome inhibitors, immunomodulatory drugs and monoclonal antibodies, with

other targeted therapies, including anti-B cell maturation antigen (BCMA) and BCL-2 family inhibitors, in the pipeline[6,109].

High dose melphalan followed by rescue therapy with autologous stem cell transplantation (ASCT) for the fittest, transplant-eligible subset of AL amyloidosis patients grants the most durable responses[110-112]. Scrupulous selection of transplant eligible patients has dramatically reduced transplant-related mortality in more recent patients' series[111]. When full dose melphalan (200 mg/m^2) is employed, the median overall survival achieved is superior than 10 years[110,111]. In patients with bone marrow plasma cell infiltration above 10%, induction therapy before ASCT to expedite lowering of toxic light chains may improve rates of hematologic response and overall survival[113,114], again stressing the importance of swiftly turning off the tap in amyloidosis[105].

Transplant-ineligible patients due to advanced disease or significant comorbidity are treated with standard or attenuated doses of chemotherapy against the plasma cell clone, using alkylating agents, proteasome inhibitors, immunomodulatory drugs, monoclonal antibodies and steroids[6]. Several drug combinations are available, and they are associated with median survivals exceeding 5 years, with the exception of patients with very advanced cardiac involvement at diagnosis, who show dismal prognosis irrespectively of the employed regimen.

The extent of reduction of the amyloidogenic light chains with respect to pre-therapy levels can be used to grade the depth of hematologic response to therapy into four main response categories, that is no response, partial response, very good partial response and complete response, which are characterized by a progressively better prognosis. Indeed, drop of the amyloidogenic, clonal light chain is paralleled by reduction of markers of heart dysfunction[115] and hematologic response to therapy is the prerequisite to halt organ function deterioration or even promote organ function recovery (i.e. organ response to therapy).

Among patients achieving the complete response status, that is the disappearance of M protein / monoclonal light chains and the normalization of serum free light chain levels, next generation flow cytometry or next generation sequencing can be employed to identify residual clonal plasma cells (defined as minimal residual disease, MRD) within the bone marrow with high (10^{-5} – 10^{-6}) sensitivity[116]. Recent studies are indicating that AL patients with MRD persistence have lower rates of organ response[117]. While the biologic bases of this observation are not clear, one possibility is that low levels of toxic, amyloidogenic light chains, below detection limits of routine diagnostic tests, may be enough to prevent organ function restoration. This would again stress the importance of completely eradicating the underlying plasma cell clone, to completely close the tap and arrest further damage.

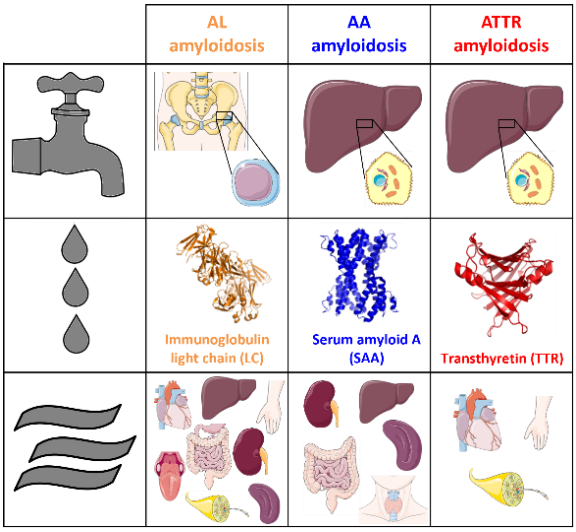

Figure 1: Most common forms of systemic amyloidosis
Source of the amyloidogenic precursors (upper panel), amyloidogenic precursor itself (middle panel) and target organs for amyloid deposition (lower panel) are depicted. AL amyloidosis: immunoglobulin light chain amyloidosis; AA amyloidosis: amyloid A amyloidosis; ATTR amyloidosis: transthyretin-related amyloidosis

	AL amyloidosis	AA amyloidosis	ATTR amyloidosis
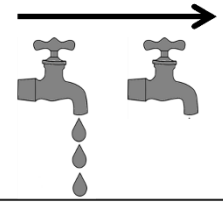	**Anti-PC (or B cells) drugs:** • Chemotherapy / ASCT • Immunomodulatory drugs • Steroids • Monoclonal antibodies	**Treatment of underlying flogosis:** • Steroids • DMARDs • Monoclonal antibodies • Antibiotics • Surgery • ...	**TTR directed interventions:** • Liver transplantation (hATTR)° • TTR tetramer stabilizers @ • *TTR* silencing agents #
	**Precursor:** monoclonal LC **Goal:** disappearance **Monitoring:** s+uEP+IFIX serum free LC levels BM studies (MRD monitoring)	**Precursor:** SAA **Goal:** SAA normalization **Monitoring:** serum SAA levels	**Precursor:** TTR **Goal:** reduced mutant TTR ° tetramer stabilization @ reduced TTR levels # **Monitoring:** tetramer stability/dissociation @ or serum TTR levels #@
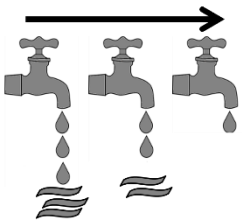	**At risk individuals:** MGUS, MM, other PC dyscrasia **Proposed screening:** • Proteinuria • NT-proBNP • ALP	**At risk individuals:** Chronic inflammation, morbid obesity (?) **Proposed screening:** • Proteinuria	**At risk individuals:** pre-symptomatic mutation carriers (hATTR) **Proposed screening** **(based on TTR mutation):** • NT-proBNP • Nerve MRI

Figure 2: Therapeutic interventions against the most common forms of systemic amyloidosis
ALP, A ALP, alkaline phosphatase; ASCT, autologous stem cell transplantation; BM, bone marrow; DMARDs, disease-modifying anti-rheumatic drugs; hATTR, hereditary ATTR amyloidosis; LC, immunoglobulin light chains; MGUS, monoclonal gammopathy of undetermined significance; MM, multiple myeloma; MRD, minimal residual disease; MRI, magnetic resonance imaging; NT-proBNP, amino-terminal pro brain natriuretic peptide; PC, plasma cell; SAA, serum amyloid A; s&uEP+IFIX, serum and urine electrophoresis with immunofixation; TTR, transthyretin. °, @ and # denote different therapeutic strategies in ATTR amyloidosis, with different goals, and whose efficacy can be monitored by Different modalities. Modified from Nevone A, Merlini G, Nuvolone M. Treating Protein Misfolding Diseases: Therapeutic Successes Against Systemic Amyloidoses. *Front Pharmacol*, 2020 Jul 10;11:1024. DOI: 10.3389/fphar.2020.01024

The Ubiquitin proteasome system

The ubiquitin proteasome system (UPS) is the most important protein degradation complex ubiquitously present in eukaryotic cells, and it is involved in the control and regulation of numerous cellular pathways including DNA repair, stress response, apoptosis, immune response, cell-cycle, chromatin remodeling and signal transduction[118,119].

The UPS system is composed by a major complex, called 26S proteasome, and by a large set of proteins, whose work is finely orchestrated in order to enable substrate selectivity and processing efficiency and to achieve regulation precision of a vast diversity of substrates, coping all the cellular proteolytic needs[118].

The selective degradation of a protein begins with the labelling of the protein through a cascade process called ubiquitination. This is a reversible process through which ubiquitins are attached to proteins for degradation, and it is exerted by ubiquitylating enzymes. The opposite process of ubiquitin removal, called deubiquitination, is catalyzed by deubiquitylating enzymes (DUBs), and it is crucial for recycling ubiquitins, regulating protein degradation, activation/inactivation of proteins[119].

Three different classes of ubiquitylating enzymes are identified: E1 ubiquitin-activating enzymes, that bind ubiquitins to activate them; E2 ubiquitin-conjugating enzymes, to which ubiquitins are transferred, and that form a complex with E3; E3 ubiquitin-ligase enzymes that mediates the specific binding of ubiquitins to the corresponding substrates (**Fig. 3**). Due to the increasing of specificity needed in this cascade, the eukaryotic cells possess few E1 enzymes, several E2 enzymes, and several hundreds of E3 enzymes[118]. As a result, a single ubiquitin, or several ubiquitin molecules at distinct sites, or polyubiquitin chains can be bound to the target protein through a process respectively called monoubiquitylation, multiubiquitylation and polyubiquitylation, and this acts as degradation signal for directing the protein to the 26S proteasome[118].

The interaction between ubiquitinated substrates and 26S proteasome occurs through a series of ubiquitin receptors that can be extrinsic or intrinsic. There are several extrinsic UBL (ubiquitin-like) – UBA (ubiquitin-associated) ubiquitin receptors, such as Rad23, Dsk2 and Ddi1, and at least three intrinsic receptors (so called because intrinsically residing in the 26S proteasome complex itself) including Rpn1 (PSMC2/S7), Rpn10 (PSMD4/S5a), and Rpn13 (ADRM1)[118,119].

The protein degradation complex, responsible for protein hydrolyzation into small peptides, is called 26S proteasome, and it is composed by 50 subunits divided in 2 sub-complexes: the 20S proteolytic core particle (CP) and the 19S regulatory particle (RP) (**Fig. 3**) [118,119]. The 20S core

particle is constituted by 14 α-type and 14 β-type protein subunits, organized in four heptameric rings in an α-β-β-α arrangement, stack into a cylinder-shaped barrel.

The β-rings form a catalytic chamber, consisting of the active sites of peptidases here sequestered, whose caspase-, trypsin-, and chymotrypsin-like activities allow protein breakdown. Heptameric α-rings, positioned on both sides of the catalytic chamber, control substrate entry into this space.

The 19S regulatory particle finely regulates proteasome activity through substrate recognition, recruitment, and unfolding. It consists of at least 18 subunits, divided in one or two subunits that caps either or both sides of the core particle: the base, which functions as a receptor for the uptake of polyubiquitinated proteins, promotes substrate unfolding and mediates the opening of the 20S gate, and the lid, which deubiquitinates the captured proteins. The base includes RPN1 (PSMD2/S2), RPN2 (PSMD1/S1), and six paralogous, distinct Regulatory Particle ATPase (RPT) subunits. The lid comprises 9 Regulatory Particle Non-ATPase (RPN) subunits: RPN3 (PSMD3/S3), RPN5 (PSMD12), RPN6 (PSMD11/S9), RPN7 (PSMD6/S10), RPN8 (PSMD7/S12), RPN9 (PSMD13/S11), RPN11 (PSMD14/Poh1/Pad1), RPN12 (PSMD8/S14), and RPN15 (PSMD9/Dss1/Sem1).

Deubiquitination, as previously mentioned, is the process through which the ubiquitin or polyubiquitin chain is removed from a variety of substrates, before entering the proteasome, therefore regulating the degradation process and consequently a plethora of other processes and functions[120]. The proteases involved in this process are called DUBs, and to date around 100 have been identified, divided in 5 subfamilies according to their sequence and structural features: ubiquitin-specific proteases (USPs), ubiquitin carboxyl-terminal hydrolases (UCHSs), ovarian-tumor proteases (OTUs), JAMM motif proteases (JAMMs), Machado-Joseph disease protein proteases (MJD)[120].

However, other gene families acting on the UPS to modulate protein ubiquitination status may exist, and this should be considered when developing DUB inhibitors and targeted therapies[121].

Among the human deubiquitylating enzymes, three of them are associated with 19S regulatory particle including Rpn11, USP14/Ubp6 and UCHL5/Uch37[ref.121-123].

Rpn11 is a zinc-dependent DUB of the JAMM family protein and is intrinsically located above the proteasome, guarding the translocation of substrates into the core particle and catalysing the *en bloc* substrate deubiquitylation[118]. USP14/Ubp6 and UCHL5/Uch37 belong to the ubiquitin-specific proteases (USP) and the ubiquitin carboxyl-terminal hydrolases (UCH) families, respectively. Although their role in the 19S RP has not been fully understood, USP14 and UCHL5 seem to have a crucial role in regulating proteasome activity, preventing non-selective protein degradation and ATP consumption[124]. UCHL5 requires to be combined to its receptor Rpn13/ADRM1 at the base of

19S RP to deubiquitinate substrates. The complex thus formed is functionally active only after its integration in the 19S RP. USP14 also binds to a receptor (Rpn1) at the base of 19s RP though not in a constituent manner[125].

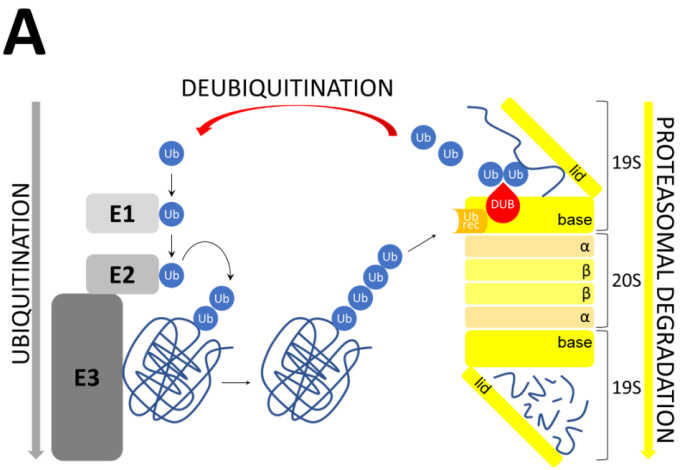

B

CLASS	TARGET	DRUG		REFERENCE
		INHIBITOR	PROTEIN DEGRADER	
DUB Deubiquitinating enzymes	USP7	P5091		Chauhan et al. Cancer Cell 2012
	USP14 / UCHL5	b-AP15, VLX1570		Tian et al. Blood 2014, Rowinsky et al. Invest New Drug 2020
	USP1	SJB3-019		Das et al. Clin Cancer Res 2017
	Rpn11	RA190	WL40	Song et al. Leukemia 2016
Ub rec Ubiquitin receptors	Rpn13	OPA		Song et al. Oncogene 2017

Figure 3: Ubiquitin proteasome system
A As professional secretory cells, plasma cells are highly dependent on the proteo-catabolic activity of the UPS. Proteins that are to be degraded, including misfolded secretory proteins that are retrogradely transported from the endoplasmic reticulum back to the cytoplasm, are tagged with a poly-ubiquitin tail by the action of ubiquitin ligases. These poly-ubiquitinated proteins are then recognized by ubiquitin receptors (Ub rec), their poly-ubiquitin tail is removed by the action of proteasome-associated deubiquitinating enzymes (DUBs) and the proteins are finally degraded by the multiple catalytic activities of the proteasome.
B Molecular targets of DUBs inhibitors. Modified from Nuvolone M, Merlini G. Redirecting proteoxicity. *Leukemia*, 2020 Dec, 34(12):3109–3110. DOI:10.1038/s41375-020-01028-w

Redirecting toxicity to treat AL amyloidosis: inhibiting the proteasome, ubiquitin receptors and deubiquitinating enzymes

The introduction of the proteasome inhibitor bortezomib has revolutionized the treatment of plasma cell disorders, and so of AL amyloidosis[126,127]. In fact, due to the exceptional high response rates to the drug highlighted by several trials, either given as a single agent or in combination with other standard treatments, bortezomib is part of the gold standard of treatment in absence of

contraindications, such as pulmonary fibrosis or peripheral neuropathy. Bortezomib is used for induction/consolidation after high-dose melphalan and autologous stem cell transplantation and constitutes the backbone of frontline therapies for transplant-ineligible patients[14,15,128-130].

The combination of bortezomib, melphalan and dexamethasone (BMDex) is superior to oral melphalan and dexamethasone alone, both in terms of progression-free and overall survival and has a strong biologic ration, with melphalan possibly overcoming the partial resistance of t(11;14)-positive clones towards bortezomib, and bortezomib possibly overcoming the partial resistance of gan1q21-positive clones towards melphalan[131].

On the other hand, clinical data revealed that a significant proportion of patients do not satisfactorily respond to bortezomib, a problem of critical clinical significance, considering that a non-negligible subgroup of patients not responding to first line therapy die before having the chance to start a rescue therapy with potentially effective second-line anti-plasma cell drugs. Addition of the anti-CD38 monoclonal antibody daratumumab to cyclophosphamide bortezomib and dexamethasone resulted in unprecedented deep and rapid hematologic and organ responses and improved event-free survival, also in patients with the t(11;14) translocation, pointing towards a new standard-of-care for patients affected by AL amyloidosis[132].

In general, understanding the biological bases underlying the resistance to proteasome inhibitors and overcoming it will constitute a significant step towards the cure of AL amyloidosis.

Recently, Oliva and coworkers had suggested that the amyloidogenic light chains instability may aggravate the delicate proteostatic equilibrium of AL amyloidosis plasma cells, demonstrating that the expression of unstable, amyloidogenic light chains renders AL amyloidosis plasma cells particularly susceptible to bortezomib, even more than multiple myeloma clones, which instead secrete stable light chains[57]. These observations have pointed towards the expression of unstable, amyloidogenic light chains as a sort of Achille's heel for the underlying amyloidogenic plasma cell clone, which could be exploited for the therapeutic purposes to fight against the clone itself[57,106,133].

In light of the possible clinical significance of targeting the proteasome for destabilizing AL amyloidosis plasma cells, a great interest rose for recent works testing DUBs, enzymes upstream of the proteasome (that is the target of bortezomib), which direct polyubiquitinated proteins to proteasome for degradation, as novel promising targets in cancer, including multiple myeloma[134]. Of note, several members of the DUBs family were shown to be dysregulated in multiple myeloma cells[135-138]. Importantly, novel small molecule DUBs inhibitors were shown to have therapeutic potential against multiple myeloma plasma cells, to act also in *in vivo* preclinical models of multiple myeloma, to overcome resistance to proteasome inhibitors and to synergize with other anti- plasma

cell drugs. Whether the deubiquitination pathway is affected in amyloidogenic plasma cells and is a valid therapeutic target for AL amyloidosis is presently unknown.

Objective of the thesis

In the present study, we aimed at studying the potential deregulation of the deubiquitinating system in AL plasma cells through global and targeted transcriptional analyses, as well as to evaluate the therapeutic potential of small molecule drug inhibitors of selected ubiquitin receptors and deubiquitinating enzymes in AL amyloidosis, through the establishment of suitable molecular assays and preclinical cellular models of AL amyloidosis.

Materials and Methods

Human Cell Atlas (HCA)

The Human Cell Atlas (HCA) software, named HCA Bone Marrow viewer (http://www.altanalyze.org/ICGS/HCA/splash.php)[139], comprising transcriptomic data from 35 bone marrow-derived cell populations of 8 healthy subjects, was used for an *in silico* study of gene expression levels of selected deubiquitinating enzymes and ubiquitin receptors (*UCHL5, USP14*, *ADRM1*, *PSMD14, USP1* and *USP7*). To verify the validity of expression data present in this database, expression levels of transcripts characteristic of a selected set of cell types were investigated across the different cell populations: *SDC1* and *CD19* (plasma cells and B cells), *CD3* (T cells), *CD14* (monocytes/granulocytes) and *HBA1* (erythroid progenitors). To retrieve information about gene expression levels of such genes, the combined donors view was selected.

Gene Expression Omnibus (GEO)

The Gene Expression Omnibus (GEO) portal [140,141] was interrogated to identify datasets containing transcriptomic data of primary bone marrow-derived plasma cells from patients with AL amyloidosis, MM and other plasma cell dyscrasias compared to healthy subjects. Two suitable data sets were selected.

The first dataset (GSE73040) reports the genomic, transcriptomic and phenotypic characterization of plasma cells of a small population of AL patients (n=9) and healthy donors (n=5), obtained with a micro-array analysis[73].

The second dataset (GSE6477) collects data of a large population of patients with plasma cell dyscrasias including MGUS (n=22), smoldering MM (n=24), newly diagnosed MM (n=73) and relapsed MM (n= 28) together with healthy donors (n=15)[142].

Ethical statements

Clinical records and biological samples were from subjects referred to the Italian Amyloid Center – Fondazione Istituto di Ricovero e Cura a Carattere Scientifico Policlinico San Matteo, Pavia, Italy, for diagnostic workout in the suspicion of systemic amyloidosis. In accordance with the Declaration of Helsinki, all patients gave their written informed consent for the use of their clinical data and biological samples for research purposes, in agreement with the Institutional Review Board guidelines.

Clinical evaluations in patients diagnosed with AL amyloidosis

Twenty-nine therapy-naïve patients with suspected AL amyloidosis and three relapsed/refractory AL amyloidosis patients evaluated between September 2017 and July 2021 at Amyloidosis Research and Treatment Center, University Hospital San Matteo (Pavia, Italy), for which a bone marrow aspiration was performed as part of the diagnostic workout and with diagnostic leftover of bone marrow aspiration available for analysis, were included in this study.

The diagnosis of AL amyloidosis and the definition of organ involvement were based on clinical examination, echocardiographic, electrocardiographic, serological, cytological and histological analysis according to consensus criteria of the International Society of Amyloidosis[143].

The presence of an M protein was assessed by: 1) capillary electrophoresis of serum proteins, which was performed with a commercial CAPI 3 PROTEIN(E) 6 kit on a CAPILLARYS 3 TERA apparatus (Sebia); 2) a semiautomated serum and urine immunofixation electrophoresis, which was performed with a commercial Hydragel 2IF/BJ(HR) kit on a Hydrasys apparatus (Sebia); 3) the κ/λ ratio of serum free light chain concentrations, assessed by latex-enhanced nephelometry (Freelite assay™, The Binding Site), on a Behring BNII Nephelometer (Dade Behring)[144]. Reference limits for serum FLC concentrations are, respectively, 3.3-19.4 mg/L for κ and 5.7-26.3 mg/L for λ (reference κ/λ ratio interval 0.26–1.65) [145].

To quantify the bone marrow plasma cell compartment, bone marrow (first aspirate) was collected in the presence of sodium citrate, smeared onto a glass slide and stained with May-Grünwald Giemsa according to standard techniques.

To identify amyloid deposit, periumbilical fat tissue was aspirated using a fine needle and smeared onto glass slides, stained with Congo red as previously described[146] and examined with an Eclipse e600 microscope (Nikon) under polarized light. Amyloid deposits were identified based on the presence of the characteristic birefringence by an experienced operator. To type amyloid fibrils, immuno-electron microscopy was performed as previously described[147].

Cell cultures and reagents

The human AL amyloidosis cell lines ALMC-1 (RRID:CVCL_M525), kindly provided by Dr. Enrico Milan (IRCCS San Raffaele Policlinic, Milan, Italy), and ALMC-2 (RRID:CVCL_M526), kindly provided by Dr. Diane F. Jelinek (Mayo Clinic, Rochester, MN)[59], were cultured in Iscove Modified Dulbecco's Medium IMDM (1X) + GlutaMAX (Gibco, Life Technologies), supplemented with 10% heat-inactivated fetal bovine serum (FBS) (origin: South America, Gibco,

Life Technologies), 1% pen/strep (penicillin 10000 units/mL + streptomycin 10000, Gibco, Life Technologies), 10 ng/mL insulin-like growth factor-1 (IGF-1, Gibco, Life Technologies) and 1 ng/mL interleukin-6 (IL-6, Gibco, Life Technologies).

The two human multiple myeloma cell lines, KMS-12-BM (RRID: CVCL_1334) [ref.148] and U266B1 (RRID: CVCL_0566) [ref.149], kind gift of Prof. Antonino Neri (IRCCS San Raffaele Policlinic, Milan, Italy), were cultured in RPMI-1640 Medium (1X) + GlutaMAX (Gibco, Life Technologies), supplemented with 10% heat-inactivated FBS (origin: South America, Gibco, Life Technologies) and 1% pen/strep (penicillin 10000 units/mL + streptomycin 10000, Gibco, Life Technologies).

Cells were seeded at a density of 2-5 × 10^5 viable cells/mL of medium, grown in a 37°C incubator with a humidified atmosphere of 5% CO_2 in air, and split three times a week.

Throughout the study, conditioned medium of the cell lines was regularly tested with the EZ-PCR Mycoplasma test Kit (Resnova) according to the manufacturer's instructions, to verify the negativity to *Mycoplasma spp.* contamination.

The use of different cell lines required a rigorous cell line authentication procedure and quality control (**Appendix 1**).

Cell line authentication for ALMC-1 and ALMC-2 cells was performed through sequencing of the expressed immunoglobulin λ light chain gene (as described below) and comparison of the obtained sequences with the sequence reported in the original publication[59].

Cell line authentication for KMS-12-BM and U266B1 was performed through short tandem repeat (STR) profiling and comparison with the references (as described below). All the cell lines were then characterized by morphological study with May-Grünwald Giemsa coloration, interphase FISH for sex-determination and assessment of translocation t(11;14) positivity, and immunophenotyping through next generation flow cytometry, as described below.

All the DUBs inhibitors drugs, namely b-AP15, RA190, OPA, P5091 and SJB3-019A, were kindly provided by Prof. Kenneth C. Anderson and Dr. Dharminder Chauhan of the Jerome Lipper Multiple Myeloma Center and LeBow Institute for Myeloma Therapeutics, Department of Medical Oncology, Dana-Farber Cancer Institute, Harvard Medical School, Boston, MA. Powdered drugs were firstly reconstituted to achieve a final concentration of 10 mM, and then they were stocked in aliquots 200-fold more concentrated than the first in-plate desired final concentration. Bortezomib was purchased from Merck Millipore (Bortezomib-CAS 179324-69-7-Calbiochem).

Isolation of primary bone marrow-derived plasma cells of AL amyloidosis and multiple myeloma patients

Bone marrow-derived plasma cells were isolated from diagnostic leftovers of bone marrow aspirates of 29 newly diagnosed AL amyloidosis patients and 3 relapsed/refractory AL amyloidosis patients evaluated at the Amyloidosis Research and Treatment Center, Foundation IRCCS Policlinico San Matteo of Pavia between 2017 and 2021 (**Table 1**). After acquisition of a written consent, bone marrow plasma cells were isolated from bone marrow aspirates as follows. In the context of a collaboration, we received diagnostic leftovers of bone marrow aspirates of 6 newly diagnosed multiple myeloma patients and 2 treated multiple myeloma patients evaluated at the with the Department of Hematology, Foundation IRCCS Policlinico San Matteo of Pavia between October 2018 and November 2020.

Bone marrow mononuclear cells were isolated through density gradient centrifugation using a standard protocol (**Fig. 4A**). Briefly, diluted bone marrow was layered 1:1 on Lymphoprep (Cederlane) and centrifuged at 450 g for 30 minutes in a swinging bucket rotor without brake. The resulting mononuclear cell layer was collected and washed in FACS buffer (PBS, 2% FBS, 2.5 mM EDTA). Subsequently, $CD138^+$ cells were isolated from MNCs using CD138 microbeads, MS columns and an OctoMACS separation system (all from Miltenyi Biotec). Based on the number of cells obtained in the $CD138^+$ fraction, a second round of separation was eventually performed, to obtain a highly purified $CD138^+$ fraction, using the $CD138^+$ fraction of the first round as input for the second MS column. Aliquots of mononuclear cells together with $CD138^+$ and $CD138^-$ fractions of the first MS column, defined POS1 and NEG1 respectively, and $CD138^+$ and $CD138^-$ fractions of the second MS column when available, named POS2 and NEG2, were analyzed by flow cytometry to assess the success of the $CD138^+$ isolation procedure and the degree of purity of $CD138^+$ fractions, expressed as percentage (**Fig. 4B**). The remainder of the fractions was lysed in TRIzol Reagent (Invitrogen, ThermoFisher Scientific) and stored at -80°C for further processing.

Isolation of primary mononuclear cells from healthy donors

Peripheral blood mononuclear cells (PB-MNCs) were isolated from venous blood sampling of 6 healthy donors using density gradient centrifugation, according to the protocol previously described. An aliquot of cells was used for drug treatment, while the remainder of the fractions was lysed in 1 mL TRIzol Reagent (Invitrogen, ThermoFisher Scientific) and stored at -80°C for further processing.

Furthermore, primary bone marrow derived mesenchymal stromal cells (BM-MSCs) were isolated from a healthy donor bone marrow sample kindly provided by Dr. Antonia Avanzini et al., according to the protocol previously described. These mononuclear cells and CD138 depleted-mononuclear cells were used for the co-culture model system (see below).

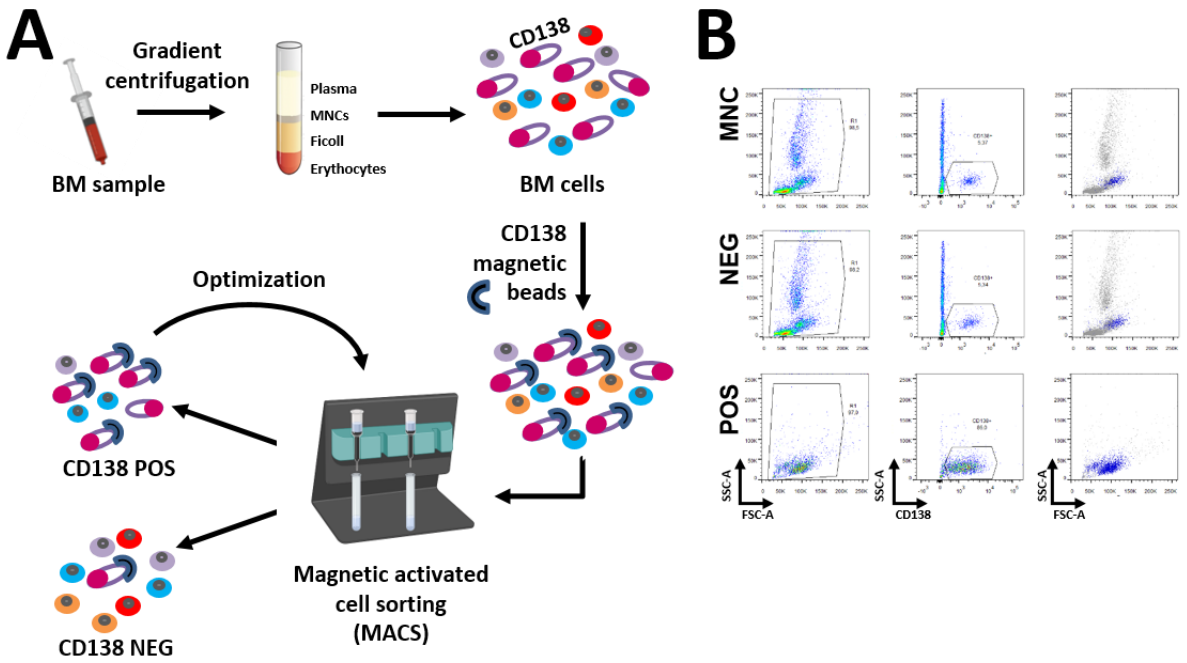

Figure 4: Isolation of CD138$^+$ cells from bone marrow aspirates
A Purification of CD138$^+$ (POS) and CD138$^-$ (NEG) fractions from bone marrow (BM) aspirates, using gradient centrifugation followed by immunomagnetic positive selection using CD138 immunomagnetic beads. One or, more commonly, two rounds of immunopurification were performed with the aim of obtaining a purity (% of CD138$^+$ cells) above 60% in the corresponding POS1 or POS2 fractions, respectively. **B** Flow cytometry analysis to investigate the percentage of CD138$^+$ cells in the initial population of mononuclear cells (MNC), in the CD138$^-$ fraction (NEG) and in the CD138$^+$ fraction (POS). Results shown as representative purification are from AL Pt. 21. Left panel: FSC / SSC plot. Middle panel: Gating of CD138$^+$ cells. Right panel: backgating of CD138$^+$ cells.

Sanger sequencing

RNA from cell lines was isolated from 1x10^6 cells lysed in 1 mL TRIzol (Invitrogen, ThermoFisher Scientific) as described below. Concentration and quality of RNAs were determined with NanoDrop Spectrophotometer ND1000 (ThermoFisher Scientific) and 1% agarose gel electrophoresis, respectively.

To sequence the entire variable region of clonal immunoglobulin light chain gene using conventional Sanger sequencing, we followed a previously described strategy of double-stranded cDNA (dscDNA) synthesis, circularization, inverse PCR and Sanger sequencing reported in [150] with minor modifications. Briefly, 1 µg of total RNAs were used for each dscDNA synthesis reaction.

Reverse transcription was performed using an Anchored Oligo $(dT)_{20}$ Primer and the SuperScript Double-Stranded cDNA synthesis kit (Invitrogen, ThermoFisher Scientific) according to the manufacturer's instructions on a ThermoMixer C (Eppendorf). The resulting dscDNA was resuspended in 10 µl of RNase-free water. The circularization of dscDNA was performed with 1 µl of T4 DNA ligase (1 U/µl), 2 µl of 5X Ligase Reaction Buffer (all from Invitrogen, ThermoFisher Scientific), 3 µl of dscDNA and RNase-free water up 10 µL of total reaction volume. The reaction was incubated overnight at 14°C.

In order to obtain an amplicon encompassing the entire variable region of the corresponding light chain, the ligated dscDNA was then used as input in an inverse PCR with primers targeting a conserved part of the constant region of κ or λ light chain gene. The inverse PCR was performed with 2 µL of the ligated dscDNA, 2 U of Platinum Taq DNA Polymerase (Invitrogen, ThermoFisher Scientific), 1.5 mM of $MgCl_2$, 0.2 mM of dNTPs mixture and 0.5 µM of forward and reverse primers (λ-C_{LA} and λ-C_{LB}, respectively) each, in a final volume of 50 µL of PCR buffer, using a Thermal Cycler C1000, CFX96 Real-Time System (Bio-Rad), at the following conditions: 2 min at 94 °C; 35 cycles of 30 sec at 94°C, 30 sec at 56 °C and 60 sec at 72 °C; 10 min at 72 °C. PCR primer pair was characterized by the following sequences: 5'-AGTGTGGCCTTGTTGGCTTG-3' (λ-C_{LA}) and 5'-GTCACGCATGAAGGGAGCAC-3' (λ-C_{LB})[150].

PCR products were then resolved through electrophoresis on 1% agarose gel, cDNA bands of the expected size (700-800 bp) were cut, and amplicons were purified using the Mini Elute Gel Extraction Kit (QIAGEN) following the manufacturer's protocol. Purified amplicons underwent Sanger Sequencing using a 3500Dx Genetic Analyzer (Applied Biosystems). The obtained sequences were analyzed using IMGT/V-QUEST (http://www.imgt.org/IMGT_vquest/input).

Short tandem repeat (STR) profiling

DNA from cell lines was isolated from $1x10^6$ cells using TRIzol Reagent according to manufacturer's instructions and DNA was resuspended in 50 µL of 8mM NaOH. Concentration and quality were determined with NanoDrop Spectrophotometer ND1000 (ThermoFisher Scientific) and electrophoresis on 1% agarose gel, respectively. Short tandem repeat profiling was determined by multiplex PCR and capillary electrophoresis of 16 STR loci (*D3S1358, TH01, D21S11, D18S51, PENTA E, D5S818, D13S317, D7S820, D16S539, CSF1PO, PENTA D, AMEL, vWA, D8S1179, TPOX, FGA*) using PowerPlex 16 HS System kit (Promega), according to manufacturer's instructions. Using CLASTR (https://web.expasy.org/cellosaurus-str-search/), a tool that allows the

comparison of STR profiles with a collection of all the STR profiles currently known, the obtained STR profiles were analyzed to verify their unicity and, when the comparison was possible, their homology to the expected profiles, according to several data banks (ATCC, CCRID, JCRB, Cosmic-CLP, DSMZ, ECACC).

Morphological study

For morphological study, $1x10^6$ cells from each cell line were collected, spun down at 400 g for 10 min at room temperature and resuspended in PBS (60 µL for $0,25x10^6$ cells). For each cell line, 4 slides were obtained using the Cytocentrifuge Cellspin II (Tharmac) at 400 g, for 12 min, at room temperature. Afterwards, the slides were stained with May-Grünwald Giemsa, according to a standard protocol.

Interphase Fluorescence In Situ Hybridization (iFISH) cytogenetic analysis

Cell lines were analyzed by interphase FISH to verify the presence or the absence of the t(11;14)(q13;q32) chromosomal translocation. A Vysis probe (LSI *CCND1*/*IGH* XT Dual Fusion FISH Probe Kit, Vysis Abbott) was used to identify breakpoints and reciprocal translocation involving the 11q13 region, in which *CCND1* gene is located and the 14q32 region, where the *IGH* gene is present.

Additionally, another Vysis probe pair was employed for sex determination of cell lines [LSI CEP (DXZ1) Spectrum Green / CEP (DYZ3) Spectrum Orange Probe, Vysis-Abbott].

In brief, two aliquots of $15x10^6$ cells of each cell line were cultured in two flasks containing 5 mL of Chromosome Medium M (Celbio). Only one culture for each cell line was supplied with 100 µL of Synchroset A (Celbio) to synchronize cells. After an overnight incubation at 37°C with a humidified atmosphere of 5% CO_2 in air, 100 µL of Synchroset B (Celbio) was added to synchronized cultures, while 80 µL of 10 µM thymidine was added to the other cultures. After an incubation of 5 hours and 50 minutes, 50 mL of Demelcolcine Solution (Sigma-Aldrich) was added to block mitosis process in metaphase. After a series of centrifugations and incubations, cell pellets were resuspended in 6-10 mL of Carnoy fixative (Methyl alcohol:Acetic acid 3:1), and samples were incubated at 4°C overnight. Cells with fixed metaphases and interphasic nuclei were then centrifuged at 1600 rpm for 8 minutes and resuspended with 0,5-1 mL of Carnoy fixative, before being placed on slides. Samples were heat-fixed by passing the slides 3–4 times through the flame and then air-dried.

Finally, slides were dehydrated through 3 passages in ethanol ascending concentration (70%, 85% and 100%) and air-dried, while the Abbott/Vysis probes were prepared according to the manufacturer's instructions. Denaturation of the probe and samples were performed simultaneously on the ThermoBrite plate (Abbott) preheated at 37°C, heating the plate for 1 minute at 75°C, followed by an incubation at 37°C overnight. Finally, after a series of washes to remove non-specific bindings, slides were counter-stained with DAPI (Sigma-Aldrich) and read with a fluorescent microscopy.

To assess the translocational status of patients evaluated for the suspicion of AL amyloidosis included in this study, the same protocol was used to analyze $2x10^5$ primary plasma cells obtained after $CD138^+$ isolation procedure.

Flow cytometry

Cell lines were analyzed by next generation flow cytometry for the definition of their immunophenotype. Staining, acquisition, and analysis were performed using two eight-colour panels according to the EuroFlow guidelines [151]. In brief, $1x10^6$ cells of each cell line were incubated 30 minutes at RT in the dark with eight antibodies directed to membrane antigens, that are CD19- PECy7 (5µL), CD27-BV510 (10 µL), CD38-FITC (6 µL), CD45-PerCPCy5.5 (10 µL), CD56-PE (2 µL), CD81-APCC750 (10 µL), CD117-APC (5 µL) and CD138-BV421 (2 µL). Labelled antibodies were purchased from BD Bioscences (San Jose, CA, USA), Cytognos S.L. (Salamanca, Spain) and BioLegend Inc. (San Diego, CA, USA).

Cells were washed and resuspended in PBS with 0.5% BSA until acquisition. In a second tube with the same cell amount, the procedure was repeated with the omission of anti-CD81-APCC750 antibody. According to the fixation-permeabilization protocol (Fix and Perm, ValterOcchiena, Italy), APCC750-CyIgλ (5 µL) and APCC750-CyIgκ (5 µL) were added. After an incubation of 15 minutes at RT in the dark, cells were washed and resuspended in PBS with 0.5% BSA. Finally, cells were acquired in a BD FACSCantoII cytometer and data analysis was performed with Infinicyt software (version 1.7; Cytognos Salamanca, Spain).

The flow cytometry analysis of apoptosis after drug treatment was performed using eBioscience Annexin V-FITC Apoptosis Detection Kit (ThermoFisher Scientific). After treatment, ALMC-2 cells were washed with cold PBS (450 g for 7 min at 4°C) and resuspended in 95 µL of 1X binding buffer. Then, 5 µL of Annexin V-FITC were added, and cell suspension was incubated at 4°C for 10 minutes. Again, cells were washed and resuspended in 95 µL of 1X binding buffer to which 5 µL of anti-CD138-BV421 antibody (Becton Dickinson Biosciences, BD) were added and cell

suspension was incubated at 4°C for 15 minutes. Finally, cells were washed and resuspended in 95 µL of 1X binding buffer to which 10 µL of propidium iodide (PI) were added just before the analysis. Finally, flow cytometry was performed using a BD FACSCantoII cytometer and data analysis was conducted with Flow Jo software (Becton Dickinson Biosciences, BD).

Furthermore, to control the success of the $CD138^+$ isolation procedure from patients' bone marrow aspirates, mononuclear cells, as well as the positive and negative fractions obtained after immunomagnetic separations, were incubated with the anti-CD138-BV421 (5 µL; Becton Dickinson Biosciences, BD) antibody for 15 minutes in the dark at 4°C. Then, cells were fixed with the BD FACS Lysing solution 10X (Becton Dickinson Biosciences, BD) with a 10-minute incubation. Finally, primary cells were washed, resuspended in 200 µL of PBS, acquired in a BD FACSCanto II cytometer. Data analysis was conducted with Flow Jo software (Becton Dickinson Biosciences, BD).

The phenotypic characterization of healthy donor mesenchymal stromal cells was performed by flow cytometry and monoclonal antibodies specific for CD34, CD73, CD90, HLA-I, CD31, CD14, CD45, CD105 and HLA-DR, FITC- or PE-conjugated were used for this purpose (all from Beckman Coulter). In brief, cells were incubated with specific antibodies at the recommended concentrations for 30 minutes at 4°C. Cells were washed in PBS 0.1% BSA, centrifuged at 1000 rpm for 10 minutes and resuspended in 300 µl of PBS. Data acquisition and analysis of cellular populations were performed by direct immunofluorescence with FACS Navios cytometer (Beckman Coulter).

RNA extraction and cDNA synthesis

RNA from cell lines (both treated and untreated) and primary, peripheral blood mononuclear cells (PB-MNCs) was isolated using the RNeasy Mini Kit (QIAGEN), starting from an aliquot with a total amount of cells comprised between $1x10^6$ cells (as for cell lines) and $10x10^6$ cells (as for PB-MNCs), lysed in 1 mL of TRIzol (Invitrogen, ThermoFisher Scientific). Starting from these aliquots, 200 µL of chloroform was added per 1 mL of TRIzol. After a gradient centrifugation (12'000 g for 15 minutes at 4°C), the upper aqueous phase was transferred in a new tube and one volume of 70% ethanol was added. Then each sample was loaded in an Easy Mini column, processed according to manufacturer's instructions and finally, RNA was eluted in 30 µL of RNAse-free water.

RNA from primary bone marrow-derived plasma cells from MM and AL amyloidosis patients (both treated and untreated) was extracted using RNeasy Plus Micro Kit (QIAGEN), starting from an

aliquot with a total amount of cells comprised from $3x10^4$ cells up to $5x10^5$ cells, lysed in 1 mL TRIzol. Also in this case, 200 µL of chloroform was added per mL of TRIzol used. After a centrifugation, the aqueous phase was transferred in a new tube and one volume of 100% ethanol was added. Then, all the sample was loaded in a RNeasy spin column, processed according to manufacturer's instructions and finally, RNA was eluted in 14 µL of RNase-free water. For all RNA samples, concentration and quality of RNA were determined with NanoDrop Spectrophotometer ND1000 (ThermoFisher Scientific).

Reverse transcription of RNA samples was performed using the QuantiTect Reverse Transcription kit (QIAGEN), according to the manufacturer's instructions, on a ThermoMixer C (Eppendorf). For each sample, 100 ng of total RNA was used as input material for retrotranscription and the resulting cDNA was diluted at 10^{-1}, with the exception of the ALMC-2 cDNA used for dynamic range assessment, obtained from the retrotranscription of 1000 ng of total RNA and aa dilution from 1:10 to $1:10^5$.

Primer identification

Primer sequences for the genes of interest were designed following a strategy established in our laboratory (**Appendix 2**). Gene features and primer sequences are listed in **Table 2**. Briefly, primer pairs were identified with NCBI/Primer-BLAST website (https://www.ncbi.nlm.nih.gov/tools/primer-blast/), using default parameters for the Refseq mRNA database of *Homo sapiens*, except the following: PCR product size – Min 70 bp Max 120 bp; Exon intron selection – Primer must span an exon-exon junction.

Once candidate primer sequences were obtained, the presence of known single nucleotide polymorphisms (SNPs) in the corresponding genomic regions was verified, using Ensembl (https://www.ensembl.org/index.html) and dbSNP (https://www.ncbi.nlm.nih.gov/projects/SNP). In order to minimize the potential detrimental impact of sequence mismatches on PCR efficiency, primer pairs with known SNPs in the last five positions of the 3' terminus were excluded[152].

For the same purpose, each gene was searched in another web portal, namely REDIportal (http://srv00.recas.ba.infn.it/atlas/search_hg.html), to exclude primer pairs that presented known A-to-I RNA editing sites within the regions of the transcripts targeted by the primers. The search was performed using default parameters, except the following: Tissue - All; Body site- All.

Finally, OligoAnalyzer 3.1 website (https://eu.idtdna.com/calc/analyzer) was interrogated using default parameters in order to check the maximum Tm of the most probable hairpin structure made

by each primer (Tm > 60°C was not accepted) and the minimum ΔG of homo- and hetero-dimer for each primer and primer pair (ΔG > -10 was not accepted).
This path was iteratively followed until an adequate primer pair was identified for each candidate reference gene. Only if iteration of this path for 15 consecutive primer pairs obtained through NCBI/Primer-BLAST was unproductive, a less stringent primer pair was selected.
All the identified primer pairs were subjected to a robust technical validation, including the assessment of PCR specificity and PCR efficiency through melting curve and dynamic range analyses, respectively, and inter and intra-assay variation.

Real Time quantitative PCR (RT-qPCR)

Real Time quantitative PCR (RT-qPCR) was performed with 7 µL of SsoFast EvaGreen Supermix (Bio-Rad), 0.5 µM of forward and reverse primers each, and 5 µL of 10^{-1} diluted cDNA as template and RNA-free water up to a final volume of 14 µL. The RT-qPCR was performed using a Thermal Cycler C1000, CFX96 Real-Time System (Bio-Rad) and the protocol used, according to Vandesompele et al.[153], was set at the following conditions: 95°C for 10 min, 40 cycles of 95°C for 15 s, 60°C for 1 min. In each experiment, each sample was run in triplicate and a water sample (H_2O) and a no-RT sample (a sample without the retrotranscriptase enzyme in the reaction mix) were used as negative controls. After each run, a melting curve analysis was performed to assess specificity of the reaction, using the following conditions: 95°C for 10 s, 60°C to 95°C for 5 s. For all steps, a ramp rate of 0.5°C/s was used. Furthermore, 1% agarose gel electrophoresis was performed to verify the unicity and size of each RT-qPCR amplicon.

Western blotting

To obtain cell lysates for protein biochemical analyses, $1x10^6$ cells for each cell lines were collected, spun down at 400 g, for 7 min, at 4°C and washed twice with ice-cold phosphate-buffered saline (PBS) (Invitrogen, ThermoFisher Scientific). Subsequently, cell pellets were resuspended in 100 µL of lysis buffer, prepared with PBS with 1% SDS and supplemented with proteases and phosphatases inhibitor cocktail tablets (PhosSTOP Easypack, Roche, Merck), and incubated on ice for 10 min. Finally, a mechanical lysis was performed using an insulin syringe.
The protein yield was assessed with the Micro BCA Protein Assay Kit (ThermoFisher Scientific) using the NanoQuant infinite M200 PRO plate reader (TECAN).

For the evaluation of drug-induced polyubiquitin accumulation, $3x10^6$ ALMC-2 cells were treated with b-AP15 or RA190 (both 100 nM), bortezomib (5 nM) as positive control, or DMSO as negative control, for 1, 3 and 6 hours, and cells were then lysed using the same protocol.

Five or ten micrograms of proteins (for polyubiquitin accumulation and for expression analysis of the molecular targets for DUBs inhibitors, respectively) were denaturated by boiling in reducing sample buffer, separated by SDS-PAGE in 4-15% Mini-protean TGX precast gels (Bio-Rad) and electrotransferred onto 0.2µm polyvinylidene difluoride (PVDF) membranes (Bio-Rad), using the Trans-Blot Turbo Transfer System (Bio-Rad). Membranes were blocked for 1h in PBS/Tween20 with 5% non-fat dried milk and incubated overnight at 4°C with the primary antibody.

Immunoblotting was performed using monoclonal rabbit anti-USP1 (D37B4), anti-ADRM1 (D9ZIU) and anti-PSMD14 (D18C7) antibodies (purchased from Cell Signaling), polyclonal rabbit anti-USP7 and anti-USP14 antibodies (purchased from Bethyl Laboratories), monoclonal rabbit anti-UCH37 (EP4897) antibody (obtained from abcam), mouse monoclonal anti-ubiquitin antibody (P4D1) and polyclonal rabbit anti-β actin antibody (C4), used as loading control (purchased from Santa Cruz Biotechnology).

After washing, membranes were incubated for 1h, at room temperature, with polyclonal secondary swine anti-rabbit immunoglobulins HRP antibody (Dako, Agilent), except for β-actin, for which a polyclonal secondary goat anti-mouse antibody was used. Finally, blots were developed using Immobilon Western Chemiluminescent HRP Substrate (Merck Millipore), according to manufacturer's instructions.

DUBs inhibitors treatment

For the evaluation of the DUBs inhibitors therapeutic effect, cell metabolic activity and cell viability were assessed upon DUBs inhibitors exposure.

For drug treatment, $3x10^4$ cells/well of ALMC-2 cells (density of $3x10^5$ cells/mL) were plated in a 96-well plate and treated with 6 different doses for each drug (b-AP15: 625, 312.5, 156, 78, 39 and 19 nM; RA190: 1250, 625, 312, 156, 78, 39 nM; OPA: 62.5, 31.25, 15.60, 7.80, 3.90, 1.95 µM ; P5091: 50, 25, 12.5, 6.25, 3.12, 1.56 µM ; SJB03-19: 2000, 1000, 500, 250, 125, 62.5 nM) or DMSO as vehicle, and incubated for 48 hours at 37° C. For each dose, a technical triplicate was performed, and each experiment was performed three times.

For the assessment of cell metabolic activity, the CellTiter-Glo Luminescent Cell Viability Assay (Promega) was used according to the manufacturer's instructions. Briefly, after the 48-hour incubation, one volume of CellTiter-Glo reagent was added (100 µL) and the plate was mixed for 2

minutes in the shaker Thermomixer R (Eppendorf) to induce cell lysis. After a 10 minute-incubation, the plate was read using the NanoQuant infinite F200 plate reader (TECAN). In the same plate, a fourth replicate was used for assessing cell viability through a Trypan Blue exclusion assay, using a 0.4% Trypan Blue solution (Sigma Aldrich) and Trypan Blue uptake or exclusion was evaluated under a light microscope (Labovert Leitz).

In addition to Trypan Blue exclusion assay, for the assessment of cell viability, after drug treatment apoptosis was measured using the eBioscience Annexin V-FITC Apoptosis Detection Kit (ThermoFisher Scientific), according to the manufacturer's instructions (see above, section Flow Cytometry).

In order to assess b-AP15 therapeutic effect in a set of four different AL and MM cell lines, the latter harboring the t(11;14) translocation, cell metabolic activity and cell viability were evaluated with the same protocols. To explore a broader range, two other doses was included (2500, 1250 nM) for a total of 8 different doses.

The same protocol of drug treatment was used for the evaluation of cell metabolic activity after exposure to b-AP15, RA190 or DMSO of primary bone marrow-derived $CD138^+$ and $CD138^-$ cells of AL amyloidosis patients (b-AP15 doses: 75 and 150 nM and 24h treatment; RA190 doses: 200 and 600 nM and 48h treatment) and peripheral blood mononuclear cells of healthy donors (b-AP15 doses: 37.5, 75, 150 and 300 nM; RA190 doses: 1200, 600, 200, 100 nM). The IC_{50} values were calculated using the GraphPad Prism software, based on the normalized data from the cell metabolic activity assay.

To study gene expression levels of *HMOX-1* and *HSPA6*, two genes associated with oxydative and proteotoxic stress, respectively, upon drug treatment, cells were treated with micromolar concentration of b-AP15. For this purpose, $1x10^6$ cells/well of ALMC-2 cells (density of $3x10^5$ cells/mL) were plated in a 6-well plate and treated with 2µM of b-AP15 or DMSO as vehicle, and incubated for 1, 3 and 6 hours at 37° C in a humidified atmosphere 5% CO_2. For each time point, a technical triplicate was performed. After the incubation, cells were collected, spun down and lysed in 1 mL of TRIzol for further RT-qPCR analysis. The same procedure was used to treat AL patient primary BM-derived $CD138^+$ cells, plating $3x10^4$ cells/well in a 96 well plate and incubating for 1 and 3 hours.

ALMC-2 cell line/BM-MSCs co-culture

Primary, BM-derived mesenchymal stromal cells (BM-MSCs) from a healthy subject were isolated from a bone marrow aspirate by density gradient centrifugation. After CD138 depletion,

mononuclear cells and CD138 depleted-mononuclear cells were plated on uncoated polystyrene cell culture flasks (Corning Costar) at a density of $1,6x10^5$ cells/cm^2 in DMEM-LG medium (Gibco, Life Technologies), supplemented with 50 mg/mL gentamicin (Gibco, Life Technologies) and 10% fetal calf serum (FCS) (Mesencult, Voden). Cells were grown at 37°C in a humidified atmosphere 5% CO_2 and culture medium was replaced twice a week. Mesenchymal stromal cells were harvested until reaching ≥80% confluence. Then, using recombinant Trypsin-EDTA (Euroclone), cells were re-plated for expansion at a density of 4000 cells/cm^2 and cultured until passage 4 (P4). The characterization of MSCs was performed following the criteria defined by the International Society for Cellular Therapy (ISCT) for morphology, clonogenic capacity, immunophenotype and differentiation capacity[154]. Clonogenic capacity is defined as the number of Colony Forming Unit fibroblasts (CFU-)F at P0 after 14 days of culture, when the number of clones were counted under a light microscope. The proliferative capacity of MSC was defined as cumulative Population Doublings (cPD), calculated by summing the PD of the single passage using the formula:

$$PD = \log_{10}(N_1/N_0) / \log_{10}2$$

where N_0 is the number of seeded cells and N_1 the number of harvested cells.

Mesenchymal stromal cells were phenotypically characterized by flow cytometry and cells were tested for their ability to differentiate into osteoblasts and adipocytes at early passages (P3). Briefly, to induce osteogenic differentiation, cells were cultured in specific differentiation medium: αMEM (Lonza) supplemented with 10% FCS (Euroclone), dexamethasone (10^{-7} M), and ascorbic acid (50 g/mL). Starting from day +7 of differentiation culture, 5 mM β-glycerolphosphate (Sigma-Aldrich) was added. For adipogenic differentiation, cells were cultured in αMEM, 10% FCS and 2 mM L-glutamine supplemented with 10^{-7} M dexamethasone, 50 mg/mL L-ascorbic acid, 100 mg/mL insulin, 50 mM isobutyl methylxanthine, 0.5 mM indomethacin (Sigma-Aldrich) and 5 mM β-glycerolphosphate. Before evaluating differentiation, both osteogenic and adipogenic cultures were incubated for two weeks at 37°C with 5% CO_2 and media were replaced twice per week. To detect osteogenic differentiation, cells were stained for alkaline phosphatase (AP) activity using Fast Blue (Sigma-Aldrich) and for calcium deposition with Alizarin Red (Sigma-Aldrich). Adipogenic differentiation was assessed based on the morphological appearance of fat droplets after staining with Oil Red O (Sigma-Aldrich). MSCs were expanded until they entered the senescence phase, defined as the passage (P) when the number of detached cells is less than or equal to the number of plated cells.

For the co-culture experiment and b-AP15 treatment, three conditions were tested: the monoculture of ALMC-2 cell line, the monoculture of MSCs and the co-culture of ALMC-2/BM-MSCs. To

obtain these 3 different cultures, at day 1 BM-MSCs (100 µL with $1,5x10^4$ cells/well) were plated in a 96-well plate and incubated at 37° C. At day 2, 90 µL of MSC medium was discarded in the wells dedicated to the co-culture and substituted with 85 µL of medium with ALMC-2 cells ($3x10^4$ cells/well). The same day, b-AP15 treatment was performed by adding 5 µL of the pre-diluted drug (two doses tested: 312.5 and 625 nM) or DMSO as control. At day 3, 18 hours before the analysis, 25 µL of ^{3}H-thymidine was added to each well and ^{3}H-thymidine incorporation was assessed on a gamma counter. After 48 hours of incubation, cell metabolic activity was assessed using the CellTiter Glo assay, according to manufacturer's instructions.

Statistical analyses

For microarray data sets, adjusted p values generated through the GEO portal were used.

Unless otherwise stated, data are reported as mean ± standard deviation (SD). Statistical analysis was performed using the GraphPad Prism software. Statistical significance ($P<0.05$, *; $P<0.01$, **; $P<0.001$, ***; $P<0.0001$, ****) was determined by two-tailed unpaired t-test, two-tailed paired t-test and one-way ANOVA.

Table 1: List of patients and clinical characteristics

# Pt	Age (year)	Sex	Diagnosis	Serum M protein type	Urine M protein type	% PC infiltration	FLC κ	FLC λ	% CD138$^+$ purity	t(11;14)	Gain1q
AL Pt. 01	48	M	MM + AL	None	BJPκ	22,5	3400	16,4	93,7 #	NA	NA
AL Pt. 02	73	F	AL	IgGλ	BJPλ	8	10,3	14,1	95,4	NA	NA
AL Pt. 03	64	M	AL	FLCλ	BJPλ	13	9,7	185	93,2	NA	NA
AL Pt. 04	68	M	AL	FLCλ	BJPλ	7	41,8	496	80,1	NA	NA
AL Pt. 05	66	M	AL	FLCλ	BJPλ	3	8,7	507	87,5 #	Positive	Negative
AL Pt. 06	56	M	AL	IgGλ	BJPλ	15	10,8	458	77,8	Positive	Negative
AL Pt. 07	61	M	AL	IgAλ + FLCλ	BJPλ	12	7,1	560	92,1	Negative	1q21 63%
AL Pt. 08	76	F	AL	IgAλ	None	7	33,9	286	80,1	Positive	Negative
AL Pt. 09	76	M	AL	IgAλ	BJPλ	13	153	309	89,4	Negative	1q21 73%
AL Pt. 10	50	M	AL	FLCλ	BJPλ	**NA**	7,93	71,7	70,2	NA	NA
AL Pt. 11	74	F	MM + AL	IgAλ + IgGλ	BJPλ	25	**NA**	**NA**	91,3	NA	NA
AL Pt. 12	64	F	AL	IgGλ	None	11,5	9,91	375	80,4	Positive	Negative
AL Pt. 13	58	M	AL	IgGλ + FLCλ	BJPλ	30	2,5	179	84,5	Negative	Negative
AL Pt. 14	54	M	AL	IgGλ + FLCλ	BJPλ	30	11,2	67,6	94,6	Positive	Negative
AL Pt. 14*	56	M	AL	IgGλ + FLCλ	BJPλ	**NA**	13,2	72,45	63,6*	Positive	Negative
AL Pt. 15	58	M	Other + AL	IgGκ + IgGλ	BJPλ	7	25,5	234	87,2	NA	NA
AL Pt. 16	73	M	AL	IgGλ + FLCλ	BJPλ	18	16,2	434	78	Negative	1q21 60%
AL Pt. 17	59	F	AL	IgDκ	BJPκ	9	118	17,1	79,1	Positive	Negative
AL Pt. 18	86	F	AL	IgGλ + FLCλ	BJPλ	9	17,4	83,9	80,0	Negative	Negative
AL Pt. 19	74	M	AL	IgAλ + FLCλ	BJPλ	8	26,3	1000	80,6	Negative	1q21 11%
AL Pt. 20	73	M	AL	None	BJPλ	4,5	68,1	398,6	68	Positive	Negative
AL Pt. 21	67	F	AL	FLCλ	BJPλ	14	21	337	86,0	Positive	Negative
AL Pt. 22	61	M	AL	FLCλ	BJPλ	NA	NA	NA	NA	Negative	Negative
AL Pt. 23	64	M	AL	IgGλ	BJPλ	4	14,8	60,2	79,5	Positive	Negative
AL Pt. 24	71	F	AL	IgMλ + FLCλ	BJPλ	9	28,2	257	77,9	Negative	1q21 27%
AL Pt. 25	73	F	AL	FLCκ	BJPκ	6,5	654	13,1	84	Positive	Negative
AL Pt. 26	73	M	MM + AL	FLCκ	BJPκ	10	1000	8,7	85,5	Positive	Negative
AL Pt. 27	69	F	AL	κ	None	6	137	16,9	81,4	Positive	Negative

AL Pt. 28	57	M	AL	λ	None	11	9,1	233	61,6	Negative	Negative
AL Pt. 29	71	M	AL	FLCλ	None	14	26,4	180	72,4	Positive	Negative
AL Pt. 30	83	M	AL	IgGκ	BJPκ	3	25,3	10,6	72,6	Negative	Negative
AL Pt. 31	80	M	AL	IgAλ + IgGλ	BJPλ	11	27,6	488	92,0	Negative	Negative
MM Pt. 01	70	M	MM	IgAκ	BJPκ	NA	37,6	2,05	77,1 #	NA	NA
MM Pt. 02	NA	F	MM	IgAκ	BJPκ	NA	NA	NA	71,3 #	NA	NA
MM Pt. 03	NA	F	MM	IgGλ	BJPλ	NA	NA	NA	84,2	NA	NA
MM Pt. 04	68	F	MM	IgAκ	BJPκ	80-90	93,6	5,91	74,7	NA	NA
MM Pt. 05	49	M	MM	IgGκ	BJPκ	90	20,1	5,18	89,1 #	NA	NA
MM Pt. 06	56	M	MM	FLCκ	BJPκ	10-15	251	12,7	70,2	NA	NA
MM Pt. 07	59	F	MM	IgAλ	BJPλ	30	9,9	36,9	80,4	NA	NA
MM Pt. 08	73	F	MM	IgGκ	None	70-80	402	5,94	90,2	NA	NA

Percentage of $CD138^+$ purity was assessed in POS2 fraction, except for patients AL Pt. 01, 05 and MM Pt. 01, 02 and 05 for which the percentage of $CD138^+$ purity was assessed in POS1 fraction, indicated with the hashtag (#). The asterisk (*) indicates the patient at the time of disease relapse. For AL Pt. 15, AL amyloidosis was accompanied by biclonal gammopathy (indicated as "Other"). AL = AL amyloidosis; BJP = Bence Jones Protein; FLC = free light chain; HC = Heavy chain; Ig = immunoglobulin; LC = light chain; MM = multiple myeloma; NA = not available; PC = plasma cells; Pt = patient.

Table 2: Gene characteristics and primer sequences

Gene symbol	Accession number	Gene name	Alias	Function	Location	Forward sequence (5'->3')	Reverse sequence (5'->3')	Amplicon size (bp)
ACTR3	NM_005721.4	ARP3 actin related protein 3 homolog	*ARP3*	Major constituent of the ARP2/3 complex	2q14.1	ACACACCACATGCAGCGATA	TTGGTAGAACTCAGGCGTGG	72
ALG9	NM_024740.2	α-1,2-mannosyltransferase		Lipid-linked oligosaccharide assembly	11q23.1	TCATCCAGCCTCACAAAGAGG	CTGTGCTGAAGTGCAGAGAGA	94
ESD	NM_001984.1	Esterase D		Serine hydrolase of the esterase D family	13q14.2	TGTCTACTTACCACCAAAGGCA	TTGCTCTGTGCAAGTTAAACC	79
GAPD	NM_002046.6	Glyceraldehyde-3-phosphate dehydrogenase	*GAPDH, G3PD*	Involved in carbohydrate metabolism	12p13.31	CATTGACCTCAACTACATGGTTTAC	CTTGACGGTGCCATGGAATTTG	73
HMOX-1	NM_002133.3	Heme oxygenase 1	*HMOX1D, HO-1, HSP32*	Essential enzyme in heme catabolism	22q12.3	AAGTTCAAGCAGCTCTACCGC	CTCCTCAAAGAGCTGGATGTTG	120
HSPA6	NM_002155.5	Heat shock protein family A (HSP70) member 6	*HSP70B*	Involved in protein quality control system	1q23.3	GCACCTTCGATGTGTCGGT	TGGTTCACGAGCCGGTTG	112
ADMR1	NM_007002.3	Adhesion regulating molecule 1	*Rpn13*	Component of the proteasome, recruits the deubiquitinating enzyme	20q13.33	GCGCGAGGCAGGATGAC	GCCCGAAACTCCACCAAGT	95
PSMD14	NM_005805.5	Proteasome 26S subunit, non-ATPase 14	*Rpn11*	Component of the 26S proteasome, mediates substrate deubiquitination	2q24.2	AGTGTGGAGGCAGTTGATCC	CATCTCCGGCCTTCCTGTCT	75
UCHL5	NM_015984.4	Ubiquitin C-terminal hydrolase L5	*UCH37, UCH-L5*	Component of the proteasome, deubiquitylating enzyme	1q31.2	ACAACTTGCAGAGGAGGAACC	GCAACTTCTGACTGAATAGCACT	75
USP14	NM_005151.3	Ubiquitin specific peptidase 14		Member of the UBP family of proteases, is a deubiquitylating enzyme	18p11.32	AGGAGGAACGCTAAAGGATGATG	TTTGGCTGAGGGTTCTTCTGG	109
USP1	NM_003368.4	Ubiquitin specific peptidase 1		Member of the UBP family of proteases, is a deubiquitylating enzyme	1p31.3	TGAACAGCTCCAGGCTAGTTT	GGTTGAGTTCCCTCAGTGTGTT	101
USP7	NM_003470.2	Ubiquitin specific peptidase 7		Member of the peptidase C19 family, is a ubiquitinyl hydrolases	16p13.2	CCGAGGACATGGAGATGGAA	CACTCAGGGCCACATTCCC	88

Gene information were retrieved from NCBI Gene and Ensembl. Underlined letters denote bases annealing with a genomic region with a known SNP, according to Ensembl and dbSNP.

Results

Expression of deubiquitinating enzymes and ubiquitin receptors in healthy conditions and in plasma cell dyscrasias

In an effort to explore the therapeutic potential of five small molecule inhibitors of selected deubiquitinating enzymes or ubiquitin receptors in preclinical models of AL amyloidosis, we first opted to study the expression pattern of their molecular targets (listed in **Fig. 3B**), both in healthy conditions and in plasma cell disorders.

Firstly, we performed an *in silico* analysis of mRNA expression levels of these molecular targets in different bone marrow cell populations (including bone marrow plasma cells and other hematopoietic cells) in healthy conditions. For this purpose, we exploited the Human Cell Atlas (HCA) data set, which collects transcriptomic data from 35 bone marrow-derived cell populations of 8 healthy subjects[139]. To confirm the reliability of this transcriptomic data set, we initially selected a set of five cell population marker genes, and we examined their gene expression levels in order to verify the selectivity of their expression in the corresponding cell population(s). *SDC1* (the gene encoding for CD138 or syndecan 1) and *CD19* gene expression was specific for the B cell lineage, while *CD3E* was restricted to the T cell lineage. The monocytes and granulocytes specific marker *CD14* was highly expressed by eosinophils, neutrophils and monocytes, while expression of the *HBA1* gene, encoding for hemoglobin subunit alpha 1, was peculiar to the erythroid population, as expected (**Fig. 5**). We then analyzed mRNA expression levels of the different molecular targets of interest across different bone marrow cell populations. Based on transcriptional data from the Human Cell Atlas, a ubiquitous expression of DUBs inhibitors molecular targets was observed in all the 35 bone marrow cellular compartments explored across all 8 examined human healthy subjects. Only modest differences in the magnitude of expression were detected in mRNA levels of all the six molecular targets among the different cellular populations examined. Additionally, for all the analyzed target genes, bone marrow plasma cells showed transcript levels in the lower range of the expression spectrum (**Fig. 5**).

Next, we decided to investigate transcriptional expression levels of the six molecular targets in the bone marrow plasma cell compartment from patients with different types of plasma cell dyscrasias, including AL amyloidosis, as opposed to healthy bone marrow plasma cells. In this regard, we exploited two publicly available microarray-based transcriptional studies of different plasma cell dyscrasias.

The first data set (GSE73040) collects transcriptional profiles of bone marrow-derived plasma cells of healthy subjects (n=5) and plasma cells from AL amyloidosis patients (n=9)[73]. According to this data set, a modest increase in expression in plasma cells from AL amyloidosis subjects compared to healthy controls was identified in four genes, *UCHL5* (+ 3.1%), *USP14* (+ 4.8%), *ADRM1* (+4.1%) and *PSMD14* (+5.6%); conversely *USP1* and *USP7* showed a moderate decreased expression in plasma cells from AL amyloidosis subjects compared to healthy controls (-1.8% and -4.2%, respectively). However, none of these differences in expression levels reached statistical significance (adjusted p-values: 0.91 for *UCHL5*, 0.81 for *USP14*, 0.56 for *ADRM1,* 0.78 for *PSMD14*, 0.90 for *USP1* and 0.79 for *USP7*, **Fig. 6**).

The second data set (GSE6477), based on a large patient population, covers the spectrum of plasma cell dyscrasias from bone marrow plasma cells of healthy donors (n=15) to the pre-malignant state of monoclonal gammopathy of undetermined significance (MGUS, n=22), up to smoldering MM (n=24), newly diagnosed MM (n=73), and relapsed MM (n= 28)[142]. In this data set, *UCHL5* expression levels showed higher intra-group variation, with a moderate decrease when progressing from healthy conditions to MGUS and smoldering MM, followed by an increase towards newly diagnosed MM and relapsed MM (adjusted p-value 4.14×10^{-1}, **Fig. 6**). *USP14*, *ADRM1* and *PSMD14* expression levels progressively increase with increasing levels of plasma cell malignity, with healthy subjects, MGUS and smoldering MM plasma cells showing lower levels of expression compared to plasma cells from newly diagnosed MM and relapsed MM patients (adjusted p-values: 4.65×10^{-3} for *USP14*, 3.71×10^{-1} for *ADRM1* and 4.27×10^{-4} for *PSMD14*, **Fig. 6**). An opposite trend was observed in *USP1* and *USP7*, that showed a progressively reduced expression with increasing levels of plasma cell malignity, thus showing higher levels of expression in plasma cells from healthy subjects and MGUS patients compared to plasma cells from newly diagnosed MM and relapsed MM patients (adjusted p-values 1.65×10^{-1} for *USP1* and 2.19×10^{-1} for *USP7*, **Fig. 6**).

Finally, we tested the expression levels of the six genes of interest encoding for the molecular targets of the above-mentioned DUBs inhibitors in primary bone marrow-derived $CD138^{+}$ cells from patients with AL amyloidosis (n=12) and patients with MM (n=8). For this purpose, we used a validated RT-qPCR assay. The process of selection of suitable reference genes for normalization of RT-qPCR data exploiting publicly available transcriptomic datasets has prompted the development of a strategy which could be applied also in other experimental and clinical settings (**Appendix 2**).

The primer pairs identified for the assessment of the molecular targets' gene expression were subjected to a rigorous technical validation. We used agarose gel electrophoresis and melting curve analysis to verify PCR specificity for each primer pair, and we tested serial dilutions of cDNA synthetized from 1 μg of RNA over 5 orders of magnitudes (from 10^{-1} to 10^{-5}) to explore the

dynamic range of each assay and calculate PCR efficiency. The linear dynamic range spanned 4 orders of magnitude of cDNA dilution for *USP1* and 5 order of magnitudes for the remaining genes. PCR efficiency ranged between 96.4% for *ADRM1* and 108.4% for *USP14*. The data on linear dynamic range, PCR efficiency and specificity are shown in **Fig. 7A**. For each of these, we analyzed 6 technical replicates in one run to assess intra-assay variation. The coefficient for intra-assay variation ranged from 0.34% for *USP7* to 0.92% for *USP1* (**Fig. 7B**). Finally, for each gene we analyzed technical triplicates in three runs on separate days to assess inter-assay variation. The coefficient for inter-assay variation ranged from 0.46% for *USP7* to 1.2 for *UCHL5* (**Fig. 7C**).

According to the RTq-PCR gene expression analysis, for all the molecular targets of interest, patients affected by AL amyloidosis showed a trend toward higher expression levels compared to the MM patients (+65.9% for *UCHL5*, +46.7% for *USP14*, +66.1% for *ADRM1*, +19.2% for *PSMD14*, +68.3% for *USP1* and +94.1% for *USP7*), with only *USP7* upregulation reaching a statistical significance (p value = 0.0122) (**Fig. 8**).

Therapeutic effect and mechanism of action of DUBs inhibitors in ALMC-2 cell line

To test the therapeutic effect of DUBs inhibitors in AL amyloidosis plasma cells and to study their mechanism of action, we initially elected to use the ALMC-2 cell line as a model system[59]. This cell line was established from the bone marrow aspirate of a 50-year-old female patient with AL amyloidosis and a plasma cell clone secreting an IgGλ and λ free light chain M-protein.

The ALMC-2 cell line was obtained at the time of clinical relapse after peripheral blood stem cell transplant, when the clinical condition evolved into overt multiple myeloma[59]. The immunoglobulin gene sequencing study revealed that the germline genes used for λ light chain production were *IGLV6-57* gene for the V region and *IGLJ3* gene for the J region[59]. Noteworthy, the ALMC-2 immunoglobulin λ light chain proved to be amyloidogenic also *in vitro*, confirming this cell line as a suitable cellular system to investigate the biology of amyloidogenic plasma cells[59].

For cell line authentication purposes (**Appendix 1**), we first performed immunoglobulin light chain sequencing, which confirmed the presence of a λ light chain sequence derived from *IGLV6-57*03* and *IGLJ3*02* genes, with 100% identity with the published sequence for this cell line (and the corresponding AL amyloidosis patient), providing further confirmation of the authenticity of the cell line (**Fig. 9A**).

Then, we performed a through phenotypic and molecular characterization of the ALMC-2 cell line, by investigating key biologic features, including cell morphology, the presence of the sexual chromosomes, the presence of the t(11;14) chromosomal translocation, the immunophenotype and

the STR profiling (**Fig. 9B-E**). May-Grünwald Giemsa staining confirmed a plasma cell morphology. The presence of two copies of the probe mapping to the X chromosome (although 12% of observed nuclei presented only one such signal) and the absence of signal from the probe mapping to the Y chromosome (**Fig. 9B**) was ascertained by molecular cytogenetics through interphase FISH (iFISH), confirming the female gender of the AL amyloidosis patient from whom the cell line was originated[59]. Furthermore, iFISH confirmed the absence of colocalization of the two probes mapping to chromosomes 11 and 14, therefore indicating the absence of the t(11;14) translocation (**Fig. 9C**), in agreement with the reported karyotype of this cell line[59]. Immunophenotyping through multiparametric next-generation flow cytometry showed expression of CD138, CD38, CD81 and CD27 cell surface markers (MFI value: 82477, 8911, 19164 and 3123, respectively), dim expression of CD45, CD117 and CD56 expression (MFI value:1293, 159 and 755, respectively), lack of CD19 expression and confirmed the λ light chain restriction of this plasma cell line (**Fig. 9D**). Short tandem repeat profiling of ALMC-2 was assessed by multiplex PCR and capillary electrophoresis (**Fig. 9E**). Even though the short tandem repat profile of this specific cell line has not been previously reported, comparison of the obtained profile from ALMC-2 cells with known profiles from cell lines available in public repositories through CLASTR confirmed its uniqueness. Finally, a PCR-based assay confirmed the negativity for *Mycoplasma spp* possible contamination in ALMC-2 cell line (**Fig. 9F**).

Next, as a prerequisite for the use of ALMC-2 cells to study the mechanism of action and therapeutic effects of the DUBs inhibitors of interest, we verified whether this cell line indeed expresses the corresponding molecular targets, both at the mRNA and at the protein level. Of note, RT-qPCR and Western blotting confirmed the expression of UCHL5 and USP14 (targets of b-AP15), ADRM1 (target of RA190), PSDM14 (target of OPA), USP1 (target of SJB-019) and USP7 (target of P5091) in ALMC-2 cells, at the mRNA and protein level, respectively (**Fig. 10**).

Having verified the expression of the molecular targets in ALMC-2 cells, we then performed an initial screening of the potential therapeutic effects of the 5 small molecule DUBs inhibitors of interest against this cell line. The ALMC-2 cell line was exposed to 6 different doses of each drug (1:2 serial dilution, from 625 nM to 19 nM for b-AP15; from 1250 nM to 39 nM for RA190; from 62.5 μM to 1.95 μM for OPA; from 2000 nM to 62.5 nM for SJB03-19; from 50 μM to 1.56 μM for P5091) or DMSO as vehicle for 48 h. We first assessed the impact of the drug treatment on cellular metabolic activity, using a luciferase-based assay to quantify ATP levels as a measure of the metabolic activity of cells[155], as well as on cell viability, using the trypan blue exclusion test, which can distinguish between dead cells, which uptake trypan blue, from living cells, which do not[156].

All tested drugs led to a dose-dependent reduction of both cellular metabolic activity and viability. The half maximal inhibitory concentration (IC_{50}) of b-AP15, RA190, OPA, SJB3-019A and P5091 on ALMC-2 cells was 156 nM, 451 nM, 6.41 μM, 162.2 nM and 11.03 μM respectively, when considering the effect on metabolic activity (**Fig. 11A**), and 407.05 nM, 622.6 nM, 6.64 μM, 332.9 nM and 10.56 μM respectively, when considering the effect on cell viability with trypan blue exclusion test (**Fig. 11B**).

We then assessed whether the exposure of ALMC-2 cells to DUBs inhibitors can induce apoptosis. To this purpose, we exposed ALMC-2 to each of the five DUBs inhibitors, or to vehicle, and used the flow cytometry-based Annexin V and propidium iodide staining test quantify early apoptotic (Annexin V-positive and propidium iodide-negative) and late apoptotic cells (Annexin V-positive and propidium iodide-positive). Noteworthy, 48-hour exposure to all five tested drugs induced apoptosis in ALMC-2 cells, with an IC_{50} of 159 nM, 594 nM, 8.1 μM, 494 nM and 9.1 μM for b-AP15, RA190, OPA, SJB3-019A and P5091, respectively (**Fig. 11C**). Overall, these data indicate a therapeutic effect of the tested small molecule DUBs inhibitors against the human amyloidogenic plasma cell line ALMC-2.

Based on these observations and on drug availability, we decided to prioritize b-AP15 and RA190 drugs for further investigations.

Mechanism of action and therapeutic effect of b-AP15 in human plasma cell lines

Recent literature indicates that, upon inhibition of the deubiquitinating enzymes USP14 and UCHL5, exposure to b-AP15 triggers a progressive accumulation of intra-cytoplasmatic polyubiquitinated proteins, eventually resulting in apoptosis induction and cell death.

ALMC-2 cells were exposed to 100 nM of b-AP15 and analyzed at 1, 3 and 6 hours after treatment. At each analyzed time point, bortezomib (5 nM) and the vehicle DMSO were included as positive and negative control, respectively. Western blotting of cell lysates showed a substantial time-dependent accumulation of polyubiquitinated proteins in ALMC-2 cells treated with b-AP15, after 3 and 6 hours upon initial drug treatment compared to DMSO-treated cells used as a baseline (**Fig. 12A**). As expected, bortezomib led to accumulation of polyubiquitinated proteins at all analyzed time points, in line with its known potent effect of proteasome inhibition.

To further explore the mechanism of action of b-AP15 in human amyloidogenic plasma cells, we also investigated the expression levels of *HMOX-1* and *HSPA6*, genes related to oxidative and proteotoxic stress, respectively, upon treatment with b-AP15. We treated ALMC-2 cells with b-AP15 (2 μM) and DMSO, as vehicle, for a short exposure of 1, 3 and 6 hours. Using RT-qPCR, we

documented an early activation of *HMOX-1*, with a mild (1.44-fold), yet statistically significant induction, which was already noticeable after 1 hour of b-AP15 treatment (p=0.02), and became more pronounced at later time points, with peak levels after 3 hours (11.27-fold induction, p<0.0001) and still a significant upregulation after 6 hours (8.02-fold induction, p<0.0001). The magnitude of *HSPA6* activation was even higher, with a progressive, time-dependent upregulation of gene expression levels (1h: 1.33-, p=0.5267; 3h: 37.27-, p=0.0006; 6h: 110.45-fold induction, p=0.0128) (**Fig. 12B**). Collectively, these results show that exposure to b-AP15 leads to an early accumulation of polyubiquitinated proteins and a substantial induction of *HMOX-1* and *HSPA6* upregulation in ALMC-2 cells.

Next, we extended the study of b-AP15 therapeutic effect in tumoral plasma cells, comparing the effect of this drug to ALMC-2 and three additional human plasma cell lines, i.e. the AL amyloidosis cell lines ALMC-1, and two multiple myeloma plasma cell lines harboring the t(11;14) translocation, that is the KMS-12-BM and the U266B1 cell lines. The ALMC-1 is the sister cell line of ALMC-2, established from the bone marrow aspirate of the same patient, but at the time of AL amyloidosis diagnosis, when the patient was therapy-naïve[59]. The human multiple myeloma KMS-12-BM cell line was produced from the bone marrow of a 64-year-old woman with refractory, terminal non-secretory multiple myeloma after combination chemotherapy[148]. The U266B1 cell line was derived from the peripheral blood of a 53-year-old man with an IgEλ secreting, refractory terminal myeloma[149].

In analogy to what was done for ALMC-2, the cell line authentication of ALMC-1, KMS-12-BM and U266B1 was performed through a series of phenotypic and molecular investigations.

For ALMC-1 cell line, immunoglobulin light chain sequencing confirmed the presence of a λ light chain sequence derived from *IGLV6-57*03* and *IGLJ3*02* genes, with 100% identity with the published sequence for this cell line (and the corresponding AL amyloidosis patient) (**Fig. 13A**)[59].

Since for KMS-12-BM and U266B1 cell lines the original STR profile is known, whereas the nucleotide sequence of the expressed light chain was not available, we authenticated both multiple myeloma cell lines through STR profiling of 16 *loci* by multiplex PCR and capillary electrophoresis. The STR profiles obtained for KMS-12-BM and U266B1 showed a 100% match with the published STR profiles for these cell lines (**Fig. 13B**).

We then proceeded with the phenotypic characterization of these cell lines. May-Grünwald Giemsa staining confirmed a plasma cell morphology in all cases. Molecular cytogenetics using iFISH confirmed the presence of two copies of the X chromosome probe and lack of Y chromosome probe for ALMC-1 and KMS-12-BM cell lines and of one copy of each probe mapping to X and Y chromosomes for U266B1 cells (**Fig. 14A**), in line with the derivation of these cell lines[59,148,149].

Interphase FISH also confirmed the absence of co-localization of the two probes mapping to chromosomes 11 and 14 in ALMC-1 cells, thus indicating the absence of the t(11;14) translocation, while the co-localization of the two probes in KMS-12-BM and U266B1 cells confirmed the presence of this cytogenetic aberration (**Fig. 14B**), consistently with the known karyotype of these cell lines[59,148,149]. Immunophenotyping of ALMC-1 cells through multiparametric next-generation flow cytometry showed expression of CD138, CD45, CD38 and CD56 cell surface markers (MFI value: 33659, 33193, 9012 and 6379 respectively), dim expression of CD27 and CD117 (MFI value: 1162 and 1100), lacked CD19 and CD81 surface expression and confirmed the λ light chain restriction of this plasma cell line[59]. KMS-12-BM cells showed an immunophenotype congruent with a non-secretory MM cell line, expression of CD138, CD38, CD27 and CD81 cell surface markers (MFI value: 55403, 63984, 109283 and 8793, respectively), dim expression of CD45 and CD56 (MFI value: 1437 and 241) and lacked CD19 and CD117 surface expression. Lastly, U266B1 cell line immunophenotype showed restriction of λ light chains, expression of CD138, CD45, CD56, CD27 and CD38 cell surface markers (MFI value: 110317, 7165, 3131, 2708 and 1058, respectively), dim expression of CD19 (MFI value: 145) and lack of CD117 and CD81 expression (**Fig. 14C**). Finally, a PCR-based assay confirmed the negativity for *Mycoplasma spp* possible contamination in all tested human cell lines (**Fig. 14D**).

Next, we verified whether ALMC-1, KSM-12-BM and U266B1 cell lines express the molecular targets of the DUBs inhibitors of interest. Molecular investigations through RT-qPCR and Western blotting confirmed the presence of all six targets, at mRNA and protein level, respectively, in all analyzed human plasma cell lines. (**Fig. 15A**). Then, ALMC-1, ALMC-2, KSM-12-BM and U266B1 cell lines were exposed to 8 different doses of b-AP15 (according to a 1:2 serial dilution, from 2500 nM to 19 nM) or DMSO as vehicle control for 48 h. We then evaluated the impact of drug treatment on cellular metabolic activity, measuring ATP from metabolically active cells with the same luciferase-based assay previously employed[155], as well as on cell viability with the trypan blue exclusion test[156]. In all the examined human plasma cell lines, b-AP15 led to a similar dose-dependent reduction of both cellular metabolic activity and viability. When considering the effect on metabolic activity, the half maximal inhibitory concentration (IC_{50}) of b-AP15 for ALMC-1, ALMC-2, KSM-12-BM and U266B1 cells was 78.7 nM, 113 nM, 245.3 nM and 120.8 nM, respectively, while when considering the effect on cell viability, the IC50 was 97.5 nM, 210.9 nM, 254.9 nM and 129 nM, respectively (**Fig. 15B-C**).

Interaction between clonal plasma cells and bone marrow stromal cells activates cytokine secretion, which mediates paracrine growth of clonal plasma cells and defends them from drug-induced apoptosis[157]. Such cellular interactions cannot be appreciated in monoculture systems, and this

could lead to a possible overestimation of the therapeutic effects of an experimental drug. In order to account for the potential cytoprotective effect of bone marrow mesenchymal stromal cells, we exposed ALMC-2 cells to 625 and 312 nM of b-AP15 for 48 hours, in the presence or absence of primary, bone marrow-derived mesenchymal stromal cells (BM-MSCs). These cells were isolated from a healthy donor bone marrow aspirate through density gradient centrifugation, purification of plastic-adhering cells and subsequent expansion in culture. To confirm their identity, the obtained cells were subjected to a series of analyses to investigate key biologic features, including morphologic analysis, clonogenic capacity, immunophenotyping and analysis of their differentiation potential. Indeed, mesenchymal stromal cells showed a peculiar fibroblast-like shape (**Fig. 15D**). These cells expressed HLA-I, CD73, CD90 and CD105 cell surface markers and lacked the expression of HLA-II, CD31, CD34, CD45 and CD80, as assessed by flow cytometry (**Fig. 15D**). Also, the analysis of the differentiation potential confirmed that the obtained mesenchymal stromal cells could be successfully differentiated into osteocytes, as demonstrated by alkaline phosphatase activity and calcium deposition, and adipocytes, as shown by Oil Red O staining (**Fig. 15D**). Worth of note, exposure to b-AP15 caused a reduction in the metabolic activity of ALMC-2 cells to a similar extent regardless of whether mesenchymal stromal cells were present or not (**Fig. 15D**). Collectively, these results indicate that b-AP15 exerts a therapeutic effect against all tested human plasma cell lines, including two amyloidogenic cell lines and two myeloma cell lines bearing the t(11;14) translocation, and said therapeutic effect is retained also in the presence of mesenchymal stromal cells in the context of co-culture *in vitro* systems.

To further investigate the potential therapeutic effect of b-AP15 against AL amyloidosis, we decided to study primary, bone marrow-derived plasma cells from patients affected by AL amyloidosis. For this purpose, we enrolled 10 consecutive, treatment-naïve AL amyloidosis patients at diagnosis, for whom diagnostic leftover of bone marrow aspirate was available for plasma cell enrichment. The main clinical data of the enrolled patients are reported in **Table 1**. The median age was 63 years (range 54 – 86) and 7 out of 10 patients were males. The median percentage of bone marrow plasma cell infiltration was 11.5% (range 4.5 – 30%) and median involved free light chain levels and differential free light chain levels were 285.5 mg/l (range: 67.6 – 1000 mg/l) and 262.25 mg/l (range: 56.4 – 973.2 mg/l), respectively. The t(11;14) translocation was present in 5 out of 9 patients (cytogenetic analysis failed for AL Pt. 10), gain1q was present in 2 cases and no patient showed both these cytogenetic abnormalities.

In all cases, $CD138^+$ plasma cells were enriched using two consecutive rounds of immunomagnetic cell sorting starting from bone marrow mononuclear cells. This procedure resulted in an average percentage of $CD138^+$ positive fraction cells of 81.58% (range 68 – 94.6%) in the target, positive

fraction, as assessed by flow cytometry (**Fig. 4B**). An aliquot of the cells from the $CD138^+$ fraction stemming from the first round of isolation was used for molecular cytogenetic analyses, namely the investigation of the presence of the t(11;14) translocation and of gain 1q, which are associated to a lower response to bortezomib-based regimens[71,158,159] and to conventional dose melphalan[69], respectively.

Cells from both the $CD138^+$ positive fraction (hereafter referred to as $CD138^+$ cells), as well as from the $CD138^-$ fraction (hereafter referred to as $CD138^-$ cells), from each patient were cultured, separately, in the presence of b-AP15 at 75 nM and 150 nM or DMSO, as vehicle, for 24 hours. Of note, b-AP15 led to a dose-dependent reduction of metabolic activity in all 10 analyzed primary $CD138^+$ cells ($p< 0.0001$). In particular, 75 nM of b-AP15 led to an average reduction in metabolic activity of 66%, with all but 2 cases (AL Pt. 13 and AL Pt. 14) showing more than 45% decrease, whereas 150 nM of b-AP15 resulted in an average decrease of metabolic activity of 82%, with all but 2 cases (AL Pt. 13 and AL Pt. 17) showing more than 75% decrease compared to vehicle treatment (**Fig. 16A**). This effect was substantially attenuated in non-$CD138^+$ cells. Indeed, among primary, bone marrow-derived, matched $CD138^-$ cells, 75 nM of b-AP15 led to an average reduction of metabolic activity of 24%, whereas the 150 nM dose resulted in an average decrease of 47% ($p< 0.0001$, **Fig. 16B**). Peripheral blood mononuclear cells from 6 healthy subjects treated with increasing doses of b-AP15 (37.5, 75, 150 and 300 nM) were used as additional non-plasma cell controls. The exposure to 75 and 150 nM of b-AP15 led to an average 31% and 44% reduction of metabolic activity, respectively, while 300 nM, that is double the concentration of the drug which was employed with bone marrow cells, resulted in an average 50% reduction of metabolic activity ($p< 0.0001$, **Fig. 16C**).

Then, we investigated the potential therapeutic effect of b-AP15 in primary, bone marrow-derived plasma cells from three relapsed/refractory AL amyloidosis patients, all treated with cyclophosphamide, bortezomib and dexamethasone (CyBorD) (**Fig. 17**). Patient 14*, with renal AL(λ) amyloidosis, experienced a hematologic progression 18 months after having initially achieved a very good partial response to 6 cycles of CyBorD frontline therapy. Of interest, sensitivity to b-AP15 for this patient had been already performed before treatment initiation, at the time of diagnosis (AL Pt. 14, see **Fig. 16**). Patient 22, with renal and soft tissues AL (λ) amyloidosis, and patient 23, also with renal AL (λ) amyloidosis, failed to respond to 2 and 3 cycles of CyBorD as frontline therapy, respectively. In all cases a re-evaluation of the bone marrow aspirate was performed to evaluate eligibility to a clinical trial for a subsequent line of therapy.

Also in this subset of patients, b-AP15 led to a dose-dependent reduction of metabolic activity in the analyzed primary, bone marrow derived cells from the $CD138^+$ cells ($p < 0.0001$), with an

average reduction in metabolic activity at 75 nM and 150 nM of 91% and 80%, respectively (**Fig. 17A**). In the matched, bone marrow derived cells from the $CD138^-$ fraction, b-AP15 led to a dose-dependent reduction of metabolic activity that on average was 30% at 75 nM and 54% at 150 nM ($p = 0.0003$, **Fig- 17B**).

We then investigated if b-AP15 is able to induce an upregulation of the expression levels of *HMOX-1* and *HSPA6* also in primary $CD138^+$ cells, as we have reported in the case of ALMC-2 cells. For this purpose, we exposed primary, bone marrow-derived plasma cells from 3 AL amyloidosis patients (AL Pt. 24, 25 and 26) at diagnosis to b-AP15 (2 μM) and DMSO, as vehicle, for 1 or 3 hours. For two of these patients (AL Pt. 25 and 26), the disease-causing plasma cell clone was positive for the t(11;14) translocation. A mild (1.7-fold), yet statistically significant induction of *HMOX-1* was already noticeable after 1 hour of b-AP15 treatment ($p=0.0010$) only in AL Pt. 26, and became evident after 3 hours, particularly in AL Pt. 25 (118-fold induction, $p<0.0001$) but also in AL Pt. 24 (5.7-fold induction, $p=0.0005$) and AL Pt. 26 (3.2-fold induction, $p=0.0010$) (**Fig. 18A**). The magnitude of *HSPA6* activation was lower, with AL Pt. 24 showing a modest but statistically significant induction already after 1 hour (1h: 2.2-, $p=0.0040$; 3h: 1.8-fold induction, $p=0.0254$) and AL Pt. 25 showing a remarkable upregulation only after 3h (17.3-fold induction, $p=0.0002$), while AL Pt. 26 no *HSPA6* activation was detected (**Fig. 18B**). Collectively, these results confirm the increased sensitivity of primary, bone marrow derived plasma cells from patients affected by AL amyloidosis to b-AP15, independently from the t(11;14) translocational status, both at diagnosis and in the relapsed/refractory setting.

Mechanism of action and therapeutic effect of RA190 in AL amyloidosis plasma cells

Previous studies showed that the small molecule named RA190 inhibits ADRM1 (**Fig. 3B**), entailing a progressive accumulation of intra-cytoplasmatic polyubiquitinated proteins and eventually resulting in apoptosis induction and cell death in different types of cancer cells, including multiple myeloma.

ALMC-2 cells were exposed to 300 nM of RA190 and analyzed at 1, 3 and 6 hours after treatment. At each analyzed time point, bortezomib (5 nM) and the vehicle DMSO was included as positive and negative control, respectively. Western blotting of cell lysates showed a time-dependent accumulation of polyubiquitinated proteins in ALMC-2 cells treated with RA190, in particular after 6 hours upon initial drug treatment compared to DMSO-treated cells used as a baseline (**Fig. 19**). As expected, bortezomib led to accumulation of polyubiquitinated proteins at all analyzed time points, in line with its known potent effect of proteasome inhibition.

As performed with b-AP15, to further explore the potential therapeutic effect of RA190 against AL amyloidosis, we studied primary, BM-derived plasma cells from 10 treatment-naïve AL amyloidosis patients at diagnosis.

The main clinical characteristics of the enrolled patients are reported in **Table 1**. The median age was 64 years (range 56 – 83) and 7 out of 10 patients were males. The median percentage of bone marrow plasma cell infiltration was 11% (range 3 – 15%) and median involved free light chain levels and differential free light chain levels were 233.5 mg/l (range: 25.3 – 560 mg/l) and 216.22 mg/l (range: 14.7 – 552.9 mg/l), respectively. The t(11;14) translocation was present in 5 out 9 patients (cytogenetic analysis failed for AL Pt. 15), while gain1q was present only in one case (AL Pt. 07) and no patient showed both these cytogenetic abnormalities. In all cases, $CD138^+$ plasma cells were enriched using two consecutive rounds of immunomagnetic cell sorting starting from bone marrow mononuclear cells, resulting in an average percentage of $CD138^+$ cells of 80.2% (range 61.6 – 92.1%) in the target, positive fraction, as assessed by flow cytometry (**Fig. 4B**).

Cells from both the $CD138^+$ positive fraction, as well as from the $CD138^-$ fraction from each patient were cultured, separately, in the presence of RA190 at 200 nM and 600 nM or DMSO, as vehicle, for 48 hours. Of note, RA190 led to a dose-dependent reduction of metabolic activity in all 10 analyzed primary $CD138^+$ cells ($p< 0.0001$). In particular, 200 nM of RA190 led to an average reduction in metabolic activity of 75%, with all but 2 cases (AL Pt. 17 and AL Pt. 27) showing more than 70% decrease, whereas 600 nM of RA190 resulted in an average decrease of metabolic activity of 89%, with all but one cases (AL Pt. 27) showing more than 80% decrease compared to vehicle treatment **(Fig. 20A)**. This effect was partially attenuated in cells from the $CD138^-$ fraction. Indeed, among primary, bone marrow-derived, matched $CD138^-$ cells, 200 nM of RA190 led to an average reduction of metabolic activity of 47%, whereas the 600 nM dose resulted in an average decrease of 73% ($p< 0.0001$, **Fig. 20B**). Peripheral blood mononuclear cells from 6 healthy subjects treated with increasing doses of RA190 (100, 200, 600 and 1200 nM) were used as additional, non-plasma cell controls. The exposure to 200 and 600 nM of RA190 led to an average 11% and 36% reduction of metabolic activity, respectively, while 1200 nM, that is double the concentration of drug which was employed with bone marrow cells, resulted in an average 82% reduction of metabolic activity ($p< 0.0001$, F**ig. 20C**). Finally, we investigated the potential therapeutic effect of RA190 in primary, bone marrow-derived plasma cells from a refractory AL amyloidosis patient, namely AL Pt. 22, treated with cyclophosphamide, bortezomib and dexamethasone, that was in parallel exposed to b-AP15 (**Fig. 20D-E**). In the analyzed primary, bone marrow derived cells from the $CD138^+$ cells of AL Pt. 22, RA190 led to a slight reduction (11%) of metabolic activity at 200 nM, while a conspicuous reduction (95%) was detected at 600 nM concentration. In the matched,

bone marrow derived cells from the $CD138^-$ fraction, RA190 did not lead to any impairment of metabolic activity at 200 nM, whereas a reduction in metabolic activity of 20% was present at 600 nM.

Collectively, these results confirm the increased sensitivity of primary, bone marrow derived plasma cells from patients affected by AL amyloidosis to RA190, independently from the t(11;14) translocational status.

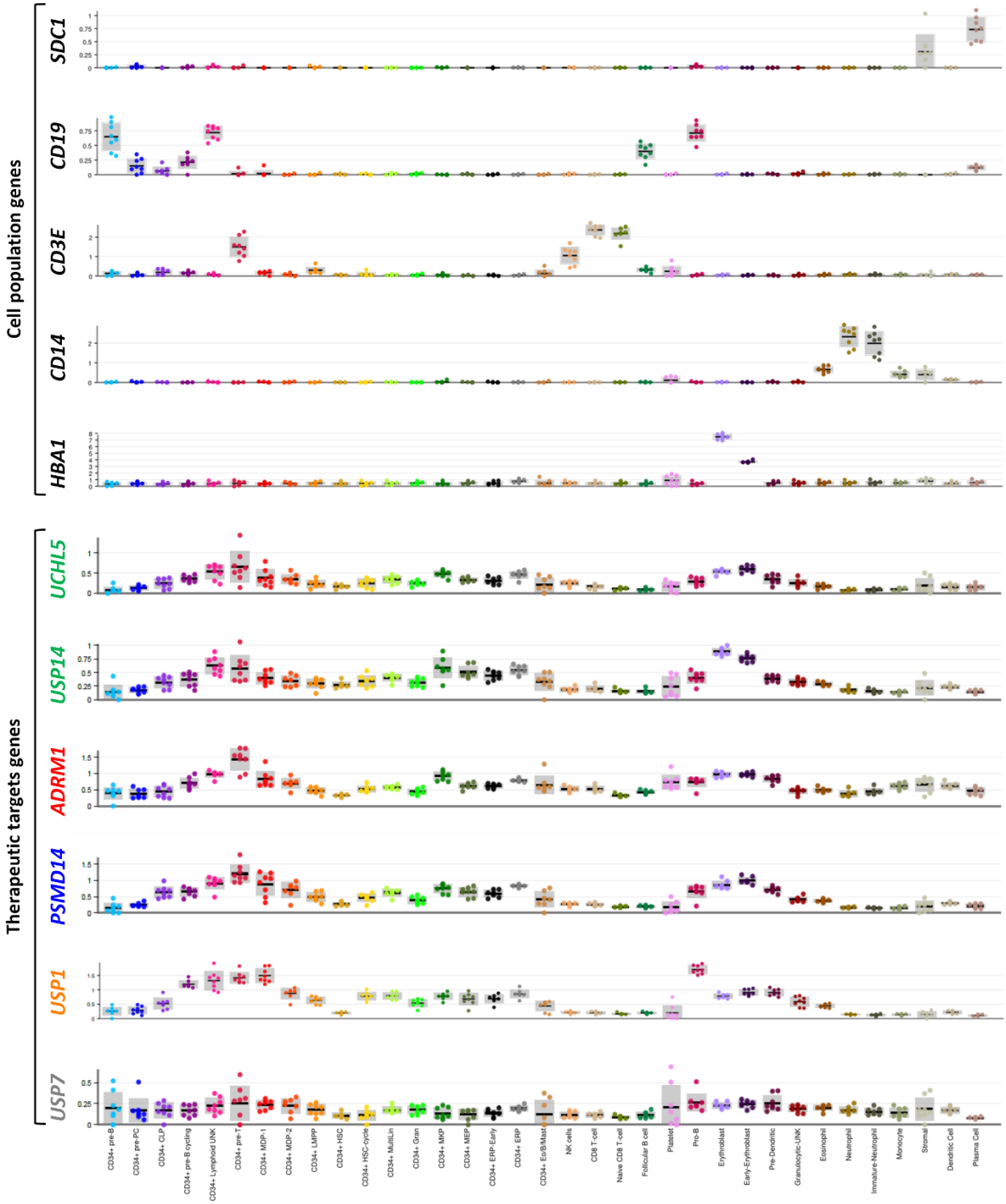

Figure 5: mRNA expression of therapeutic targets of interest in human bone marrow cellular compartments

Expression levels of deubiquitinating enzymes or ubiquitin receptors which are the molecular targets of the drugs investigated within this study (*UCHL5, USP14,* targeted by b-AP15, *ADRM1,* targeted by RA190, *PSMD14,* targeted by OPA, *USP1*, targeted by SJB3-019A, and *USP7*, targeted by P5091) and cell population marker genes (*SDC1, CD19, CD3E, CD14, HBA1*) in 35 bone-marrow derived cell populations of 8 healthy donors. Data are derived from the Human Cell Atlas[139].

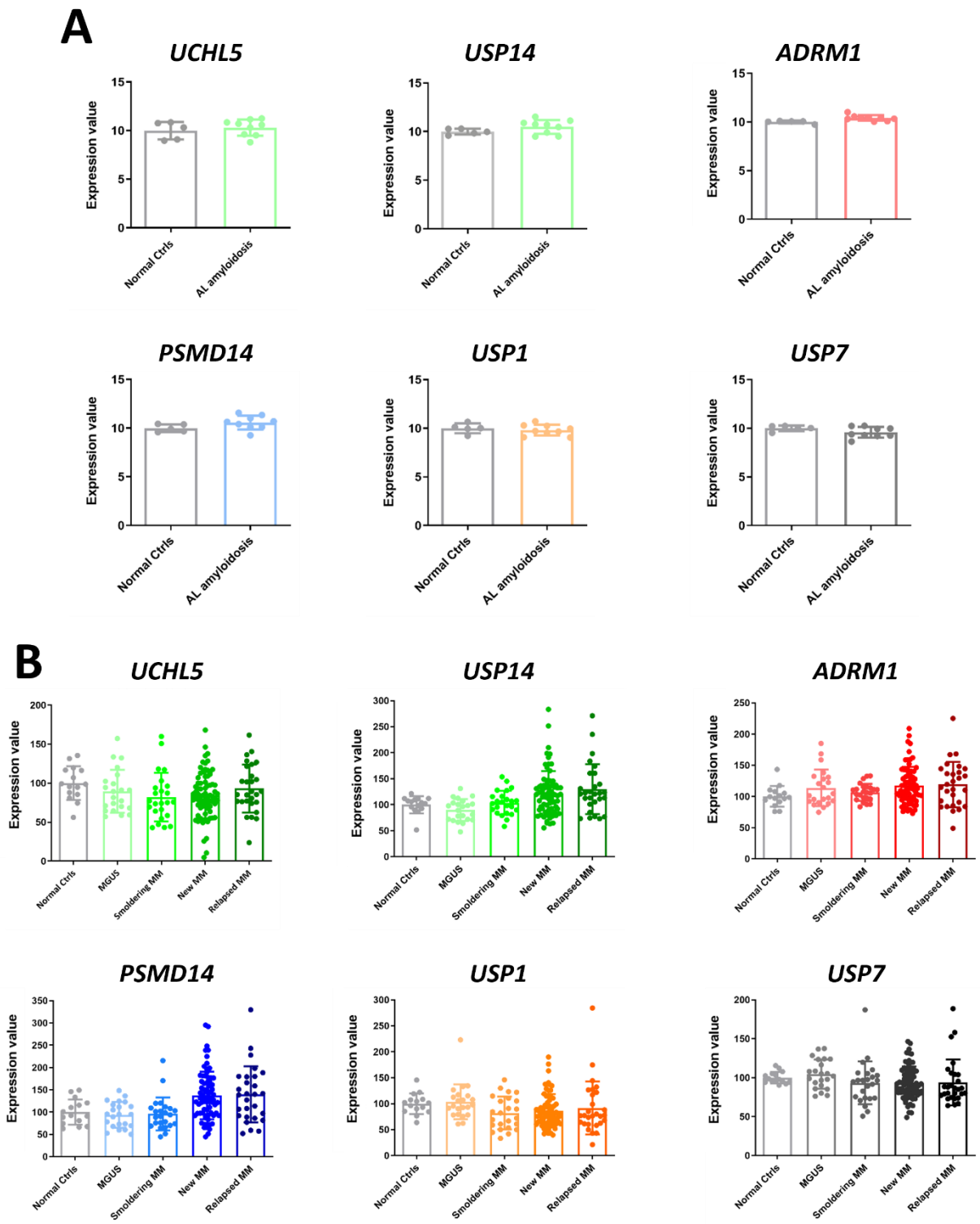

Figure 6: mRNA expression of therapeutic targets of interest in plasma cell dyscrasias
Expression levels of deubiquitinating enzymes or ubiquitin receptors which are the molecular targets of the drugs investigated within this study (*UCHL5, USP14,* targeted by b-AP15, *ADRM1,* targeted by RA190, *PSMD14,* targeted by OPA, *USP1*, targeted by SJB3-019A, and *USP7*, targeted by P5091) in 9 AL amyloidosis patients and 5 healthy donors collected from the AL amyloidosis dataset (GSE73040) [73] **(A)** or in 147 patients with plasma cell dyscrasias and 15 healthy donors collected from the MM dataset (GSE6477) [142] **(B)** of the Gene Expression Omnibus (GEO) portal (each dot denotes one subject, bar denotes mean and error bar denotes standard deviation). Ctrl: controls; MGUS: monoclonal gammopathy of uncertain significance; MM: multiple myeloma.

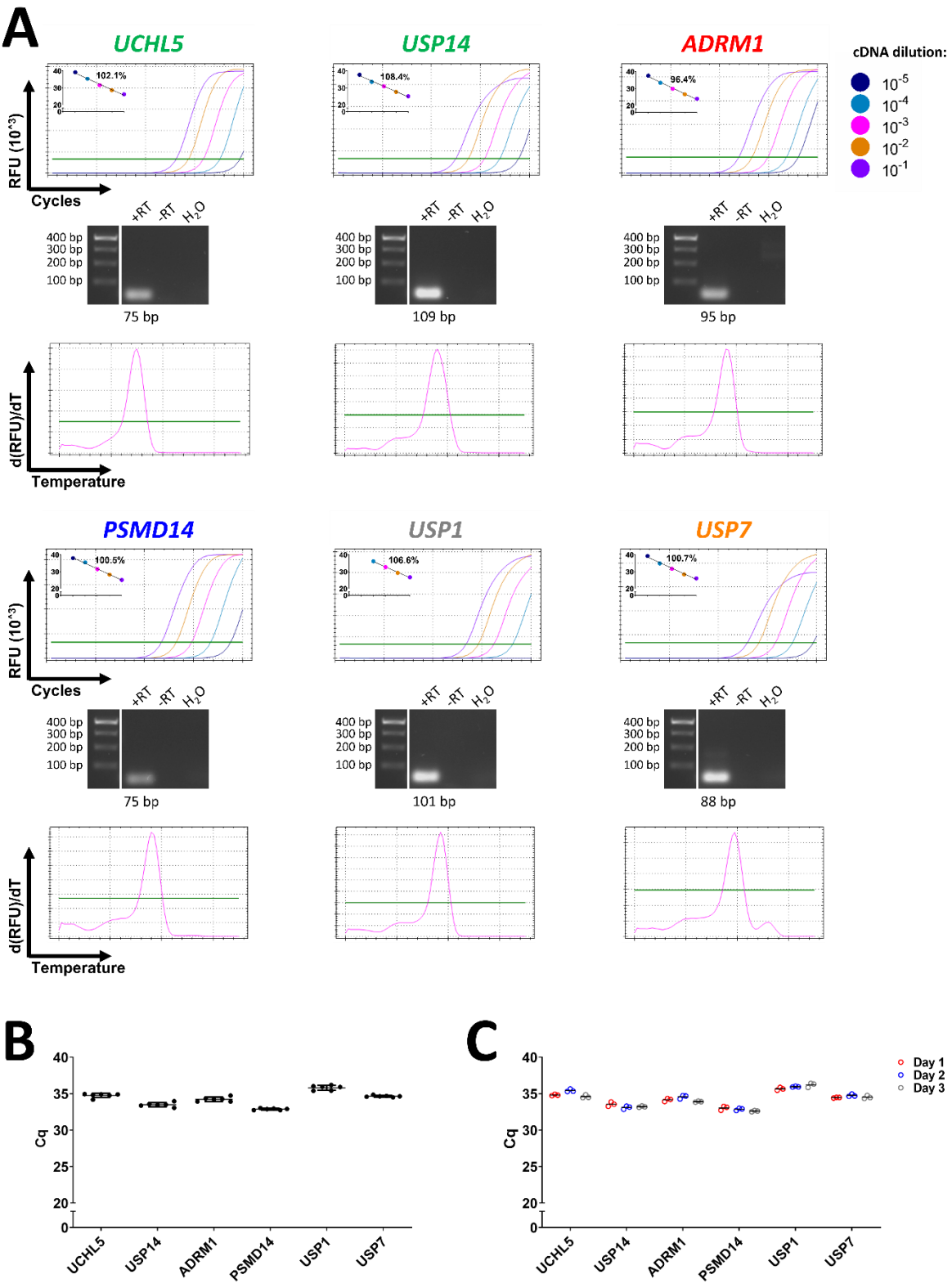

Figure 7: Technical validation of RTq-PCR assays for molecular targets of interest

(**A**) For each molecular targets of interest, from top to bottom: a plot showing the relative fluorescence unit (RFU 10^3) over cycle for the different cDNA dilutions (color-coded as in the legend), with in the left corner a plot of the correlation of cDNA dilution and C_q indicating the PCR efficiency; an agarose gel for ALMC-2 RNA retrotranscribed with or without retrotranscriptase (+RT and –RT, respectively) (n bp below each gel

indicates the expected base pair amplicon size); plot of the first negative derivative of RFU (d(RFU)/dT) over different temperature of the melting curve analysis. Dynamic range: RFU is equal to 7; melting curve: -d(RFU)/dT *UCHL5* (3), *PSMD14* (2700), *USP14*, *ADRM1*, *USP1* and *USP7* (3000). (**B**) Cq values of six technical replicates, represented by dots, for each molecular targets gene obtained within one single run. (**C**) Cq values of three technical replicates, represented by open circles, for each molecular targets gene obtained in three different runs in separate days.

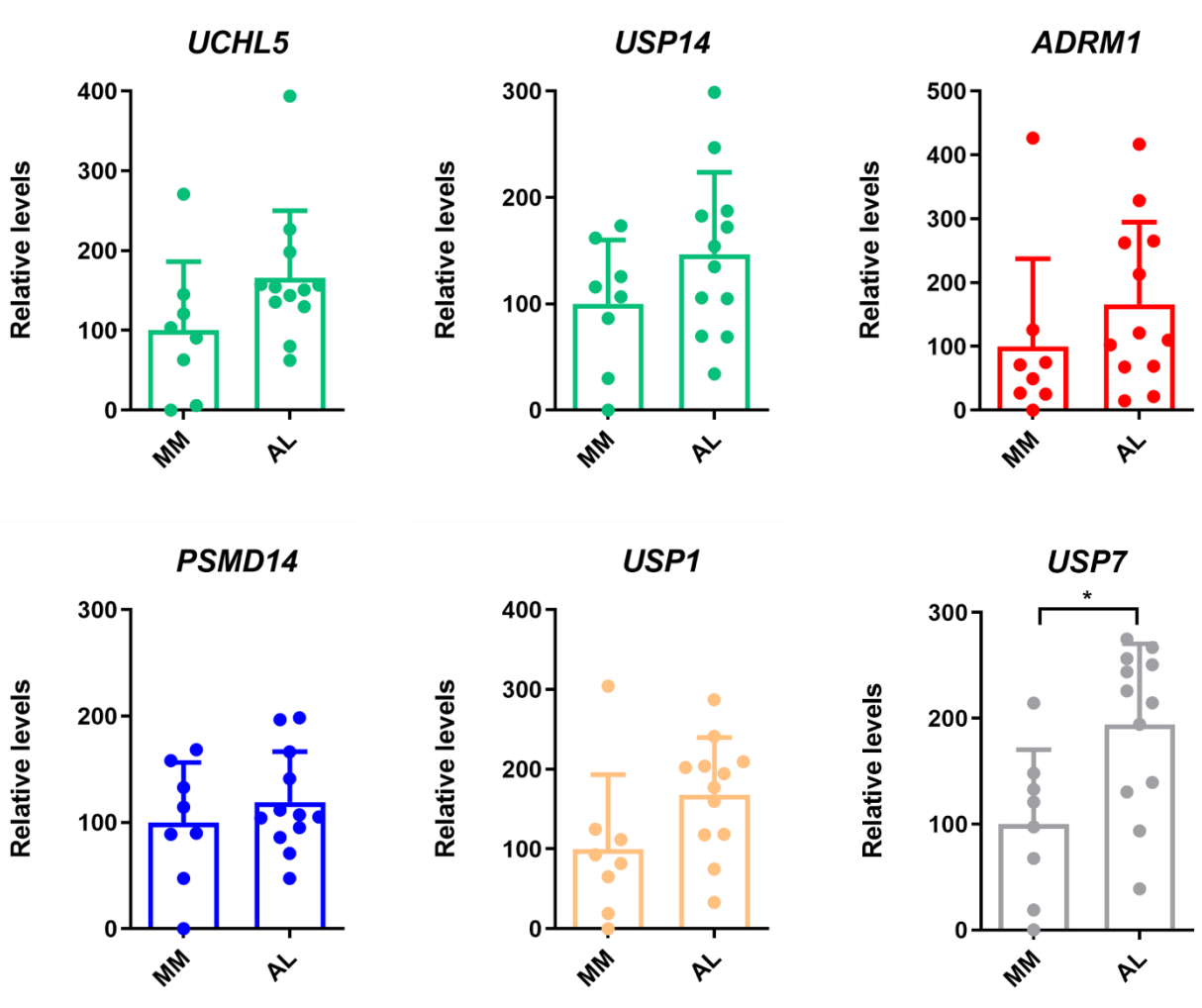

Figure 8: mRNA expression of therapeutic targets of interest in primary bone marrow-derived plasma cells

Expression levels of deubiquitinating enzymes or ubiquitin receptors which are the molecular targets of the drugs investigated within this study (*UCHL5, USP14,* targeted by b-AP15, *ADRM1,* targeted by RA190, *PSMD14,* targeted by OPA, *USP1*, targeted by SJB3-019A, and *USP7*, targeted by P5091) in primary, bone marrow derived cells from the $CD138^{+}$ fraction from 8 multiple myeloma patients (MM) and 12 AL amyloidosis patients (AL), as assessed by RT-qPCR (patients included in this analysis correspond to the patients AL Pt. 01 - AL Pt. 12 and MM Pt. 01 - MM Pt. 08 listed in **Table 1**). *ACTR3*, *ALG9* and *ESD* were used as normalizing genes. Each dot denotes one subject, bar denotes mean and error bar denotes standard deviation. Statistical significance was determined by two-tailed unpaired t-test *: p value = 0.0122.

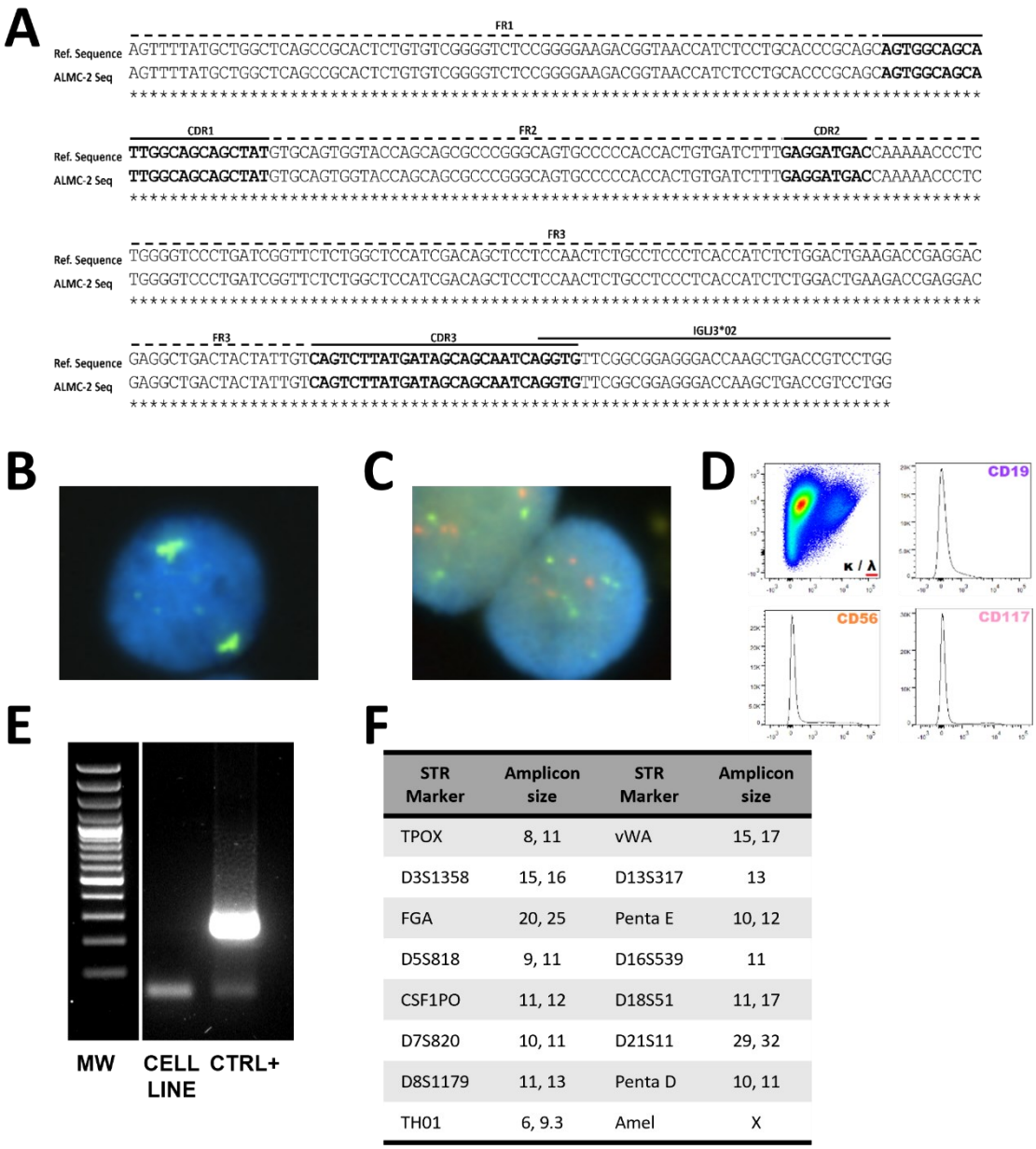

STR Marker	Amplicon size	STR Marker	Amplicon size
TPOX	8, 11	vWA	15, 17
D3S1358	15, 16	D13S317	13
FGA	20, 25	Penta E	10, 12
D5S818	9, 11	D16S539	11
CSF1PO	11, 12	D18S51	11, 17
D7S820	10, 11	D21S11	29, 32
D8S1179	11, 13	Penta D	10, 11
TH01	6, 9.3	Amel	X

Figure 9: ALMC-2 cell line authentication and characterization
(A) ALMC-2 *IGLV* gene sequences as determined by Sanger sequencing; the obtained sequence shows 100% identity with the published sequence of this cell line (Ref. sequence)[59]. FR: frame work region; CDR: complementarity-determining region. **(B)** Gender was assessed through interphase FISH with LSI CEP (DXZ1) Spectrum Green / CEP (DYZ3) Spectrum Orange Probe, Vysis-Abbott (green signal for X chromosome, red signal for Y chromosome). **(C)** The presence of translocation t(11;14) was verified through interphase FISH with LSI *CCND1*/*IGH* XT Dual Fusion FISH Probe Kit, Vysis Abbott (green signal for *IGH* on chromosome 14, red signal for *CCND1* on chromosome 11). **(D)** Immunophenotype of ALMC-2 cell line was performed by multiparametric flow cytometry. **(E)** Short tandem repeat (STR) profiling of ALMC-2 cell line used in this study. The uniqueness of the STR profile was verified with CLASTR. Amplicon size is expressed as number of repeats. (**F)** PCR amplification of genomic material from *Mycoplasma spp.* in conditioned medium of ALMC-2 cell line. A positive control (CTRL +) is included. MW: molecular weight. White lanes indicate non-consecutive lanes of agarose gel.

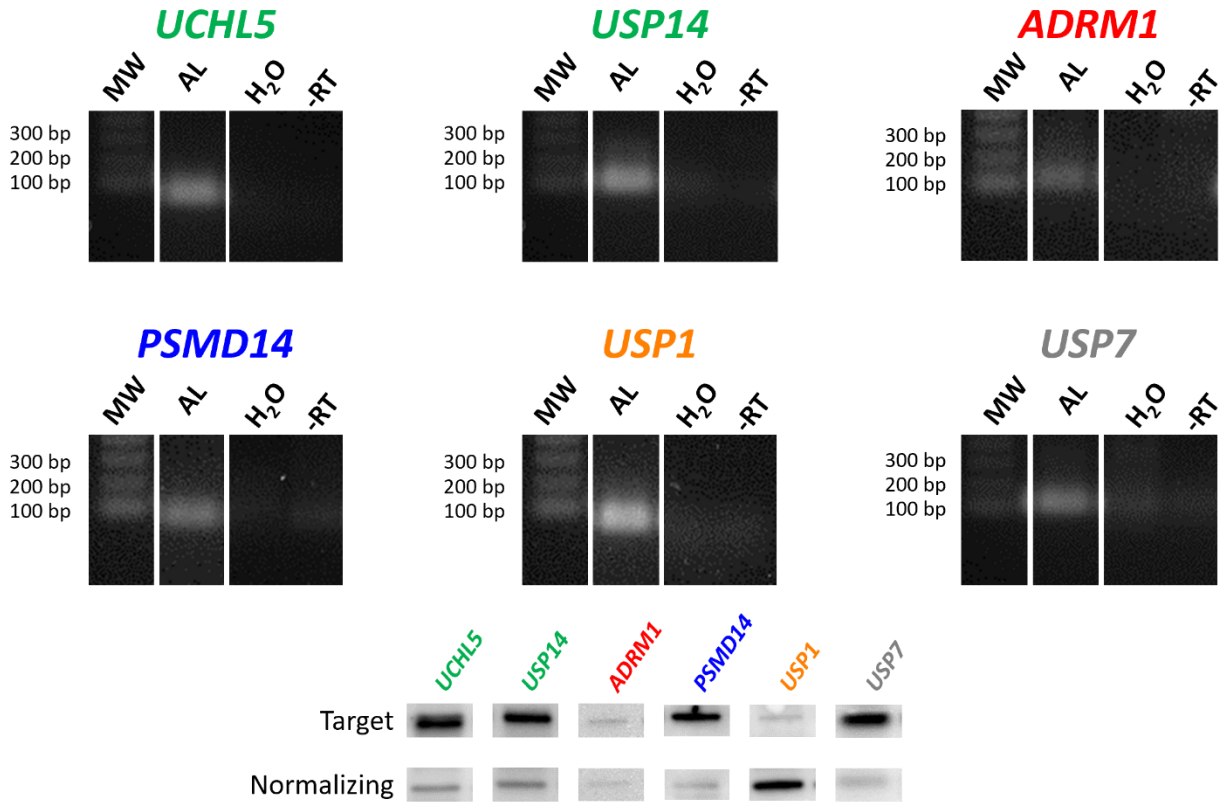

Figure 10: Expression of therapeutic targets of interest in ALMC-2 cell line.
Expression of deubiquitinating enzymes or ubiquitin receptors which are the molecular targets of the drugs investigated within this study (*UCHL5, USP14,* targeted by b-AP15, *ADRM1,* targeted by RA190, *PSMD14,* targeted by OPA, *USP1*, targeted by SJB3-019A, and *USP7*, targeted by P5091) in ALMC-2 cell line (AL) was verified both at mRNA level by RT-qPCR (upper lane) and at protein level by Western Blotting (lower lane). No cDNA (H_2O) and no reverse transcriptase (-RT) were used as negative controls in the RT-qPCR experiments. MW: molecular weight. For Western blotting, the normalizing gene used was β-actin in all cases, except for ADRM1, normalized with GAPDH.

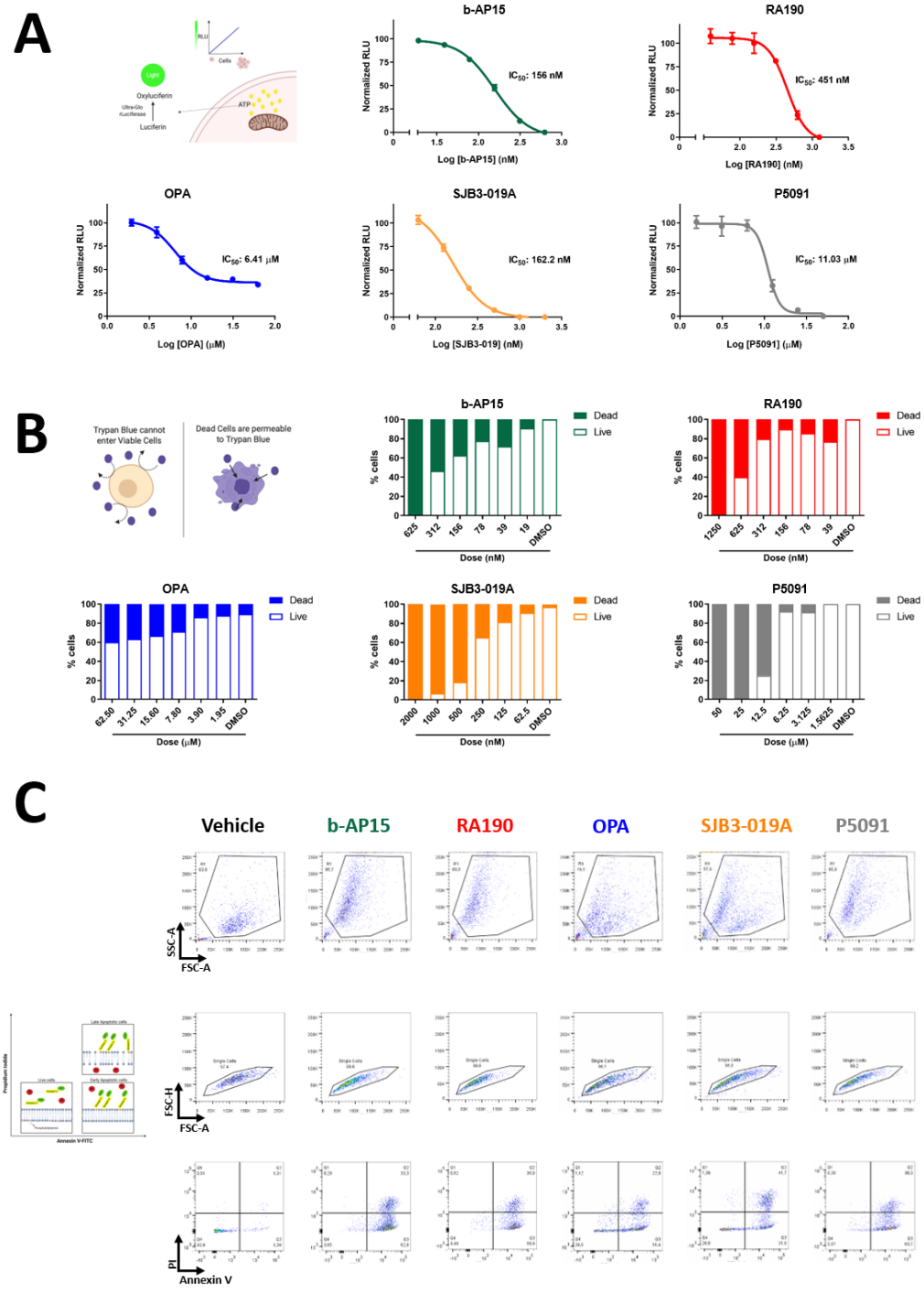

Figure 11: Therapeutic effect of DUBs inhibitors of interest in ALMC-2 cell line
(A) Graphs showing a dose-dependent impairment of cell metabolism induced by different DUBs inhibitors in ALMC-2 cell line, after 48h of treatment, as assessed by the CellTiter-Glo assay. In each experiment, the signal obtained with vehicle-treated cells was set as 100% for normalization. (**B)** Histograms showing a dose-dependent impairment of cell viability induced after 48h of DUBs inhibitors exposure in ALMC-2 cell line, as assessed by the Trypan Blue exclusion assay. **(C)** ALMC-2 cells were treated with DUBs inhibitors or DMSO, as vehicle, for 48h, followed by Annexin V/ propidium iodide (PI) staining and analysis of apoptosis using flow cytometry. For A and B, results are from three independent experiments. For C, results are from a representative dose for each drug (b-AP15: 312 nM; RA190: 625 nM; OPA: 15.6 µM; SJB3-019A: 500 nM; P5091: 25 µM).

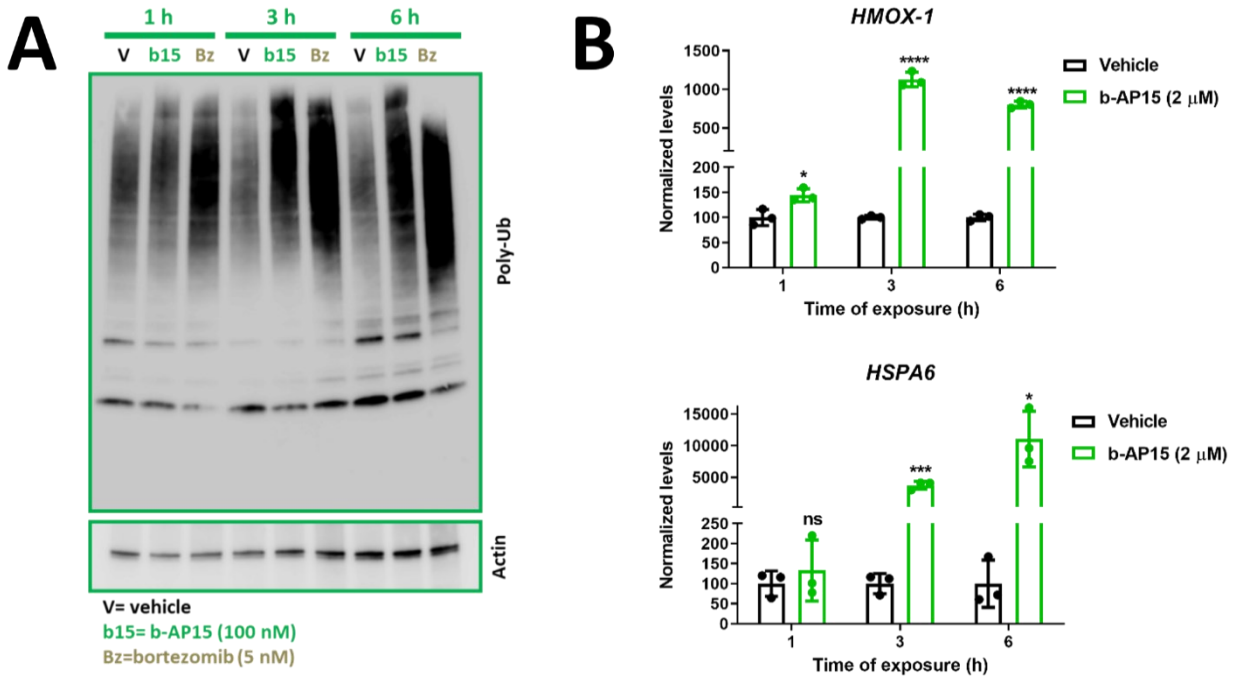

Figure 12: Mechanism of action of b-AP15 in ALMC-2

(A) Time-dependent accumulation of polyubiquitinated proteins in ALMC-2 cells exposed to b-AP15 (b15) for the indicated times, in hours (h). Bortezomib (Bz) and DMSO (vehicle, V) were used as positive and negative controls, respectively. **(B)** ALMC-2 cells were exposed to b-AP15 (2 μM) or DMSO, for 1, 3 and 6 h and the expression levels of *HMOX-1*, *HSPA6* and *GAPD*, used as control, were quantified by RT-qPCR. At each time point, gene expression levels of vehicle-treated cells were set as 100% for normalization purposes. Statistical significance was determined by two-tailed unpaired t-test – *HMOX-1* *: p value = 0.0200, ****: p value <0.0001; *HSPA6*: *: p value = 0.0128, ***: p value = 0.0006.

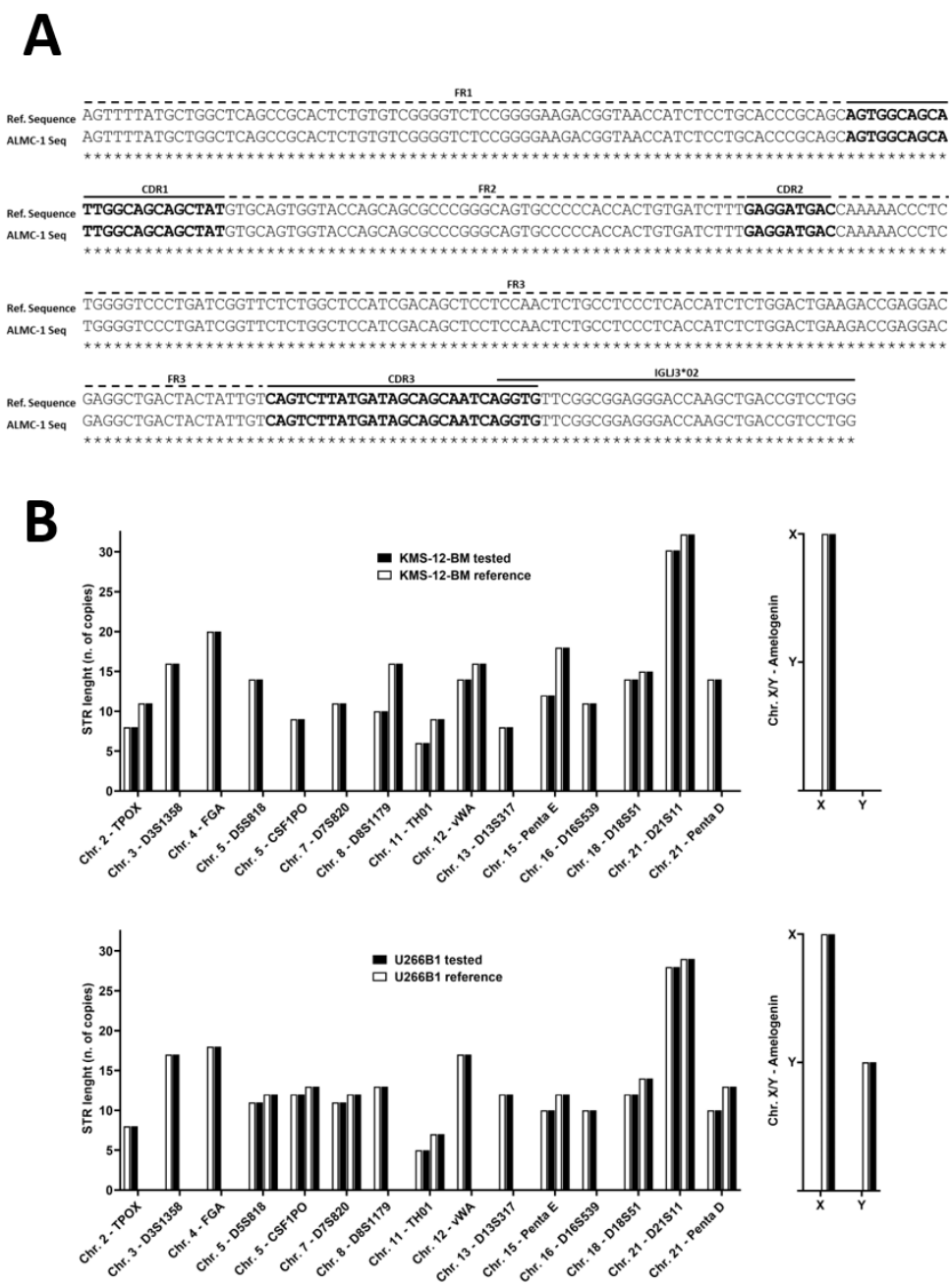

Figure 13: Authentication of ALMC-1, KMS-12-BM and U266B1 human plasma cell lines
(A) ALMC-1 *IGLV* gene sequences as determined by Sanger sequencing; the obtained sequence shows 100% identity with the published sequence of this cell line (Ref. sequence)[59]. FR: frame work region; CDR: complementarity-determining region. **(B)** Short tandem repeat (STR) profiling of KMS-12-BM and U266B1 used in this study (KMS-12-BM and U266B1 tested), in comparison with reference STR profile for these cell line (according to Cosmic-CLP; DSMZ; JCRB, labeled as KMS-12-BM reference; according to ATCC; CCRID; Cosmic-CLP; DSMZ; ECACC; Genomics_Center_BCF_Technion, labeled as U266B1 reference). Chr.: chromosome.

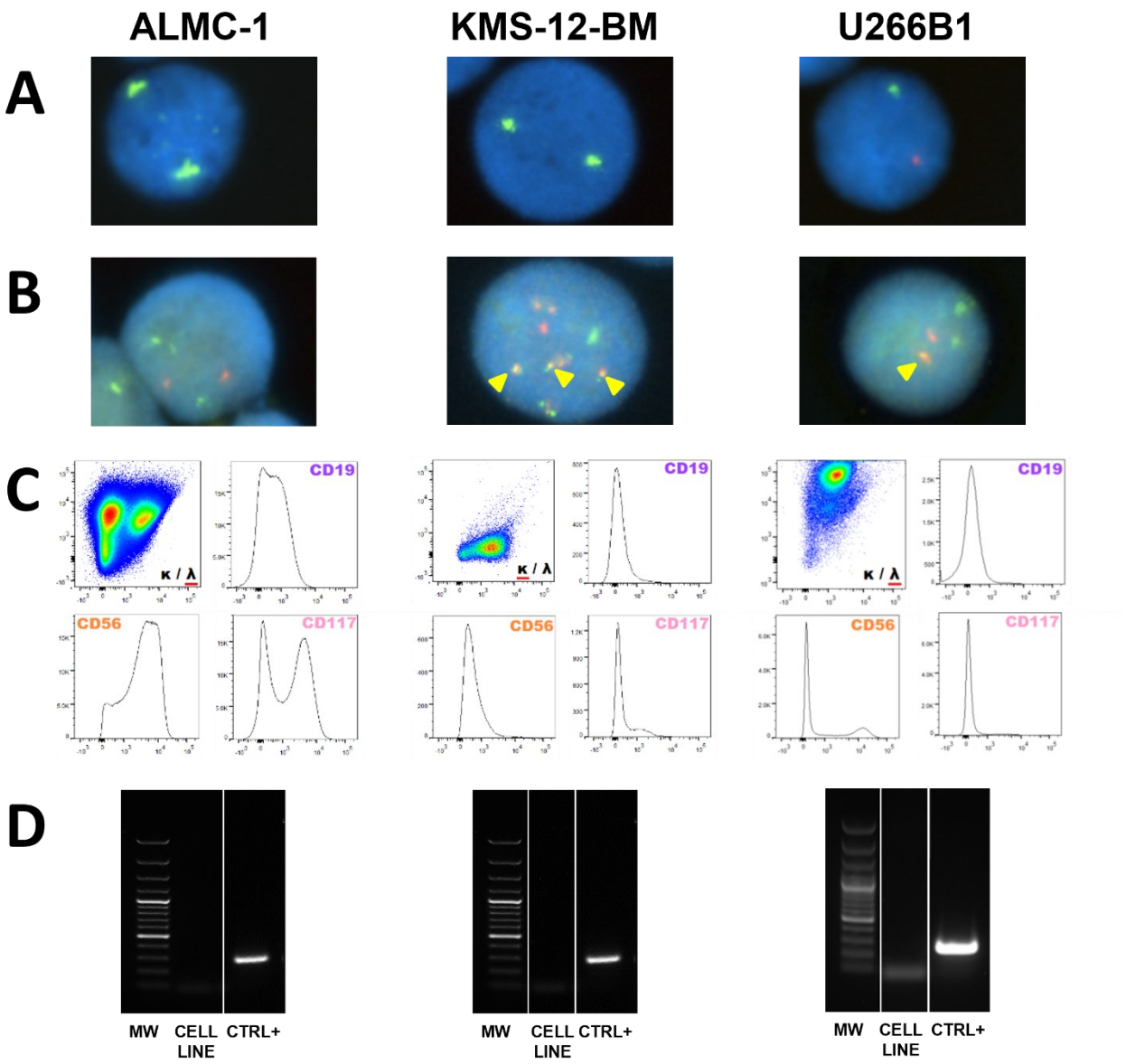

Figure 14: ALMC-1, KMS-12-BM and U266B1 cell lines characterization
(A) Gender was assessed through interphase FISH with LSI CEP (DXZ1) Spectrum Green / CEP (DYZ3) Spectrum Orange Probe, Vysis-Abbott (green signal for X chromosome, red signal for Y chromosome). **(B)** The presence of translocation t(11;14) was verified through interphase FISH with LSI *CCND1*/*IGH* XT Dual Fusion FISH Probe Kit, Vysis Abbott (green signal for *IGH* on chromosome 14, red signal for *CCND1* on chromosome 11). Yellow arrow head identified the t(11;14) in U266B1 and KMS-12-BM. **(C)** Immunophenotype of cell lines was performed by multiparametric flow cytometry. **(D)** PCR amplification of genomic material from *Mycoplasma spp.* in conditioned medium of cell lines. A positive control (CTRL +) is included. MW: molecular weight. White lanes indicate non-consecutive lanes of agarose gel.

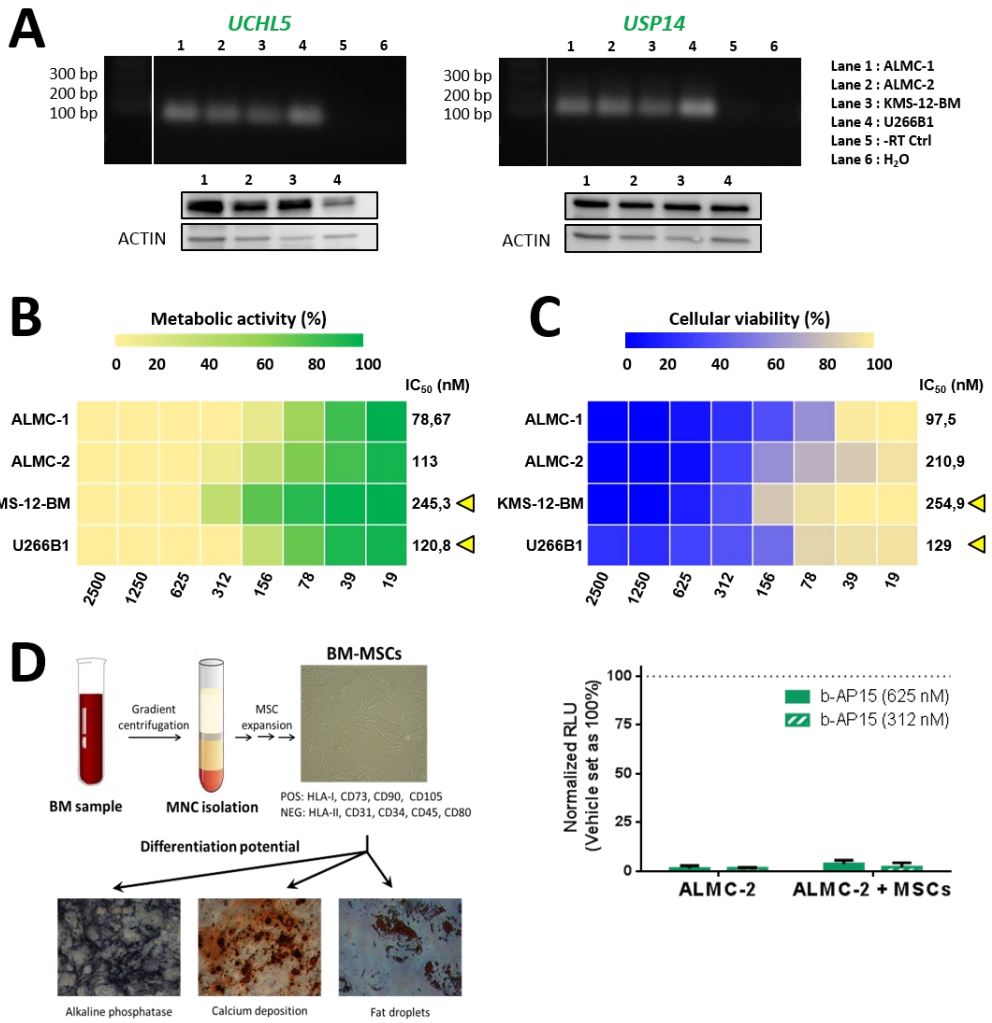

Figure 15: Expression and therapeutic effect of b-AP15 on AL and MM cell lines and sensitivity to b-AP15 of ALMC-2 cells with or without mesenchymal stromal cells

(A) Expression of deubiquitinating enzymes *UCHL5* and *USP14,* targeted by b-AP15, in the four cell lines used in this study was verified both at mRNA level by RT-qPCR (upper lane) and at protein level by Western Blotting (lower lane). No cDNA (H_2O) and no reverse transcriptase (-RT Ctrl) were used as negative controls in the RT-qPCR experiments. **(B)** Heat map showing a dose-dependent impairment of cell metabolism induced by b-AP15 in AL (ALMC-1 and ALMC-2) and MM (KMS-12-BM and U266B1) cell lines, after 48h of treatment, as assessed by the CellTiter-Glo assay. For each cell line, the signal obtained with vehicle-treated cells was set as 100% for normalization. IC_{50} was obtained from 3 independent experiments, in which each drug dose was investigated in triplicate. **(C)** Heat map showing a dose-dependent impairment of cell viability induced after 48h of b-AP15 exposure in AL (ALMC-1 and ALMC-2) and MM (KMS-12-BM and U266B1) cell lines, as assessed by the Trypan Blue exclusion assay. In B and C, yellow arrow heads indicate cell lines harboring the t(11;14) translocation. **(D)** In the left panel, scheme of derivation of primary BM-derived mesenchymal stromal cells (BM-MSCs) using gradient centrifugation, for mononuclear cell (MNC) isolation, followed by MSCs purification and expansion. The characterization of MSCs was performed by cell morphology, multiparametric immunophenotyping (positive, POS, and negative, NEG, antigens are listed above) and immunohistochemistry to define the differentiation potential towards osteocytes and adipocytes. In the right panel, ALMC-2 cells were treated alone and in co-culture with MSCs with the indicated doses of b-AP15 or DMSO, as vehicle, for 48h and cell metabolic activity was assessed using the CellTiter Glo assay.

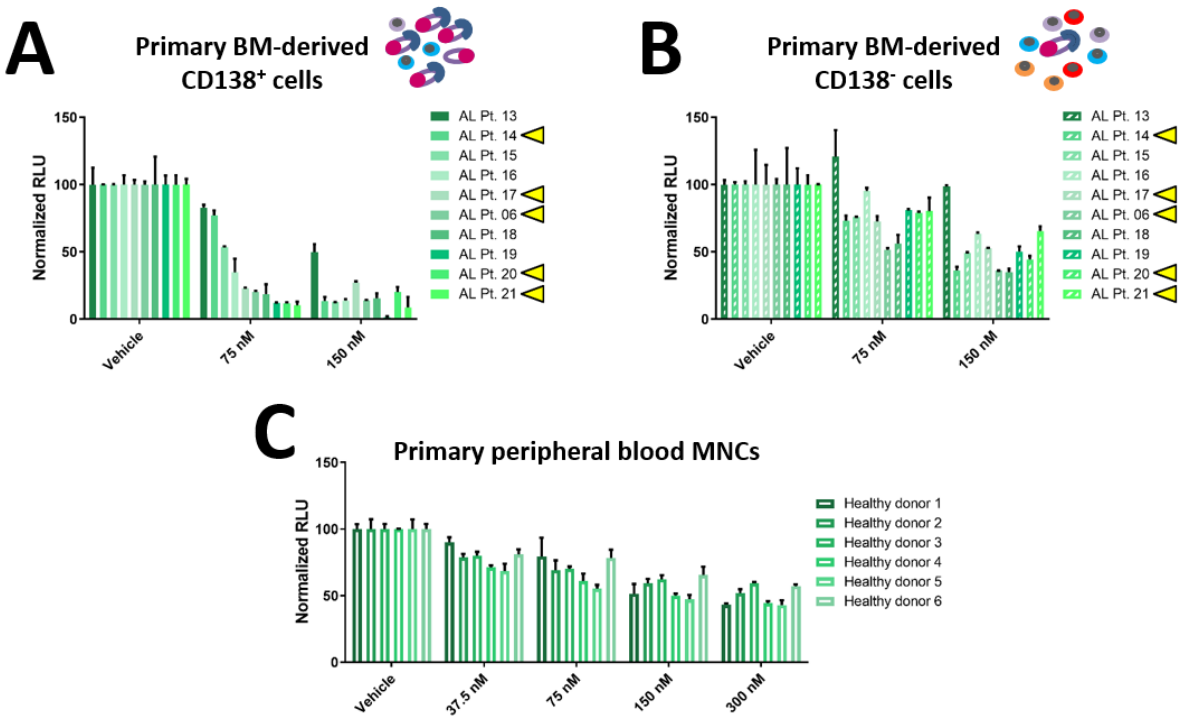

Figure 16: Therapeutic effect of b-AP15 on primary, patient-derived amyloidogenic plasma cells
Primary bone marrow-derived $CD138^+$ **(A)** or $CD138^-$ cells **(B)** of 10 AL amyloidosis patients were treated with the indicated doses of b-AP15 or DMSO, as vehicle, for 24 h and cell metabolic activity was assessed using the CellTiter Glo assay (for each patient, the signal obtained with vehicle-treated cells was set as 100% for normalization; mean ± SD, n=2). **(C)** Primary, peripheral blood mononuclear cells (PB-MNCs) from 6 healthy subjects were treated with the indicated doses of b-AP15 or DMSO, as vehicle, for 24 h and cell metabolic activity was assessed using the CellTiter Glo assay (for each patient, the signal obtained with vehicle-treated cells was set as 100% for normalization, mean ± SD, n=3). In A and B, yellow arrow heads indicate patients with a plasma cell clone harboring the t(11;14) translocation. Patient numbering corresponds to the patient ID in **Table 1**.

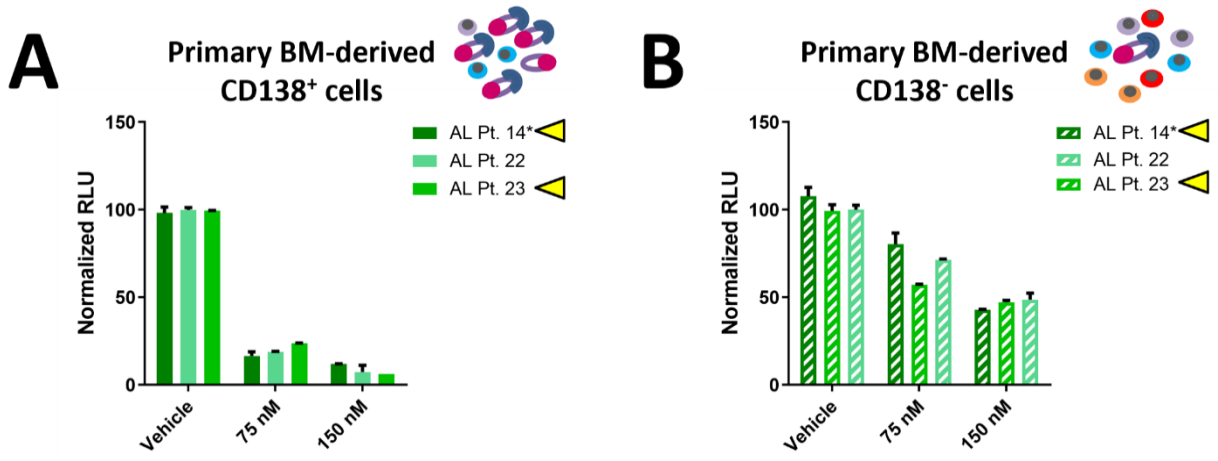

Figure 17: Therapeutic effect of b-AP15 on primary, patient-derived, bone marrow plasma cells from relapsed/refractory AL amyloidosis patients

Primary bone marrow-derived $CD138^+$ **(A)** or $CD138^-$ cells **(B)** of 3 relapsed/refractory AL amyloidosis patients were treated with the indicated doses of b-AP15 or DMSO, as vehicle, for 24 h and cell metabolic activity was assessed using the CellTiter Glo assay (for each patient, the signal obtained with vehicle-treated cells was set as 100% for normalization; mean ± SD, n=2). Yellow arrow heads indicate patients with a plasma cell clone harboring the t(11;14) translocation. Patient numbering corresponds to the patient ID in **Table 1**. The asterisk (*) indicates the patient at the time of disease relapse.

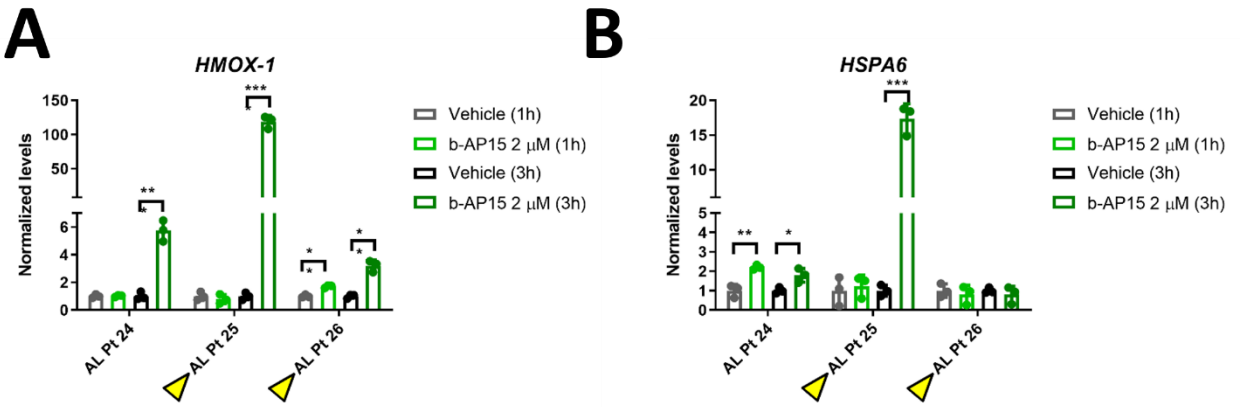

Figure 18: Mechanism of action of b-AP15 primary, patient-derived amyloidogenic plasma cells
Primary bone marrow-derived CD138^{+} cells of 3 AL amyloidosis patients were exposed to b-AP15 (2 µM) or DMSO, for 1 and 3 h and the expression levels of *HMOX-1* (**A**), *HSPA6* (**B**) and *GAPD*, used as control, were quantified by RT-qPCR. At each time point, gene expression levels of vehicle-treated cells were set as 1 for normalization purposes. Statistical significance was determined by two-tailed unpaired t-test – *HMOX-1* **: p value = 0.0010, ***: p value = 0.0005, ****: p value <0.0001; *HSPA6*: *: p value = 0.0254, **: p value = 0.0040, ***: p value = 0.0002. Yellow arrow heads indicate patients with a plasma cell clone harboring the t(11;14) translocation. Patient numbering corresponds to the patient ID in **Table 1**.

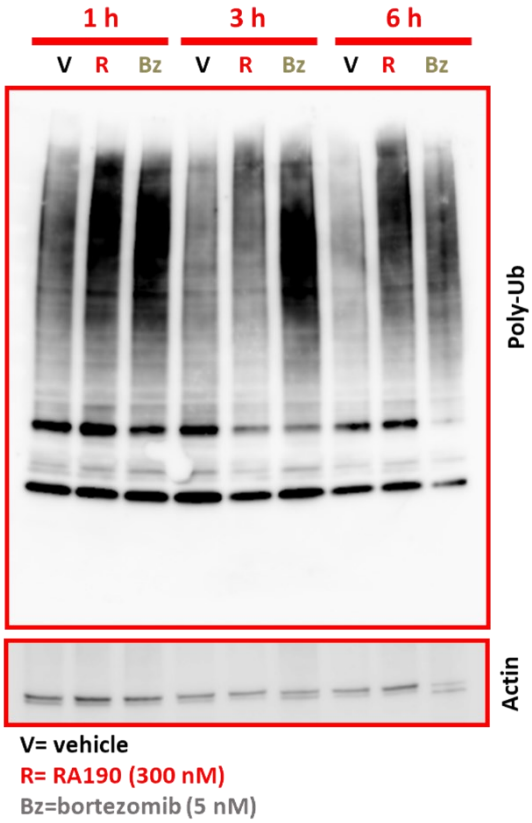

Figure 19: Mechanism of action of RA190 in ALMC-2
Time-dependent accumulation of polyubiquitinated proteins in ALMC-2 cells exposed to RA190 (R) for the indicated times, in hours (h). Bortezomib (Bz) and DMSO (vehicle, V) were used as positive and negative controls, respectively.

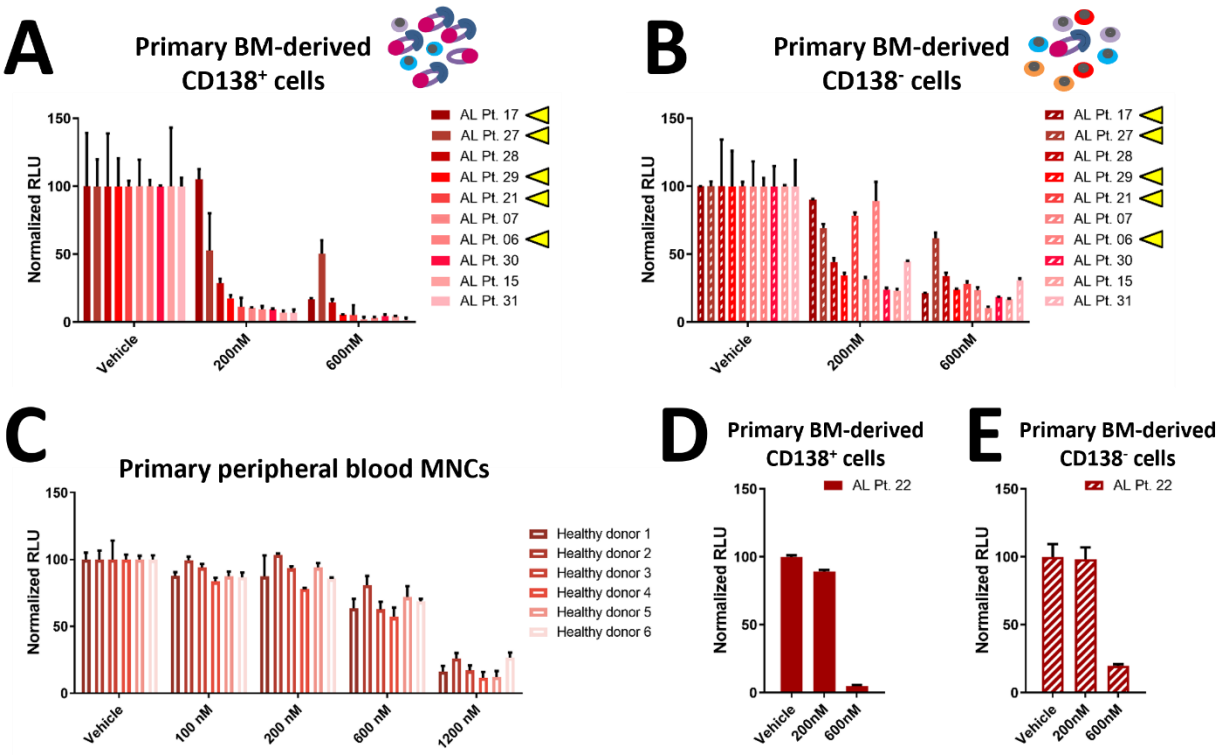

Figure 20: Therapeutic effect of RA190 on primary, patient-derived bone marrow amyloidogenic plasma cells

Primary bone marrow-derived $CD138^+$ **(A)** or $CD138^-$ cells **(B)** of 10 AL amyloidosis patients were treated with the indicated doses of RA190 or DMSO, as vehicle, for 48 h and cell metabolic activity was assessed using the CellTiter Glo assay (for each patient, the signal obtained with vehicle-treated cells was set as 100% for normalization; mean ± SD, n=2). **(C)** Primary, peripheral blood mononuclear cells (PB-MNCs) from 6 healthy subjects were treated with the indicated doses of RA190 or DMSO, as vehicle, for 48 h and cell metabolic activity was assessed using the CellTiter Glo assay (for each patient, the signal obtained with vehicle-treated cells was set as 100% for normalization, mean ± SD, n=3). Primary bone marrow-derived $CD138^+$ **(D)** or $CD138^-$ cells **(E)** of a refractory AL amyloidosis patient were treated with the indicated doses of RA190 or DMSO, as vehicle, for 48 h and cell metabolic activity was assessed using the CellTiter Glo assay (the signal obtained with vehicle-treated cells was set as 100% for normalization; mean ± SD, n=2). In A and B, yellow arrow heads indicate patients with a plasma cell clone harboring the t(11;14) translocation. Patient numbering corresponds to the patient ID in **Table 1**.

Discussion

Despite ongoing efforts at promoting the clearance of amyloid deposits from affected organs, with the aim to reduce organ damage and restore organ function [160-166], the mainstay of the treatment of systemic AL amyloidosis remains the eradication of the underlying plasma cell clone, so as to reduce or halt the supply of amyloidogenic light chains[104,105]. This is typically accomplished by exploiting therapeutic interventions originally developed for the treatment of the more prevalent plasma cell tumor, namely multiple myeloma, on the basis of the biologic similarities between these two conditions, both caused by tumoral plasma cells.

If diagnosed late and/or not responding to therapy, both AL amyloidosis and multiple myeloma can be quickly and invariably fatal. Both diseases are considered treatable but not curable due to the resilience of the underlying plasma cell clones which can resist anti-plasma cell therapies or relapse even after a long time. On the other hand, although these diseases share a similar genetic susceptibility background and degree of genomic stability, AL amyloidosis and multiple myeloma are two biologically distinct conditions[17,73]. Differences in terms of size and proliferation rate of the underlying plasma cell clone and its secreted M protein, transcriptional and mutational profile set AL amyloidosis and multiple myeloma apart[73,80]. In particular, it has been proposed that AL amyloidosis lays at the crossroad between MGUS and multiple myeloma [73,78]. Moreover, these differences can rebound on the sensitivity of the underlying plasma cell clone to drugs.

Yet, current efforts in drug discovery against plasma cell tumors have thus far focused almost exclusively on preclinical models of multiple myeloma and only drugs reaching the clinical stage of testing in multiple myeloma are eventually also tested in the setting of AL amyloidosis. This entails that if candidate therapies have not reached a clinical use for multiple myeloma, they are not tested against AL amyloidosis, thus resulting in the loss of potential effective therapies that could be employed against amyloidogenic plasma cell clones. Therefore, a paradigm shift is needed in drug discovery in the context of plasma cell disorders, towards pre-clinical studies focused specifically on investigating new therapeutic strategies for AL amyloidosis.

Due to their unique biology necessary to sustain massive antibody production, plasma cells display a critical dependence on cellular pathways ensuring protein degradation, including the ubiquitin-proteasome system (UPS) and autophagy. Indeed, a wealth of preclinical and clinical evidence indicate that the proteasome complex represents a validated target against

plasma cell tumors. Moreover, the expression of proteotoxic, unstable light chains was demonstrated to render AL amyloidosis clones even more sensitive than multiple myeloma clones towards proteasome inhibitors[130,167]. Accordingly, the first-in-class proteasome inhibitor bortezomib has revolutionized treatment of plasma cell disorders, representing the backbone of frontline therapies for transplant-ineligible AL amyloidosis patients, but being also employed in association to high-dose melphalan and autologous stem cell transplantation for induction and consolidation purposes[14,130,131]

However, a significant percentage of AL patients fails or ceases to respond to bortezomib-based treatments due to the development of resistance to this drug. This poor responsiveness is particularly reported in those cases who harbor the t(11;14) translocation the most common cytogenetic alteration in AL amyloidosis, which is observed in >40% of patients[67,71,158]. Hence, identifying drugs which can overcome resistance to proteasome inhibitors represents an urgent medical need.

The ubiquitinating/deubiquitinating system acts upstream of the proteasome and is involved in maintaining proteostasis and in tagging and directing proteins that have to be degraded towards the proteasome system itself. Current data have shown that multiple myeloma clones present a deregulation of the ubiquitylation/deubiquitylation system and drugs against this pathway have demonstrated a therapeutic potential in pre-clinical models of multiple myeloma both *in vitro* and *in vivo*[136,168]. Whether this pathway was affected in AL amyloidosis has remained largely unexplored. In this study, we set out to explore the therapeutic potential of small molecule inhibitors of selected deubiquitinating enzymes and ubiquitin receptors in preclinical models of AL amyloidosis.

Here, we have initially focused on six deubiquitinating enzymes and ubiquitin receptors, namely UCHL5, USP14, ADRM1, PSMD14, USP1 and USP7, that have been recently implicated in oncogenesis and tumor progression in a variety of different cancers (UCHL5:[136,169-173]; USP14: [174-179]; ADRM1: [137,180-183]; PSMD14: [138,184-187]; USP1: [188-193]; USP7: [194-197]). Five novel small-molecule inhibitors of these deubiquitinating enzymes and ubiquitin receptors, named b-AP15, RA190, OPA, SJB3-019A and P5091, has been recently established and their anti-tumor activity is currently tested in different solid and hematologic neoplasia (b-AP15: [136,169,170,198,199]; RA190; [137,200-202]; OPA: [184]; SJB3-019A: [188,203]; P5091: [135,204-206])

We first investigated expression levels of these deubiquitinating enzymes and ubiquitin receptors in tumoral plasma cells. Analysis of published transcriptomic data sets revealed different patterns of expression across the investigated spectrum of plasma cell malignity,

from normal plasma cells to MGUS, newly diagnosed multiple myeloma and relapsed myeloma, depending on the specific deubiquitinating enzyme or ubiquitin receptor under exam. We then opted to compare mRNA levels of these proteins of interest in bone marrow plasma cells from patients with AL amyloidosis and with multiple myeloma, using quantitative RT-PCR.

Measurement of transcriptional levels through quantitative RT-PCR critically depends on reference genes used for normalization purposes. A recent survey from our group had demonstrated that, even in studies focusing on the search for normalization genes for quantitative RT-PCR studies, adherence to international guidelines for the performance and report of quantitative PCR studies is limited[207-209] (**Appendix 3**).

In this context, we devised a strategy for the selection of suitable normalizing genes based on publicly available transcriptomic datasets (**Appendix 2**). Application of this strategy for the study of amyloidogenic and non-amyloidogenic bone marrow plasma cells led to the identification of *ACTR3*, *ESD* and *ALG9* as three suitable reference genes in this clinical setting, which proved to be superior to commonly employed normalizing genes, including *ACTB*, *GAPDH* and *B2M*, further confirming the utility of the employed strategy.

Our transcriptional studies based on validated quantitative RT-PCR assays confirmed mRNA expression for all the investigated deubiquitinating enzymes or ubiquitin receptors in bone marrow plasma cells from all investigated AL patients. Interestingly, amyloidogenic plasma cells showed a trend toward an upregulation in expression levels for all investigated deubiquitinating enzymes or ubiquitin receptors compared to myeloma plasma cells. Despite the limited number of investigated cases (n= 12 AL amyloidosis and n=8 multiple myeloma), such upregulation achieved statistical significance for the case of USP7. It will be of interest to extend these analyses to a larger number of cases to explore whether amyloidogenic plasma cells display indeed increased levels of deubiquitinating enzymes or ubiquitin receptors and to investigate whether this phenomenon might be linked with the expression of unstable, amyloidgenic light chains. In this context, the use of an inducible plasmacytoma model for the controlled expression of amyloidogenic or control light chains might help addressing these experimental questions.

We next elected to investigate the potential therapeutic effect of DUBs inhibitors in preclinical models of AL amyloidosis, starting with the use of immortalized plasma cell lines. Due to the paucity of AL amyloidosis plasma cell lines, with only two sister cell lines derived from the same AL amyloidosis patient at two different stages of the disease being available, we employed the more aggressive and supposedly more drug-resistant of the two

amyloidogenic plasma cell lines, i.e. the ALMC-2 line, for initial investigations[59]. First, we confirmed the expression of these deubiquitinating enzymes or ubiquitin receptors, both at the mRNA and protein level, in this cell line.

Next, we showed that exposure of ALMC-2 cells to all the tested molecular inhibitors, i.e. b-AP15, RA190, OPA, SJB3-019A, P5091, induced a dose-dependent decrease in cellular metabolic activity. Congruently with these results, we also verified that DUBs inhibitors reduced cell viability and resulted in a prompt induction of apoptosis.

Based on initial evaluation of data on the therapeutic effect of these drugs on the AL amyloidosis cell line ALMC-2, and based on drug availability, we decided to prioritize b-AP15, a small molecule inhibitor of the deubiquitylating enzymes USP14 and UCHL5, and RA190, targeting the ubiquitin receptor Rpn13, encoded by the *ADRM1* gene.

First, we assessed the effects of the selective targeting of UCHL5 and USP14 using b-AP15 against ALMC-2 cells. Brief exposure to nanomolar concentrations of b-AP15 led to a time dependent accumulation of polyubiquitinated proteins, thus confirming the critical role of UCLH5 and USP14 in maintaining proteostasis[125,136,168,171,174,198,199,210-217]. Evidence of the polyubiquitin accumulation was obtained at concentrations that induced decreased cell metabolism and cell viability and an increase in apoptosis in ALMC-2 cell line, hence providing a link between proteasome inhibition and cytotoxicity.

For a deeper comprehension of the mechanisms underlying b-AP15 activity, we assessed transcription levels of *HMOX-1* and *HSPA6*, two genes involved in oxidative and proteotoxic stress, respectively, which had been found to be quickly activated in HCT116 and MCF7 cancer cells upon treatment with this drug[218,219].

HMOX-1 encodes for the enzyme heme oxygenase-1 (HO-1) which catabolizes heme and plays a crucial protective role against oxidative stress. We treated ALMC-2 cells with b-AP15 for 1, 3 and 6 hours and we could detect an upregulation of *HMOX-1* already after 1h of treatment. Such an early activation of *HMOX-1* by b-AP15 has not been previously reported. A significant upregulation of *HMOX-1* was present also after 3 and 6 hours, with a peak at the 3-hour time point. *HSPA6* encodes for the Hsp70B chaperone, a heat shock induced protein involved in preventing proteotoxicity[215,218]. Of note, b-AP15 was shown to induce *HSPA6* expression, as well, at the three time points analyzed, although its upregulation did not reach statistical significance after 1 hour. The dramatic enhancement of chaperone expression (>100 fold-induction) highlights the significant proteotoxic response which occurs in b-AP15 treated cells.

The earlier increase of *HMOX-1* expression levels might be taken to suggest that oxidative stress anticipates the ER stress in ALMC-2 cells. Congruently, an accumulation of polyubiquitinated proteins, which is a potent inducer of ER stress, was reported only after 3 hours of drug treatment. On the other hand, the lack of evident accumulation of polyubiquitinated proteins at 1 h might be determined by the limited sensitivity of the Western blotting assay employed. Whether oxidative stress occurs before ER stress requires further investigation. In particular, it will be essential to dissect the early molecular perturbations induced by b-AP15 exposure, both at the transcriptional and protein levels. To this regards, next-generation sequencing-based transcriptomic analyses and proteomic analyses may be informative. Even so, the concurrent role of oxidative and proteotoxic stress in mediating b-AP15 cytotoxicity has been well described[216].

Next, we decided to investigate the sensitivity to b-AP15 in ALMC-1 cells, which represent an earlier disease stage compared to ALMC-2 cells, to assess whether the ALMC-1 line is even more sensitive to b-AP15. Interestingly, ALMC-1 showed a higher sensitivity towards b-AP15 compared to ALMC-2 when comparing the effect of this drug on the metabolic activity and viability of these sister cell lines.

Tian et al. showed that b-AP15 reduces cell viability in bortezomib resistant cell lines[136]. However, all the multiple myeloma plasma cell lines included in this study lacked the t(11;14) translocation, which is associated with a lower response rate towards bortezomib-based regimens. In addition, the t(11;14) translocation status of patients with multiple myeloma included in that study was not reported. Since the ALMC-1 and ALMC-2 cell lines also lack the t(11;14) and no additional AL plasma cell lines exists, we decided to employ two MM plasma cell lines harboring this cytogenetic abnormality, that are the U266B1 and KMS-12-BM cell lines[148,149]. Additional cell lines were also tested and interphase FISH analysis confirmed lack of the t(11;14) translocation (data not shown).

These investigations implied the use of multiple human plasma cell lines. The recognition of the frequent occurrence of cell line misidentification or cross-contamination with unrelated cell lines led to the implementation of appropriate authentication procedures based on the analysis of short tandem repeat profiles, as well the strict adherence to good laboratory practice and frequent monitoring of cell cultures[220,221].

Also, we have performed a systematic review of 149 studies on multiple myeloma cell lines published between 2018 and 2021 in the top journals within the fields of hematology, immunology, oncology or in multidisciplinary journals. This survey has revealed that in about 70% of analyzed studies there was no indication of any authentication procedure.

Limited access to short tandem profile analysis might explain, at least in part, the lack of proper authentication of cell lines in these cases. We reasoned that the sequence of expressed immunoglobulin genes might represent a molecular fingerprinting for plasma cell lines and knowledge of these sequences might be exploited for plasma cell line authentication purposes. In this context, we took advantage of a novel method to sequence expressed immunoglobulin genes in biological samples developed in our laboratory and termed Single Molecule Real-Time Sequencing of the M protein (Cascino, Nevone et al. Submitted, **Appendix 4**). SMaRT M-Seq was exploited to obtain the full-length V region of expressed kappa or lambda light chain in a panel of 19 human plasma cell lines, including the most commonly employed cell lines (**Appendix 1**). This data set could represent a resource for scientists working with human plasma cell lines and facilitate authentication procedures.

When expanding pharmacologic treatment to the additional human plasma cell lines, we observed that b-AP15 dose-dependently induced a reduction in metabolic activity and viability also in the t(11;14)-positive U266B1 and KMS-12-BM cell lines.

Bone marrow mesenchymal stromal cells (BM-MSCs) and possibly other cells within the bone marrow niche assure cytoprotection towards clonal plasma cells, possibly through paracrine effects and through adhesion molecules. These cellular interactions are nor recapitulated in monoculture systems and the lack of this cytoprotective activity may lead to an overestimation of anti-plasma cell activity of tested drugs. Therefore, we decided to study the therapeutic effect of b-AP15 against ALMC-2 in a co-culture system with primary, BM-MSCs.

We decided to expose ALMC-2 cells to b-AP15 also in the presence of primary BM-MSCs in a 2D co-culture. Of note, co-culturing of ALMC-2 with primary BM-MSCs did not prevent b-AP15-mediated cell death. Collectively, these data indicate that targeting USP14 and UCHL5 induces oxidative and proteotoxic stress, and ultimately triggers cell death in ALMC-2 cells, also in the presence of primary BM-MSCs, and the therapeutic effect of b-AP15 is observed also in t(11;14) positive MM plasma cell lines.

Work with BM-MSCs within this study was paralleled by the analysis of this cellular compartment in patients with AL amyloidosis. Mesenchymal stromal cells from patients with AL amyloidosis (AL-MSCs) were comparable to stromal cells from healthy donors (HD-MSCs) in terms of morphology, immune-phenotype, and differentiation capacities while showing a reduced proliferation rate and entering senescence at earlier passages, as already described in multiple myeloma[222,223]. Conversely, BM-MSCs from patients with AL amyloidosis showed different *in vitro* immunomodulatory effects compared to what has been

reported for BM-MSCs from patients with multiple myeloma, pointing towards a potentially different role for these cells in shaping the BM microenvironment in these two conditions[224]. Further studies addressing the bone marrow microenvironment in AL amyloidosis are needed.

Clearly, the 2D co-culture system we employed for this analysis presents some limitations, since the use of an immortalized cell line did not fully mimic the biology and heterogeneity of primary plasma cells, as well as their interaction with/dependence on the surrounding bone marrow. Furthermore, the surrounding bone marrow environment (ie, other cell types and extracellular matrix) is not taken into account in these *in vitro* models. Recently, more sophisticated systems, as 3D co-culture systems using primary bone marrow cells, are offering a convenient and feasible alternative to the animal model system for testing drugs in a system that more closely resemble the bone marrow environment[225,226]. Establishment of 3D culture systems for preclinical studies in AL amyloidosis are warranted.

After having verified the therapeutic effect of b-AP15 towards human plasma cell lines, we then analyzed its effect against primary, patients-derived cells. For this purpose, we employed primary, bone marrow derived $CD138^+$ cells, along with the $CD138^-$ fraction, the latter serving as a control.

Thus far, only few studies[13, 45,48,51] have employed primary patient cells to assess b-AP15 efficacy. Our results showed that both these drugs drastically reduced cell metabolic activity in $CD138^+$ cells. A minor effect on metabolic activity was seen in $CD138^-$ control cells. These cells, representing the $CD138^-$ fraction obtained from BM-MNCs after the first round of immunopurification, still contain some residual plasma cells, which could partially explain the reduction in cell metabolic activity detected upon exposure to the experimental drug. On the other hand, our transcriptional analysis has revealed the ubiquitous expression of *USP14, UCHL5* and *ADRM1* across different cell populations within the bone marrow, which could explain the residual, significantly milder effect of b-AP15 towards cells other than $CD138^+$ cells within this fraction. The preferential activity of these drugs against primary bone marrow-derived $CD138^+$ cells was further verified using peripheral blood mononuclear cells from healthy donors, in which even the highest tested dose of b-AP15 (300 nM, which is double of the concentration employed for the treatment of primary bone marrow-derived cells) did not suffice to induce a similar decrease in cell metabolic activity as the one detected with bone marrow-derived $CD138^+$ cells.

Finally, we evaluated the therapeutic effect of b-AP15 in primary, bone marrow derived $CD138^+$ cells (and $CD138^-$ cells, as a control) of three relapsed/refractory AL amyloidosis

patients. All patients were treated with bortezomib, dexamethasone and cyclophosphamide, for a total of 2, 3 and 6 cycles (for AL Pt. 23, AL Pt. 22 and AL Pt. 14*, respectively). Of note, both patients showed a dose dependent remarkable reduction of cell metabolic activity in $CD138^+$ cells, in a similar extent to what reported in treatment-naïve patients.

Recently, VLX1570 has been established as a novel, optimized inhibitor USP14/UCHL5 inhibitor structurally related to b-ap15[ref.219]. Of note, treatment of multiple myeloma cells with VLX1570 triggered the accumulation of proteasome-bound high molecular weight polyubiquitin conjugates and an apoptotic response, and this drug led to extended survival in xenograft models of multiple myeloma[227]. The safety, tolerability, and pharmacokinetic behavior of VLX1570 was evaluated in the context of a phase 1 clinical trial. Despite anti-myeloma effects at doses at or above 0.6 mg/kg, two patients treated at the 1.2 mg/kg dose level experienced abrupt, fatal pulmonary toxicity and the3 study was discontinued[228]. Subsequent studies showed that both b-ap15 and VLX1570 target a diverse range of proteins, resulting in nonspecific protein aggregation. Whether such molecular effects may be implicated in the pulmonary toxicity exerted by VLX1570 is currently unknown. Despite the sever toxicity reported for VLX1570, efforts directed at identifying small molecule DUB inhibitors with greater therapeutic indices are warranted based on the biologic rational, their unique mechanism of action, and robustness of preclinical antitumor activity, also in cases resistant to proteasome inhibitors[106,228].

In this context, the ubiquitin receptor Rpn13, encoded by the *ADRM1* gene, is emerging as a particularly promising molecular target against tumoral plasma cells. Targeting Rpn13 through the specific inhibitor RA-190 showed therapeutic effects in preclinical models of multiple myeloma[14].

Of note, in our study treatment of ALMC-2 cells with RA190 led to a time-dependent accumulation of polyubiquitinated proteins, and to a dose-dependent reduction in metabolic activity and viability. Importantly, RA190 showed a therapeutic effect also on primary, patient-derived bone marrow plasma cells, further confirming that inhibition of the deubiquitinating system is a promising therapeutic approach against AL amyloidosis.

Building on this knowledge , chemical linking of RA190 to the cereblon-binding drug thalidomide led to the generation of a small molecule degrader termed WL40. This drug is capable of recruiting cytoplasmic Rpn13 to a cereblon-containing E3 ligase complex, leading to Rpn13 polyubiquitination and subsequent degradation. Noteworthy, WL40 showed increased anti-myeloma effects compared to the parental drug RA190[229]. Whether such potentiated pharmacologic activity is confirmed also in amyloidogenic plasma cells will be

the subject of future studies. Further clinical development of targeted protein degradation and application of this innovative pharmacologic technology to interfere with proteoastasis against tumoral plasma cells is eagerly awaited[106].

Our results of b-AP15 and RA190 efficacy against AL amyloidosis plasma cell clones are consistent with the data reported by Tian et al. and Song Y et al. on multiple myeloma plasma cell clones[136,137]. Worthy of note, our cohort of primary, bone marrow-derived $CD138^+$ cells included cells from AL amyloidosis patients harboring the t(11;14) translocation. This result might have relevant clinical consequences for those patients carrying this translocation, who are less likely to benefit from bortezomib-based regimens. Moreover, b-AP15 and RA190 were active even in primary bone marrow-derived $CD138^+$ cells deriving from patients with a high tumor burden (BMPCs >10%) and who failed to obtain deep hematological responses (very good partial response or better) to bortezomib based frontline therapies.

These clinical considerations further highlight the promising role of these DUB inhibitors even in bortezomib-refractory patients, which is of pivotal importance given the increasing emergence of drug-resistant amyloidogenic plasma cells. In order to confirm the ability of b-AP15 and RA190 to counteract bortezomib resistance in AL amyloidosis, it will be of interest to establish a bortezomib-resistant AL amyloidosis cell line.

The therapeutic effect of b-AP15 and RA190 against different tumors, including multiple myeloma, was confirmed also in several *in vivo* studies, which also proved that this drug is well tolerated *in vivo*[136,137,174,199,201,210,213,214,230-233]. The lack of established animal models for AL amyloidosis currently hampers the conduction of such analyses. Recently, a xenoengraftment-based mouse model has been established, based on the MISTRG6 mice, where patient-derived clonal plasma cells promptly engraft and can be maintained and analyzed over time[64]. Whether primary bone marrow plasma cells from AL amyloidosis patients can successfully engraft in these mice is presently unknown. Such novel experimental model may prove instrumental to study amyloidogenic plasma cells in vivo over time, including their response to novel drugs.

Tian and coworkers reported that b-AP15 can synergize with other classes of anti-plasma cell drugs, including lenalidomide, the histone deacetylase (HDAC) inhibitor SAHA or dexamethasone, against multiple myeloma, while Song and colleagues reported synergistic anti-myeloma activity of RA190 in combination with lenalidomide, pomalidomide or bortezomib [136,137]. It will be of interest to assess whether such synergistic activities are confirmed also in the context of AL amyloidosis, and whether it can expand to other classes

of anti-plasma cell drugs (including novel proteasome inhibitors and anti-plasma cell monoclonal antibodies). Furthermore, as future perspectives, it will be of interest to extend the investigations reported in the present study also to other available DUBs inhibitors (OPA, P5091, SJB3-019A) in the context of AL amyloidosis.

Conclusions and future perspectives

In conclusion, our results demonstrated anti-tumor activity of b-AP15 and RA190 both in AL amyloidosis cell lines and primary patient-derived plasma cells, showing a specific anti-AL activity and a favorable therapeutic index. Notably, these drugs were effective even in clones harboring the t(11;14) translocation, both in immortalized plasma cell lines and primary patient-derived amyloidogenic plasma cells, as well as in clones from bortezomib-refractory patients.

Collectively these data validate inhibition of DUBs upstream of the proteasome as a novel pharmacologic approach to overcome the proteasome inhibitor resistance in AL amyloidosis. Our study, together with the notion that several DUBs inhibitors are effective also *in vivo* and act synergistically with other anti-plasma cell drugs, provides the rationale for the evaluation of DUBs inhibitor, alone and in combination, as potential therapy to improve patient outcome in AL amyloidosis.

Scientific production arisen from this thesis

Peer-reviewed publications

1. Nevone A, Girelli M, Mangiacavalli S, Paiva B, Milani P, Cascino P, Piscitelli M, Speranzini V, Cartia CS, Benvenuti P, Goicoechea I, Fazio F, Basset M, Foli A, Nanci M, Mazzini G, Caminito S, Sesta MA, Casarini S, Rognoni P, Lavatelli F, Petrucci MT, Olimpieri PP, Ricagno S, Arcaini L, Merlini G, Palladini G, Nuvolone M. **An N-glycosylation hotspot in immunoglobulin κ light chains is associated with AL amyloidosis.** *(Manuscript submitted)*
2. Cascino P, Nevone A, Piscitelli M, Scopelliti C, Girelli M, Mazzini G, Caminito S, Russo G, Milani P, Basset M, Foli A, Fazio F, Casarini S, Massa M, Bozzola M, Ripepi J, Sesta MA, Acquafredda G, Moretta A, Avanzini MA, Rognoni P, Milan E, Ricagno S, Lavatelli F, Petrucci MT, Klersy C, Merlini G, Palladini G, Nuvolone M. **Single Molecule Real-Time Sequencing of the M protein (SMaRT M-Seq): toward personalized medicine approaches in monoclonal gammopathies.** *(Manuscript submitted)*
3. Valsecchi C, Croce S, Maltese A, Montagna L, Lenta E, Nevone A, Girelli M, Milani P, Bosoni T, Massa M, Abbà C, Campanelli R, Ripepi J, De Silvestri A, Carolei A, Palladini G, Zecca M, Nuvolone M, Avanzini MA. **Bone Marrow Microenvironment in Light-Chain Amyloidosis: In Vitro Expansion and Characterization of Mesenchymal Stromal Cells.** *Biomedicines*. 2021 Oct.
4. Alameda D, Goicoechea I, Vicari M, Arriazu E, Nevone A, Rodríguez S, Lasa M, Puig N, Cedena MT, Alignani D, Garate S, Lara-Astiaso D, Vilas-Zornoza A, Sarvide S, Ocio EM, Lecumberri R, Garcia de Coca A, Labrador J, Gonzalez ME, Palomera L, Gironella M, Cabañas V, Casanova M, Oriol A, Krsnik I, Pérez-Montaña A, de la Rubia J, de la Puerta JE, de Arriba F, Fazio VM, Martinez-Lopez J, Lahuerta JJ, Mateos MV, Odero MD, Prosper F, Weiner A, Amit I, Nuvolone M, San-Miguel JFF, Paiva B. **Tumor cells in light-chain amyloidosis and myeloma show different transcriptional rewiring of normal plasma cell development**. *Blood*, 2021
5. Nevone A, Cascino P, Girelli M, Scopelliti C, Piscitelli M, Bozzola M, Sesta MA, Ripepi J, Milani P, Basset M, Palladini G, Nuvolone M. **Analisi dei livelli trascrizionali di ciclina D1 nello studio delle discrasie plasmacellulari: revisione sistematica della letteratura**. *Biochimica Clinica*, 2021 Mar.
6. Palladini G, Paiva B, Wechalekar A, Massa M, Milani P, Lasa M, Ravichandran S, Krsnik I, Basset M, Burgos L, Nuvolone M, Lecumberri R, Foli A, Puig N, Sesta MA, Bozzola M, Cascino P, Nevone A, Ripepi J, Berti P, Casarini S, Annibali O, Orfao A, San-Miguel J, Merlini G. **Minimal residual disease negativity by next-generation flow cytometry is associated with improved organ response in AL amyloidosis**. *Blood Cancer J*, 2021 Feb.
7. Nevone A, Merlini G, Nuvolone M. **Treating Protein Misfolding Diseases: Therapeutic Successes Against Systemic Amyloidoses**. *Frontiers in Pharmacology*, 2020 Jul.
8. Nevone A, Cascino P, Bozzola M, Palladini G, Nuvolone M. **Identificazione di geni di normalizzazione per studi trascrizionali con PCR quantitativa: revisione della letteratura**. *Biochimica Clinica*, 2019 Sept.

Acknowledgements

I would like to express my sincere gratitude to Dr. M. Nuvolone for supervision, teaching and mentoring; Prof. K.C. Anderson and Dr. D. Chauhan for kindly providing all the DUBs inhibitors, D. F. Jelinek for kindly providing ALMC-2 cell lines; Dr E. Milan for the kind gift of ALMC-1 cell line; Prof. A. Neri for the kind gift of KMS-12-BM and U266B1 cell lines; Dr. M. Massa and Dr. M. Sesta for the contribution to the flow cytometry analysis of cell lines; Dr. A. Avanzini and Dr. A. Maltese for kindly providing bone marrow-derived mesenchymal stromal cells; Dr. I. Dambruoso, Dr. M. Boni, Dr. R. Zappatore and Prof. L. Arcaini for cytogenetic analysis; Prof. G. Merlini, Prof. G. Palladini, Dr. M. Nuvolone, Dr. A. Foli, Dr. P. Milani, Dr R. Mussinelli, Dr. M. Basset and for patients recruitment and clinical data; Dr. M. Bozzola and Dr. P. Cascino and Dr F. Valsecchi for help with Western blot analyses and pharmacological experiments.

Part of the text and figures were reproduced or adapted from published manuscripts (Nevone et al. Front Pharmacol 2020 for introduction, Nevone et al. Biochmica Clinica 2019 for Appendix 3), from manuscripts submitted (Cascino* and Nevone* et al. for Appendix 4) or under preparation (Nevone et al. for Appendix 1 and 2), as well as from dissertations and applications to funding agencies submitted or under preparation and related to the work presented here.

This work was supported by grants from the Italian Ministry of Health (Ricerca Finalizzata, grant #GR-2018-12368387), the CARIPLO Foundation (grant #2018-0257), the Amyloidosis Foundation, and by Cancer Research UK [C355/A26819] and FC AECC and AIRC under the Accelerator Award Program.

Appendices

Appendix 1: Plasma cell lines fingerprinting through sequencing of the expressed immunoglobulin genes

Introduction

Cell lines represent a valuable tool for biomedical research, due to their ability of replacing primary cells. The recognition of the frequent occurrence of cell line misidentification or cross-contamination with unrelated cell lines (both intra- and inter-species contamination), as well as microbial contamination has stimulated the development of methods to authenticate the identity of cell lines. Authentication of cell line is crucial to guarantee cell line identity and to obtain reproducible and valid data and is recommended by the scientific community, funding agencies and scientific journals.

Over the years, different systems have been proposed to certify cell line identity, one of the most widely employed one being short tandem repeat (STR) profiling. Nevertheless, still today cell line authentication procedures are often neglected, due to limited awareness and possibly to limited access to STR profiling or other advanced molecular techniques.

Besides microsatellite profiling, cell line authentication could also rely on the identification of a peculiar biologic feature which could represent a cell line fingerprint. We reasoned that the unique immunoglobulin produced by a given B cell or plasma cell line as the result of V(D)J recombination and somatic hypermutation of immunoglobulin genes might be employed for cell line authentication purposes.

Methods

We performed a systematic review of published literature on multiple myeloma cell lines, to evaluate current practices on human plasma cell lines authentication. We compiled a list of 223 unique studies that were analyzed to extrapolate information regarding the authentication procedures applied.

We then focused on a panel of 19 human multiple myeloma cell lines (7 secreting a κ immunoglobulin light chain, while 12 secreting a λ immunoglobulin light chain). After proper authentication through STR profiling and a phenotypic and molecular characterization performed through morphological studies, next-generation, multiparametric flow cytometry

and high-resolution agarose gel electrophoresis with immunofixation, we sequenced and analyzed their expressed immunoglobulin light chain genes.

Results

The systematic review resulted in a total of 149 unique studies employing human plasma cell lines and published in the last three years. The use of more than one multiple myeloma cell line was reported in 84,6% of papers (median: 6; range: 2-37). The original references of the employed cell lines were mainly omitted. In fact, only 29 papers (19,5%) explicitly referred to the original description of each specific cell line used (Fig. 1A). The source of the employed cell line(s) is reported in 18.8% of cases, and the most frequent source of cell lines was repository (67.1%), followed by academic institutions (36.9%) and commercial providers (3.4%) (Fig. 1B). Cell line authentication procedures were performed only in a minority of studies and STR profiling was the method of election (24.83%), followed by flow cytometry (2%) and other methods used by individual publications (Fig. 1C).

Then we authenticated the cell lines using STR profile technique (data not shown). Finally, we elected to sequence the expressed immunoglobulin light chain gene of 19 among the most popular human multiple myeloma cell lines. We sequenced the immunoglobulin germline genes used for κ light chain production of KMS-26 (*IGKV1-05*03*), KJON (*IGKV1-33*01*), OH-2 (*IGKV1-39*01*), JK-6L (*IGKV2-28*01*), JJN-3 (*IGKV3-15*01*), KMS-34 (*IGKV3-15*01*) and AMO-1 (*IGKV3-20*01*) (Fig. 2.1), and λ light chain production of KMM-1 (*IGLV1-51*01*), U266B1 (*IGLV2-08*01*), ANBL-6 (*IGLV2-14*01*), MM1.S (*IGLV2-14*01/*03*), MM.1-144 (*IGLV2-14*01/*03*), RPMI-8226 (*IGLV2-14*03*), MOLP-8 (*IGLV2-23*01/*03*), L-363 (*IGLV2-23*02*), LP-1 (*IGLV3-21*02*), OPM-2 (*IGLV3-25*03*), ALMC-1 (*IGLV6-57*04*) and ALMC-2 (*IGLV6-57*04*) cell lines (Fig. 2.2). Each sequence proved to be productive and differed from the respective IGKV or IGLV germline gene by 3 or more mutations.

Conclusions

We set up a strategy for the authentication of plasma cell lines, taking advantage of their unique characteristic of producing a cell line-specific immunoglobulin monoclonal protein that can be used as a fingerprint feature for each plasma cell line. The strategy described here can be expanded to other B cell or plasma cell lines, to possibly set up a database of immunoglobulin reference sequences that can be of help for B cell or plasma cell line authentication.

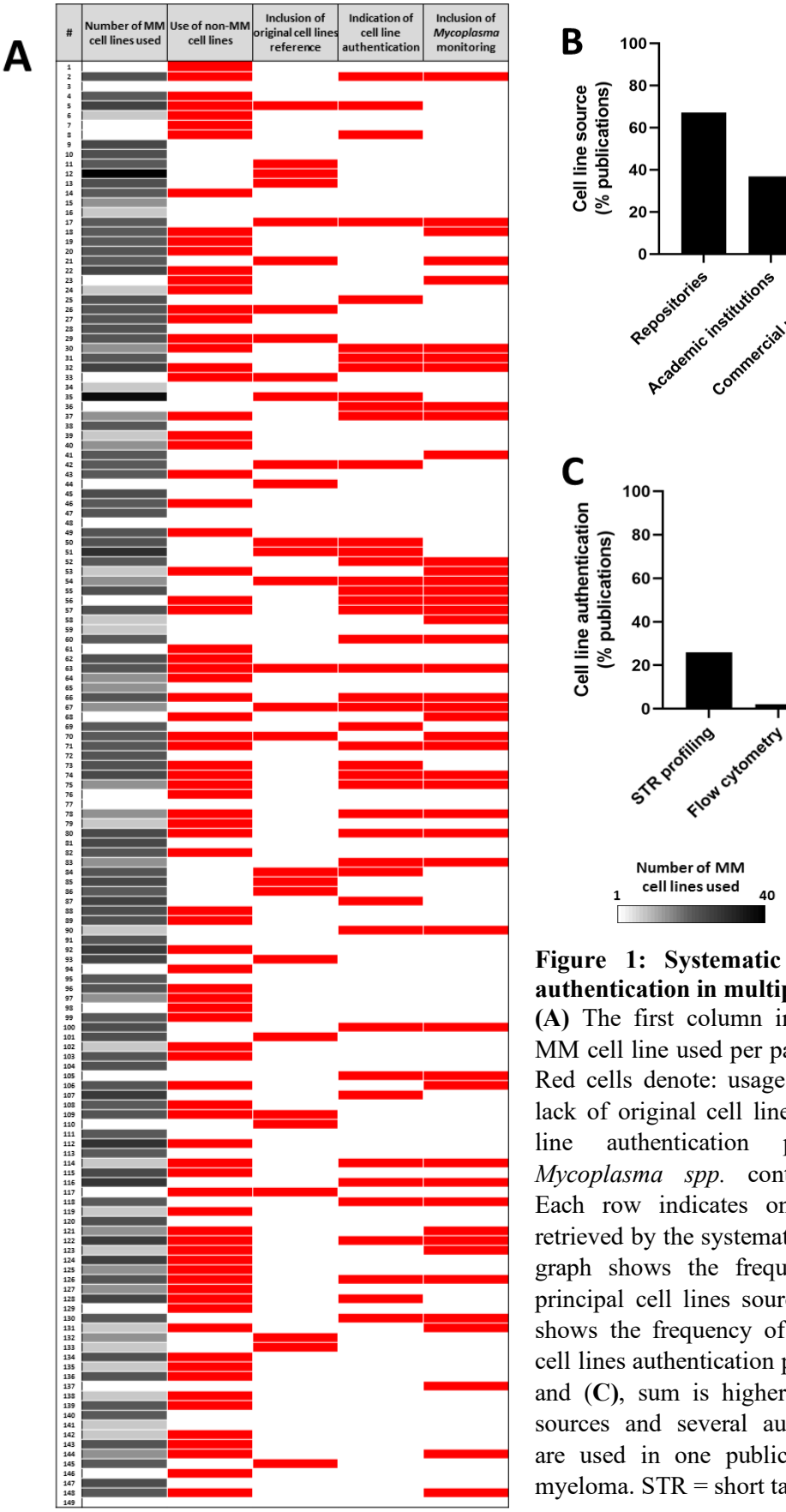

Figure 1: Systematic review on cell line authentication in multiple myeloma cell lines
(A) The first column indicates the number of MM cell line used per paper (in shades of gray). Red cells denote: usage of non-MM cell lines; lack of original cell line reference; lack of cell line authentication procedures; lack of *Mycoplasma spp.* contamination monitoring. Each row indicates one of the 149 studies retrieved by the systematic research. **(B)** The bar graph shows the frequency of usage of the principal cell lines sources. **(C)** The bar graph shows the frequency of usage of the principal cell lines authentication procedures. For both **(B)** and **(C)**, sum is higher than 100% as several sources and several authentication procedures are used in one publication. MM = multiple myeloma. STR = short tandem repeats.

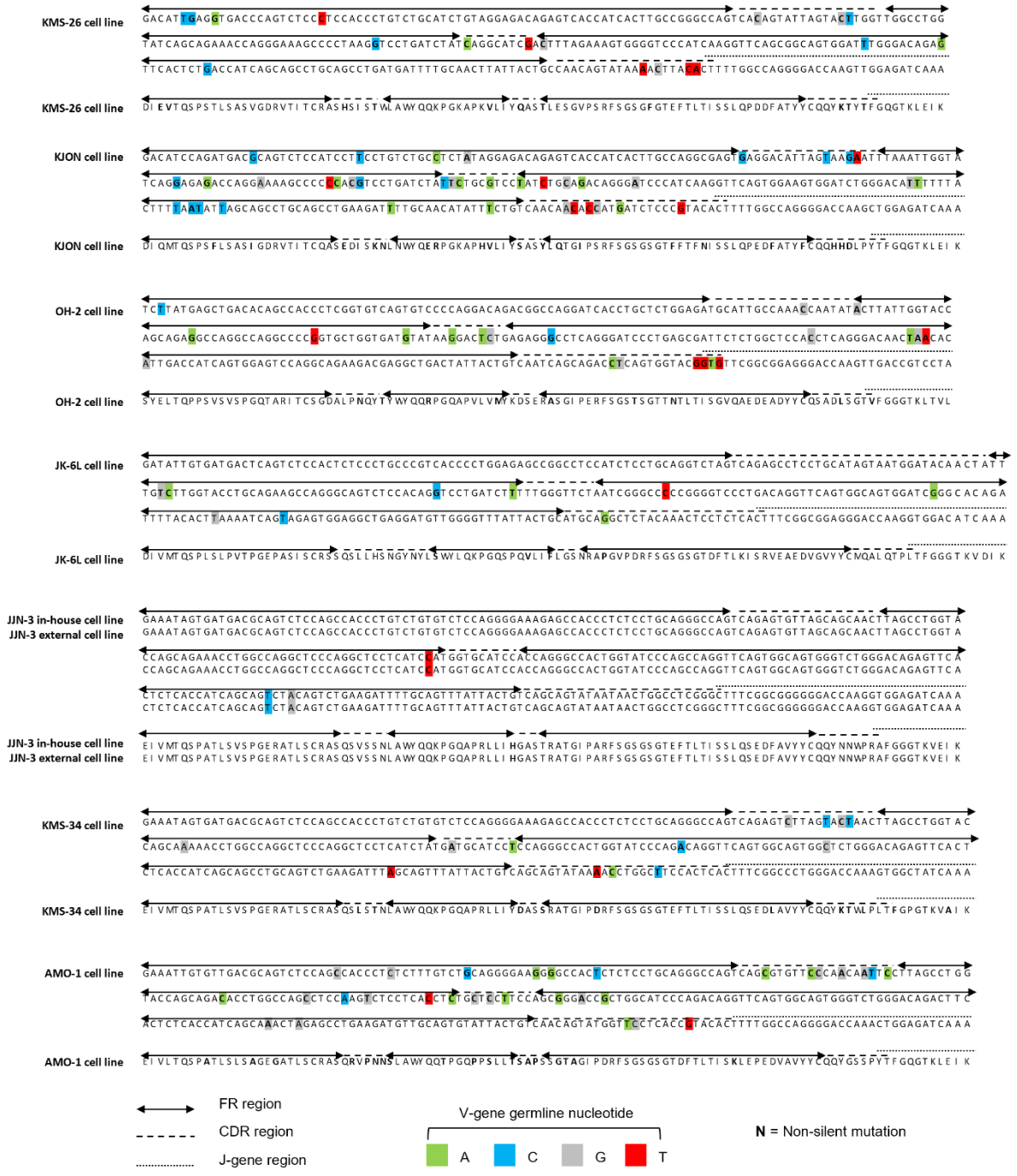

Figure 2.1: Sequence of the κ light chains expressed by human multiple myeloma cell lines
For each cell line, V and J gene sequences as determined through SMaRT M-Seq are aligned according to IMGT nomenclature. For each cell line, protein sequences as predicted based on the nucleotide sequence aligned according to IMGT nomenclature is reported. Colored squares denote sequence mismatches (≠ ref. seq.) in the cell line-specific light chain with respect to the corresponding germline gene. Bold letter indicates non silent mutation. When an aminoacidic substitution is encoded by two nucleotide substitutions, both nucleotides are indicated in bold. FR: framework region; CDR: complementarity determining region; Pt.: patient.

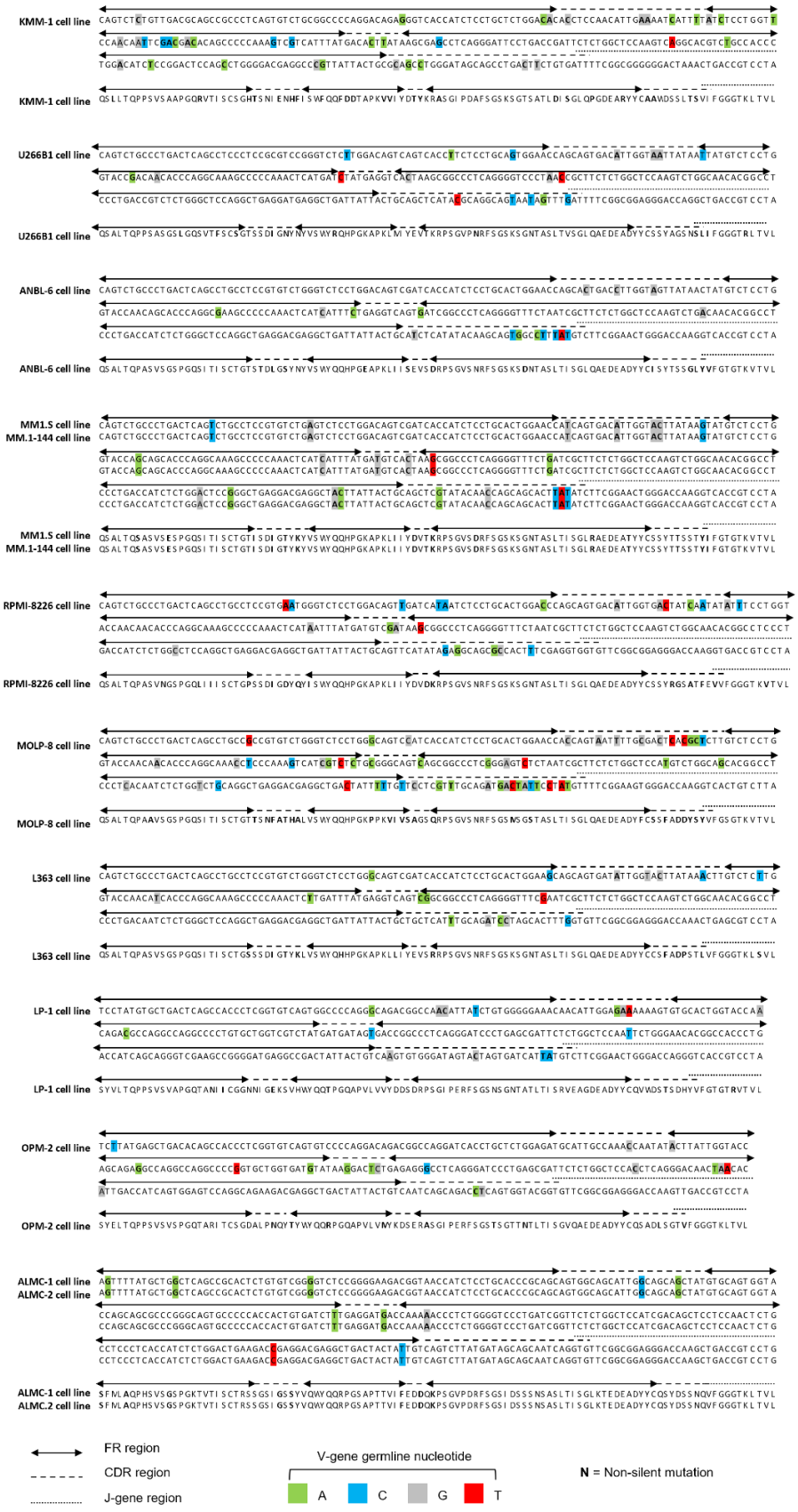

Figure 2.2: Sequence of the λ light chains expressed by human multiple myeloma cell lines
For each cell line, V and J gene sequences as determined through SMaRT M-Seq are aligned according to IMGT nomenclature. For each cell line, protein sequences as predicted based on the nucleotide sequence aligned according to IMGT nomenclature is reported. Colored squares denote

sequence mismatches (≠ ref. seq.) in the cell line-specific light chain with respect to the corresponding germline gene. Bold letter indicates non silent mutation. When an aminoacidic substitution is encoded by two nucleotide substitutions, both nucleotides are indicated in bold. FR: framework region; CDR: complementarity determining region; Pt.: patient.

Appendix 2: A strategy for the selection of RT-qPCR reference genes based on publicly available transcriptomic data sets

Introduction

In the next-generation sequencing era, reverse transcription quantitative PCR (RT-qPCR) is still widely employed for both basic research and molecular diagnostics due to its ease of use, versatility and limited costs. Measurement of transcriptional levels through RT-qPCR critically depends on reference genes used for normalization purposes. Here, we devised a strategy to select valid reference genes for a specific clinical or experimental setting based on publicly available transcriptomic data sets. As a proof of principle, we applied this strategy to identify and validate reference genes for transcriptional studies of bone marrow (BM)-derived $CD138^+$ plasma cells from patients with AL amyloidosis or control subjects.

Methods

We performed a systematic review of published literature to compile a list of 150 candidate reference genes for RT-qPCR experiments with human samples. Next, we interrogated the Gene Expression Omnibus data repository to assess expression levels of these 150 genes in published transcriptomic studies on BM-derived $CD138^+$ plasma cells from patients with different plasma cell dyscrasias and controls. For the top 14 genes with the lowest difference across examined cases and for 5 among the most commonly used normalizing genes (*ACTB*, *B2M*, *GAPDH*, *HMBS*, *HPRT1*), we iteratively used PrimerBlast, Ensembl, dbSNP and OligoAnalyzer to identify primer pairs on either exon-exon boundaries or on different exons, devoid of potentially interfering SNPs and lacking thermodynamically significant secondary structures and/or tendency to homo- or heterodimers formation. After a robust technical validation, the expression levels of the selected genes were investigated in AL amyloidosis patients and control subjects to identify the most suitable reference genes in this clinical setting, using geNorm.

Results

We used the amyloidogenic plasma cell line ALMC-2 as a source of RNA of human amyloidogenic plasma cells for technical validation of the selected 14 primer pairs. We used agarose gel electrophoresis and melting curve analysis to verify PCR specificity for each primer pair and we tested serial dilutions of cDNA over 5 orders of magnitudes (from 10^{-1} to 10^{-5}) to explore the dynamic range of each assay and calculate PCR efficiency. For the

subsequent analyses, we focused on the 11 genes (6 candidate genes and the 5 housekeeping genes) whose PCR assay had a 5-log dynamic range and an efficiency comprised between the ideal interval of 90% and 110% (Fig. 1-2).

For each of the genes under study, we analysed 6 technical replicates in one run to assess intra-assay variation. The coefficient for intra-assay variation ranged from 0.27% for *POLR2B* to 1.28% for *SDHA* (Fig. 3A). Next, for each gene we analysed technical triplicates in three runs on separate days to assess inter-assay variation. The coefficient for inter-assay variation ranged from 0.08% for *ACTR3* to 1.53% for *B2M* (Fig. 3B).

The expression profiles of the 11 investigated genes were then analyzed in $CD138^{+}$ plasma cells isolated through immunomagnetic-sorting from diagnostic leftovers of BM samples of patients with AL amyloidosis and healthy BM donors (Fig 4A). Use of geNorm identified *ACTR3*, *ESD* and *ALG9* as the most suitable reference genes in this clinical setting (Fig 4B). Of note, all the commonly used normalizing genes (*ACTB, B2M, GAPDH, HMBS, HPRT1*) performed worse than candidate genes identified with our strategy.

Conclusions

We have developed a strategy to select appropriate reference genes for normalization of RT-qPCR experiments based on publicly available and easily accessible transcriptomic data sets (Fig. 5). As a proof of principle, we have applied this strategy to identify stable reference genes for the analysis of primary, patient-derived amyloidogenic and control plasma cells, identifying *ACTR3*, *ESD* and *ALG9* as the most stable genes in this clinical setting.

The strategy presented here may be applicable to other clinical and experimental settings for which publicly available transcriptomic data sets are available.

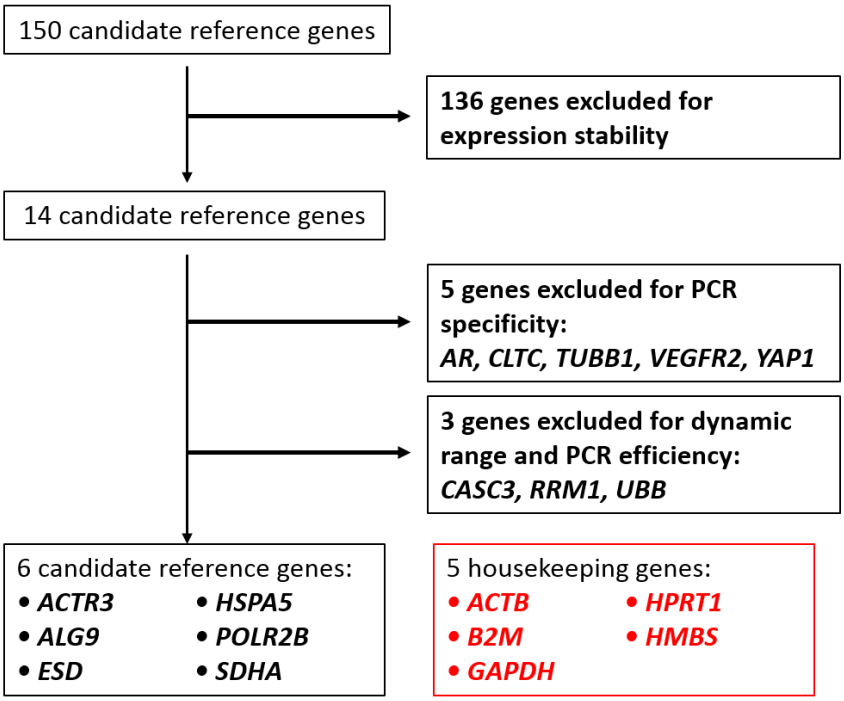

Figure 1: Flowchart of the selection of the best performing candidate reference genes
Flow chart shows the selection of the six best performing candidate reference genes based on the validation of the PCR assays of each of the 14 genes obtained from the systematic research. The expression levels of the six candidate reference genes identified (in black), as well as the expression levels of five common reference genes (in red), were then explored in the context of the AL amyloidosis

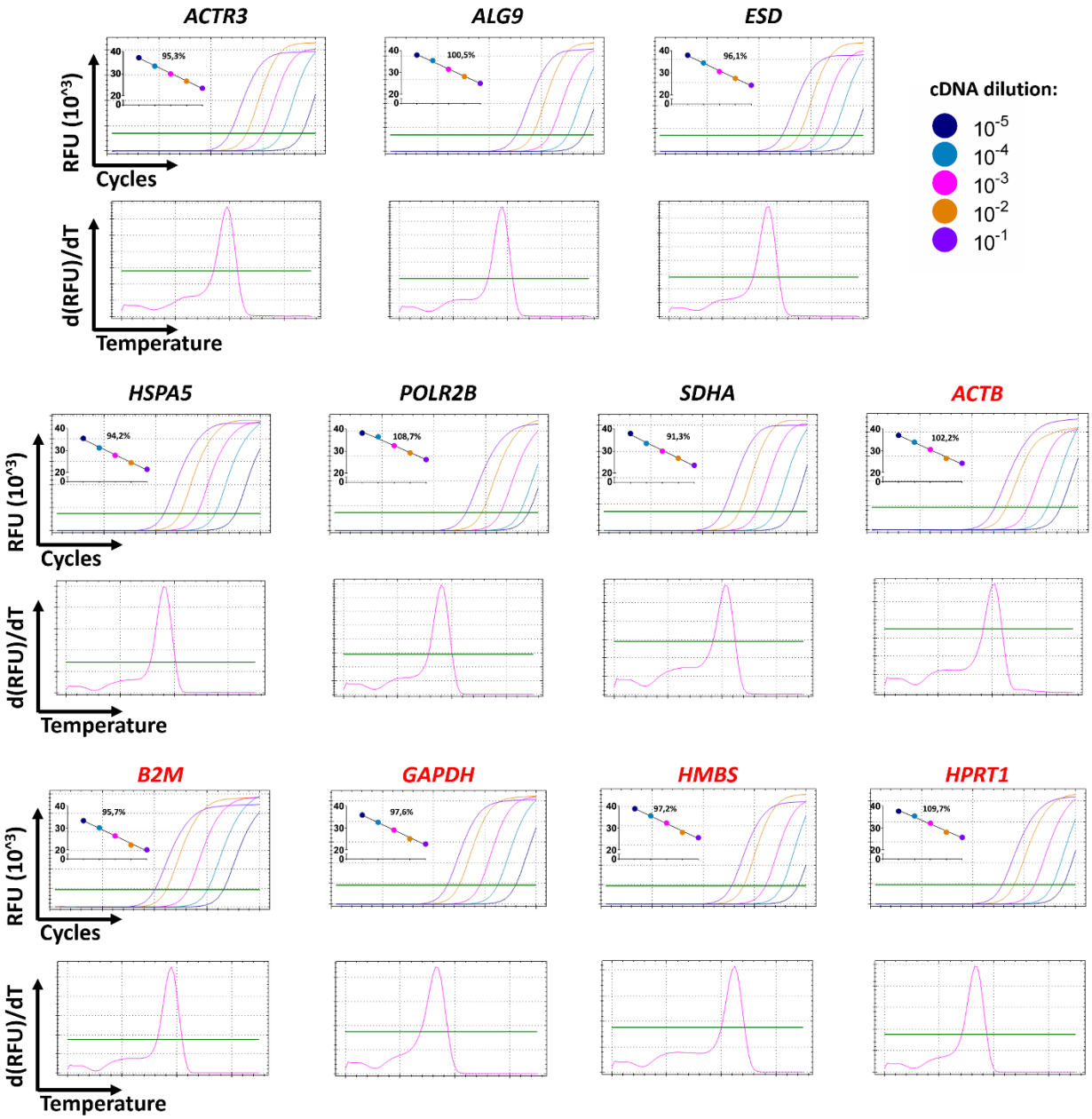

Figure 2: Dynamic range, PCR efficiency and specificity of candidate reference genes and common refence genes

For each gene, the upper plot shows the relative fluorescence unit (RFU 10^3) over cycle for the different cDNA dilutions (color-coded as in the legend), and in the left corner a plot of the correlation of cDNA dilution and Cq indicates the PCR efficiency; the lower plot shows the first negative derivative of RFU (d(RFU)/dT) over different temperature of the melting curve analysis. Dynamic range: RFU is equal to 20 for *ACTB*, 25 for *GAPDH*, *HMBS* and *HPRT1*, 30 for *B2M*, 40 for *ACTR3*, *ALG9*, *ESD*, *POLR2B* and *SDHA*, 50 for *HSPA5*; melting curve: -d(RFU)/dT *ALG9*, *ESD*, *POLR2B* (8000), *ACTR3* (7000), *SDHA* (6000), *B2M* and *HPRT1*(5000), *GAPDH* and *HMBS* (4000), *ACTB* (3000), *HSPA5* (10). Black color indicates candidate reference genes identified with the proposed strategy; red color indicates the commonly used reference genes.

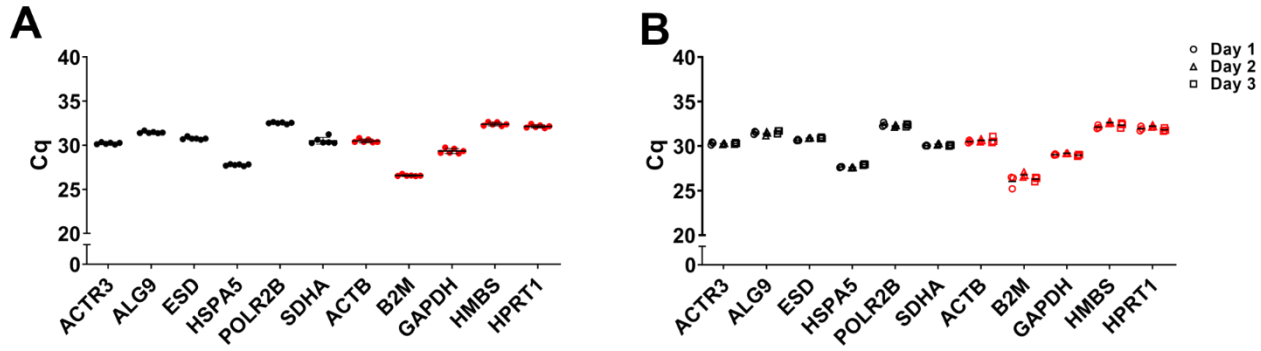

Figure 3: Technical validation of the assays of the candidate reference genes and the common reference genes

(A) Cq values of six technical replicates, represented by dots, for each candidate reference gene (in black) or common reference gene (in red) obtained within one single run. (**B)** Cq values of three technical replicates for each candidate reference gene (in black) or common refence gene (in red) obtained in three different runs in separate days, each symbol (circle, triangle, square) indicates a day.

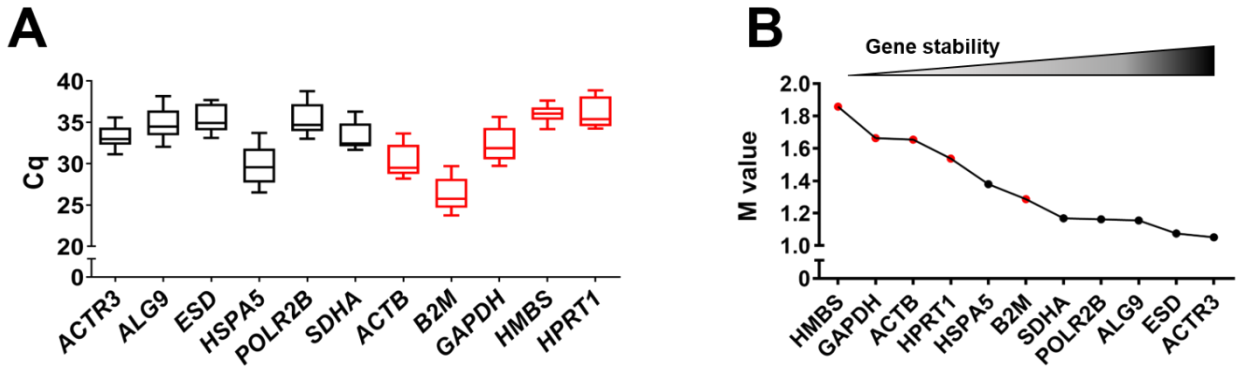

Figure 4 Distribution of expression levels and stability analysis of candidate and common reference genes in AL amyloidosis patients and controls.

(A) Distribution of quantification cycle (C_q) values of candidate reference genes (n=6, in black) and the common reference genes (n=5, in red) across all the study subjects (patients with AL amyloidosis: n=6; healthy donors: n=3). (**B)** Stability ranking of candidate reference genes (n=6, in black) and the common reference genes (n=5, in red) based on the M value determined by geNorm across all the study subjects (patients with AL amyloidosis: n=6; healthy donors: n=3). The triangle above the graph shows how the stability grade increases as the M value decreases (shades of gray).

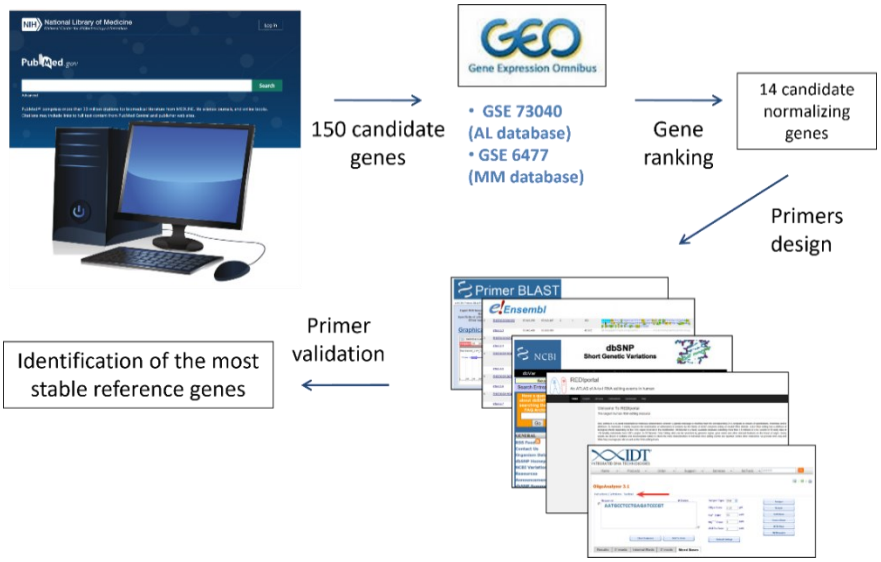

Figure 5: Strategy for the identification of RT-qPCR reference genes based on published transcriptomic data sets

Scheme of the proposed strategy for the identification of appropriate reference genes for RT-qPCR studies based on published transcriptomic data sets.

Appendix 3: Identification of genes for normalization of RT-qPCR gene expression data: a review of published literature.

Introduction

Reverse-transcriptase quantitative Polymerase Chain Reaction (RT-qPCR) is a well-established technique to quantify gene expression levels and critically depends on reference genes for data normalization. In light of the importance of identifying suitable genes for normalization of RT-qPCR data, in recent years numerous studies have been conducted to investigate candidate genes for normalization in the context of specific experimental settings. By virtue of the potential impact of this type of studies, which could suggest the use of specific genes and specific PCR assays for a particular sector of studies, it is desirable that the experimental design of these studies and the type of information reported in the related publications comply with the indications of international guidelines (namely "The Minimum Information for Publication of Quantitative Real-Time PCR Experiments – MIQE – guidelines"), in order to ensure interpretability and reproducibility of the data.

However, a systematic overview of the practices of normalization genes research for RT-qPCR assays is currently lacking.

Methods

We performed a review of biomedical literature to analyse the usage of RT-qPCR in relation to other techniques for transcriptional investigations and to describe practices for the identification of suitable reference genes for RT-qPCR. We also analysed transparency and good laboratory practices based on adherence to the MIQE guidelines, using selected validated evaluation criteria. Finally, using Ensembl and dbSNPs we investigated the frequency with which employed primers showed sequence mismatches with respect to known mutations and polymorphisms, investigating in case of the mismatch their position within the oligonucleotide.

Results

Analysis of relevant biomedical literature demonstrated that RT-qPCR remains the most commonly used technique for transcriptional studies, with a frequency of usage showing a progressive increase over time (Fig. 1).

In the 81 analysed studies, 3 genes (*GAPD*, *ACTB*, *B2M*) were included in ≥70% of cases (Fig. 2) but ranked among the most stable genes only in ≤1/3 of cases (Table 1). The most

frequently used normalizing algorithm was geNorm (83%), followed by NormFinder (73%) and BestKeeper (32%) (Fig. 3). Of note, these algorithms were more often used in combination (75% of cases), with 1 normalizing system used in 25% of studies, compared to 2 normalizing systems in 39%, 3 systems in 25% and more than 3 systems used in 11% (Fig. 4). In the 57% of the publications using more than one normalization systems, there was a concordance in the results obtained.

Overall, key MIQE criteria were satisfied in ≥50% of analyzed studies, but only four criteria (details of employed kit/enzyme for reverse transcription, priming method, primers/probes and DNA polymerase) were satisfied in ≥90% of cases. Data on assay repeatability were reported only in 15% of studies. The presence of pseudogenes as a potential confounder of assay specificity was evaluated only in 13% of studies. Finally, as few as 6% of studies accounted for the presence of known mutations of single nucleotide polymorphisms when designing assay primers/probes (Fig. 5).

Fifteen primer pairs of 15 different genes were randomly selected to analyze whether they matched a genomic region free of known mutations or polymorphisms. On average, there were 7.5 mismatches per primer (range: 1-20) and 24 primers (80%) exhibited mismatch in the last 5 positions in 3' (Fig. A1.6). Overall, only for one of the 15 investigated genes both primers were found to be free of mutations and known polymorphisms in the last 5 bases in 3'.

Conclusions

Despite the availability of methods allowing global, transcriptomic analyses at increasingly lower costs, RT-qPCR remains a widely used method for transcriptional studies. The need to identify stable genes for RT-qPCR data normalization and to design and validate suitable qPCR assays for the selected reference genes is crucial, and publicly available transcriptomic and genomic datasets could be employed to refine the identification of suitable normalizing genes and to assist assay design. Reporting the results of RT-qPCR studies with transparency and clarity ensures reproducibility and therefore, better adherence to the MIQE guidelines should be encouraged.

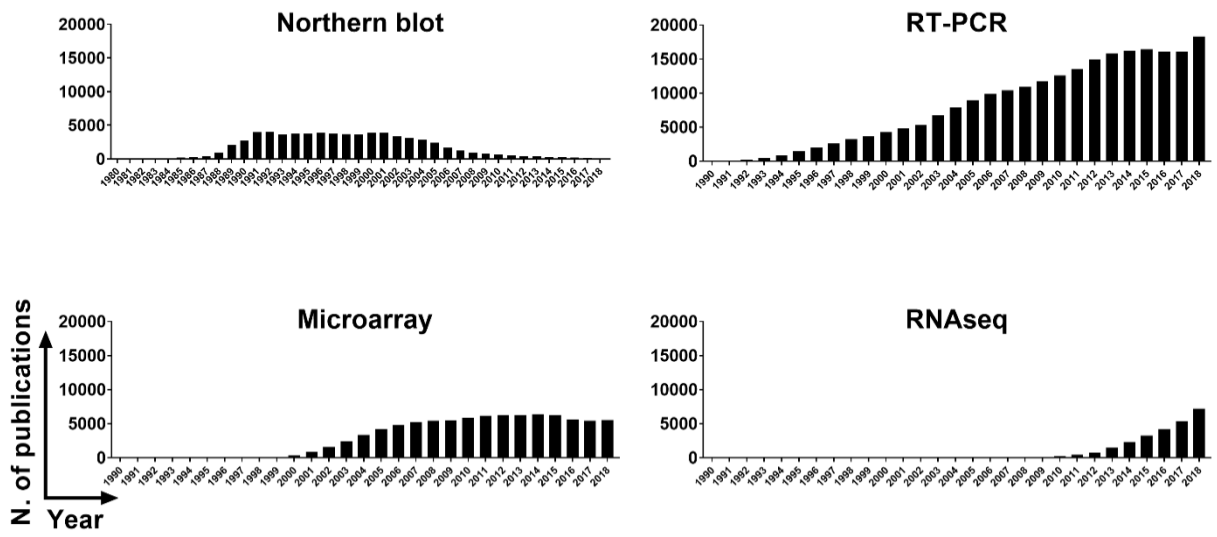

Figure 1: Annual trend in the usage of techniques for transcriptional studies in biomedical literature

The bar graphs show the number of publications per year of four techniques for transcriptional studies. Data was obtained from Pubmed, using one of the following keyword: "Northern blotting" OR "Northern blot"; "RT-qPCR" OR "RT-PCR" OR "qPCR" OR "quantitative PCR" OR "Real time PCR"; "microarray" OR "gene expression microarray"; "RNAseq" OR "RNA-seq" OR "RNA sequencing".

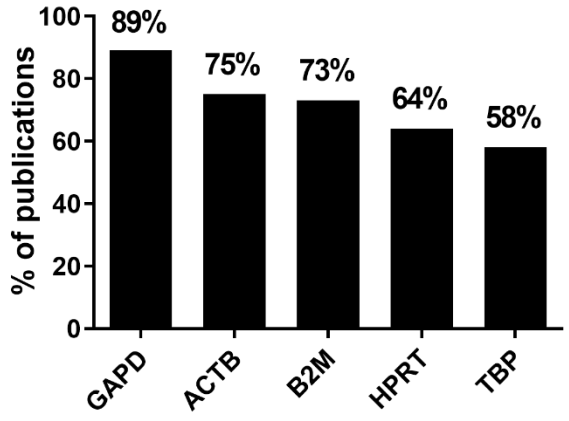

Figure 2: Frequency of the top five reference genes used in transcriptional studies in biomedical literature

The bar graph shows the frequency of usage of top 5 reference genes employed for normalizing the results in the analyzed literature. Data are based on 81 publications. Sum is higher than 100% as several normalizing genes are used in one publication.

Table 1: List of 62 genes stably expressed in the examined biomedical literature
The 62 genes resulted among the most stable genes in the 81 publications studied are here ordered by frequency. For each gene it is reported the frequency and percentage in which they were studied in the 81 articles ("Gene investigated") and the frequency and percentage in which they ranked among the most stable genes among the articles in which they were tested (“Stable Gene”).

Gene name	Investigated gene		Stable gene		Gene name	Investigated gene		Stable gene	
GAPD	72/81	88,89%	24/72	33,33%	*ALAS1*	5/81	6,17%	2/5	40,00%
ACTB	61/81	75,31%	19/61	31,14%	*CYC1*	5/81	6,17%	2/5	40,00%
B2M	59/81	72,84%	11/59	18,64%	*MTATP6*	4/81	4,94%	2/4	50,00%
HPRT1	52/81	64,20%	18/52	34,61%	*RPL37A*	4/81	4,94%	1/4	25,00%
TBP	47/81	58,02%	13/47	27,66%	*HSPCB*	4/81	4,94%	3/4	75,00%
18S	42/81	51,85%	7/42	16,67%	*RPL32*	4/81	4,94%	1/4	25,00%
PPIA	30/81	37,04%	9/30	30,00%	*ATP5B*	4/81	4,94%	2/4	50,00%
YWHAZ	30/81	37,04%	9/30	30,00%	*EF1A*	3/81	3,70%	2/3	66,67%
HMBS	29/81	35,80%	5/29	17,24%	*TMBIM6*	3/81	3,70%	2/3	66,67%
GUSB	29/81	35,80%	4/29	13,79%	*G6PDH*	3/81	3,70%	1/3	33,33%
RPLP0	26/81	32,10%	12/26	46,15%	*PSMB6*	3/81	3,70%	1/3	33,33%
SDHA	24/81	29,63%	8/24	33,33%	*RPS13*	3/81	3,70%	1/3	33,33%
UBC	22/81	27,16%	6/22	27,27%	*CHCHD1*	2/81	2,47%	1/2	50,00%
RPL13	20/81	24,69%	7/20	35,00%	*GNB2L1*	2/81	2,47%	1/2	50,00%
POLR2A	18/81	22,22%	4/18	22,22%	*TPT1*	2/81	2,47%	1/2	50,00%
PGK1	18/81	22,22%	2/18	11,11%	*UBCH5B*	2/81	2,47%	2/2	100,00%
TFRC	17/81	20,99%	4/17	23,53%	*PSMC4*	2/81	2,47%	1/2	50,00%
PUM1	16/81	19,75%	7/16	43,75%	*ALG9*	1/81	1,23%	1/1	100,00%
IPO8	13/81	16,05%	3/13	23,07%	*CTBP1*	1/81	1,23%	1/1	100,00%
MRPL19	8/81	9,87%	1/8	12,5%	*CYCA*	1/81	1,23%	1/1	100,00%
TUBB	7/81	8,64%	2/7	28,57%	*DDX5*	1/81	1,23%	1/1	100,00%
RPS17	7/81	8,64%	2/7	28,57%	*HIST*	1/81	1,23%	1/1	100,00%
CASC3	6/81	7,41%	2/6	33,33%	*HUEL*	1/81	1,23%	1/1	100,00%
EIF2B1	6/81	7,41%	2/6	33,33%	*MDH1*	1/81	1,23%	1/1	100,00%
PES1	6/81	7,41%	1/6	16,67%	*RPL4*	1/81	1,23%	1/1	100,00%
POP4	6/81	7,41%	2/6	33,33%	*SRSF9*	1/81	1,23%	1/1	100,00%
RPL30	6/81	7,41%	1/6	16,67%	*TFCP2*	1/81	1,23%	1/1	100,00%
ELF1	5/81	6,17%	2/5	40,00%	*U6*	1/81	1,23%	1/1	100,00%
PMM1	5/81	6,17%	1/5	20,00%	*UBXN6*	1/81	1,23%	1/1	100,00%
RPL29	5/81	6,17%	1/5	20,00%	*VIL1*	1/81	1,23%	1/1	100,00%
CDKN1β	5/81	6,17%	1/5	20,00%	*ZNF410*	1/81	1,23%	1/1	100,00%

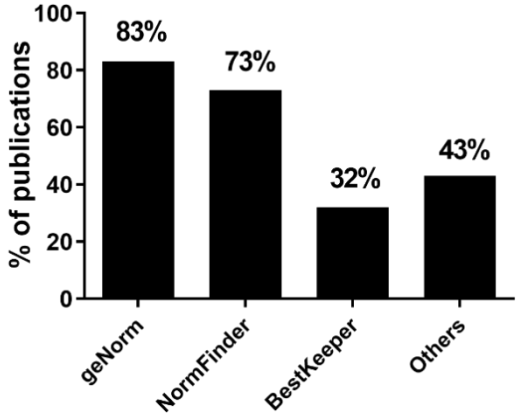

Figure 3: Frequency of the normalizing systems used in transcriptional studies in biomedical literature
The bar graph shows the frequency of the normalizing systems employed in a single publication. Data are based on 81 publications. Sum is higher than 100% as several normalizing systems are used in one publication.

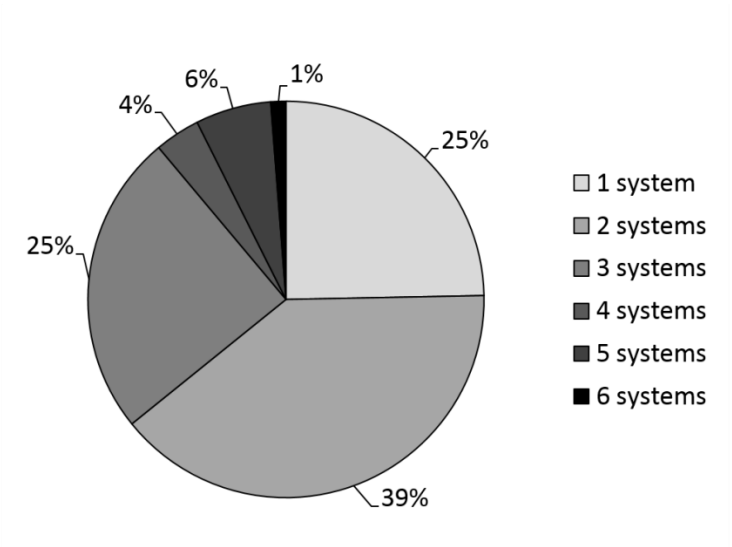

Figure 4: Frequency of the number of normalizing systems used in a single publication
The pie chart shows the percentage distribution of the number of normalizing systems employed in a single publication. Data are based on 81 publications.

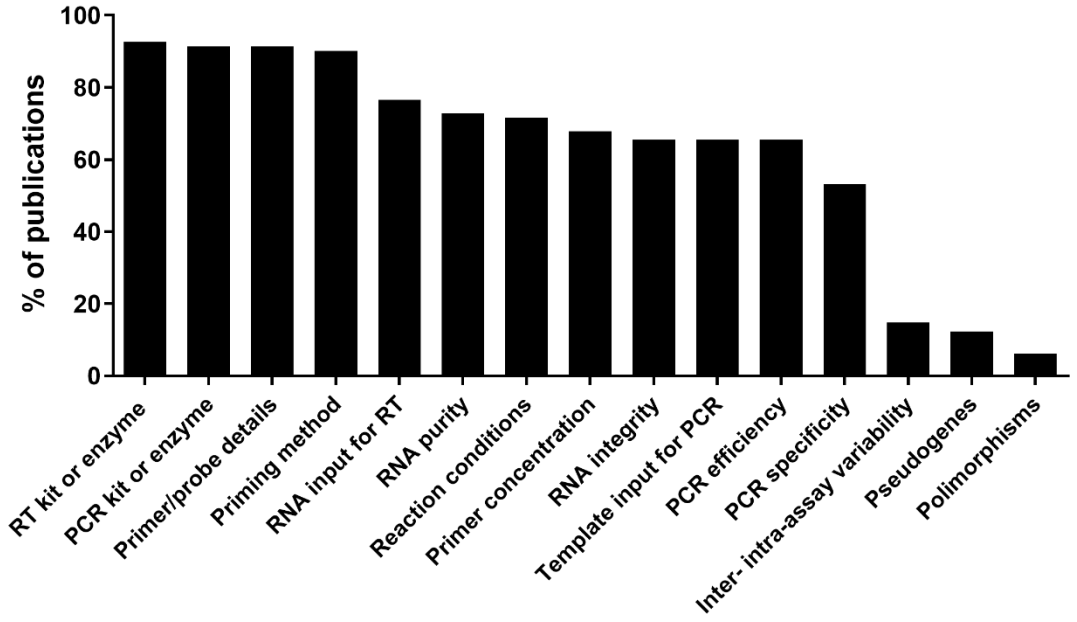

Figure 5: Analysis of adherence to MIQE guidelines
The bar graph shows the frequency of adherence to MIQE guidelines on the basis of the presence of experimental parameters data. Data are based on 81 publications.

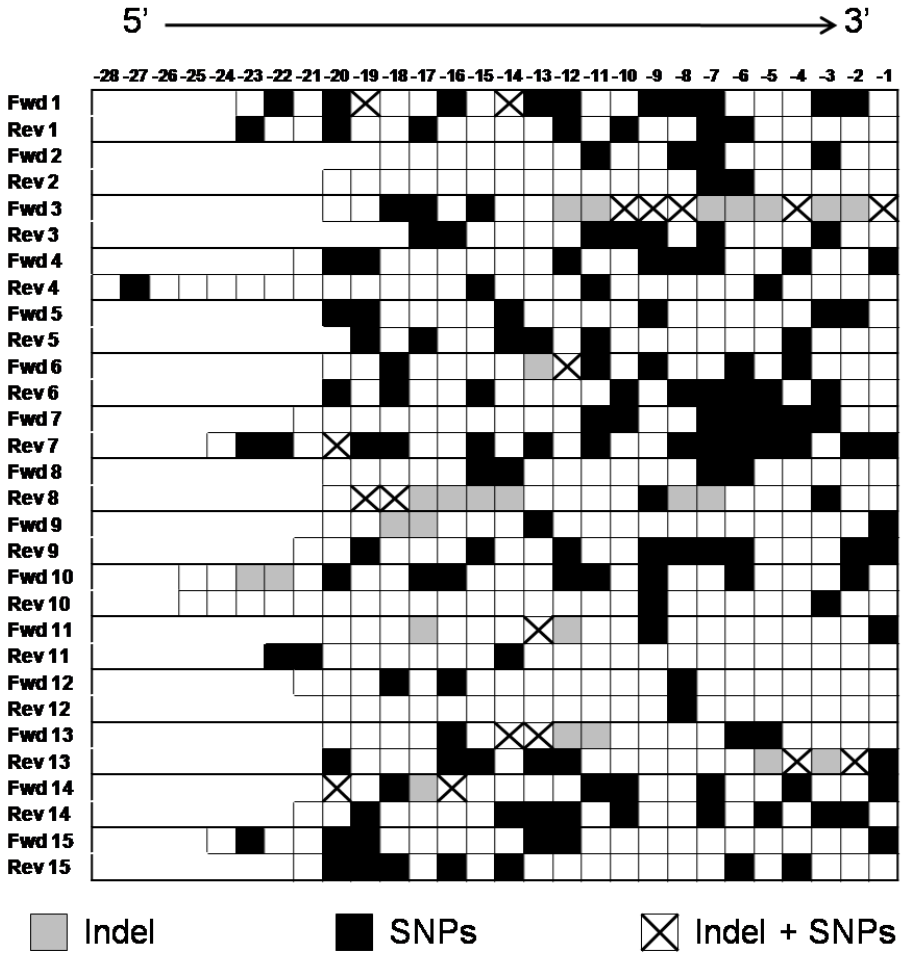

Figure 6: Localization of known mutations in 15 primer pair sequences randomly selected from the analyzed literature

Localization of known insertions/deletions (Indel), known single nucleotide polymorphisms (SNP) or both (Indel + SNP) in the genomic regions corresponding to a set of 15 randomly selected primer pairs (indicated as Fwd n and Rev n, where Fwd and Rev indicate forward and reverse primers, and n indicates the arbitrary number of the primer pair under examination) from 15 different genes, selected from the 81 publications analyzed. Each box indicates a primer nucleotide, numbered from -1 onwards starting from terminal 3'.

Appendix 4: Single Molecule Real-Time Sequencing of the M protein (SMaRT M-Seq): toward personalized medicine approaches in monoclonal gammopathies

Introduction

In patients affected by monoclonal gammopathies, tumoral B cells or plasma cells secrete a monoclonal antibody (termed M protein), which can be used to track the presence of the tumor itself. Moreover, the M protein can directly cause potentially life-threatening organ damage, which is dictated by the specific, patient's unique clonal light and/or heavy chain, as in patients affected by immunoglobulin light chain (AL) amyloidosis. Yet, the current paradigm in the diagnosis and management of these conditions treats the M protein as a simple tumor biomarker to be identified/quantified. Patients' specific M protein sequences remain mostly undefined and molecular mechanisms underlying M-protein related clinical manifestations are largely obscure.

Methods

By combining the unbiased amplification of expressed immunoglobulin genes with long-read, single molecule real-time DNA sequencing and bioinformatics analyses, we have established a method to identify the full-length sequence of the variable region of expressed immunoglobulin genes and to rank the obtained sequences based on their relative abundance, thus enabling the identification of the full-length variable sequence of M protein genes from a high number of patients analysed in parallel (Fig. 1).

Results

The assay, which we termed Single Molecule Real-Time Sequencing of the M protein (SMaRT M-Seq), has undergone an extensive technical validation. Sequencing of contrived bone marrow samples generated through serial dilutions of plasma cell lines into control bone marrow, as well as sequencing of *bona fide* bone marrow samples from AL patients and comparison with gold-standard techniques of immunoglobulin gene sequencing showed:

1) 100% sequence-accuracy at the individual base-pair level;
2) High repeatability (CV<0.8% for sequencing of pentaplicates) in defining the molecular clonal size (i.e. the fraction of total immunoglobulin sequences coinciding with the clonal sequence);

3) A high sensitivity in identifying clonal immunoglobulin sequences (10^{-3} when employing low-coverage sequencing on multiple, pooled samples) (Fig. 2).

Noteworthy, SMaRT M Seq was applied to a cohort of 86 consecutive patients with AL amyloidosis (17 κ and 69 λ; median BMPC infiltration 9%, IQR 6-13%; median dFLC 176 mg/L, IQR 75-370 mg/L), including cases with small clonal burden and M protein which was undetectable with conventional M protein studies. A full-length sequence of the variable region of the clonal light chain was obtained in all patients (median molecular clonal size of 88.3%, IQR: 70.7 – 93%) (Fig. 3). The most common κ germline genes were *IGKV1-33* and *IGKV4-01* (24% each of the 17 κ AL patients), and the most common λ germline genes were *IGLV6-57* (26% of the 69 λ AL patients), *IGLV2-14* (17%), *IGLV3-01* (17%) and *IGLV1-44* (10%). The most frequent λ and κ germline genes together (*IGLV6-57*, *IGLV2-14*, *IGLV3-01*, *IGLV1-44*, *IGKV1-33* and *IGKV4-01*) accounted for 66% of all the clones. Germline gene usage correlated with selected clinical features.

Sequence information was then exploited to improve mass spectrometry-based amyloid typing on fat pad aspirates (Fig. 4) and to enable the sensitive detection of clonotypic sequences using short-read DNA sequencing of the involved light chain isotype (data not shown).

Conclusions

We have established SMaRT M-Seq as a novel valuable assay to reliably identify the full-length variable sequence of M proteins. SMaRT M-Seq has undergone extensive technical validation, showing high accuracy, repeatability and sensitivity. The latter is determined by the number of reads analyzed per sample. This is in turn dictated by the sequencing output of the employed sequencing platform, and by the number of pooled samples analyzed in a given sequencing round, thus proving to be scalable. Even when analyzing multiple samples on a sequencing platform with low sequencing output, the achieved sensitivity of SMaRT M-Seq significantly exceeds the requirements for the identification of clonal B cells/plasma cells in patients with AL amyloidosis.

Sequencing disease-associated M proteins from large cohorts of patients has the potential to uncover molecular mechanisms of M protein-related clinical manifestations which have remained largely unexplored so far and could enable approaches of personalized medicine for the sensitive detection of patients' specific M proteins at diagnosis and after anti-clonal therapy.

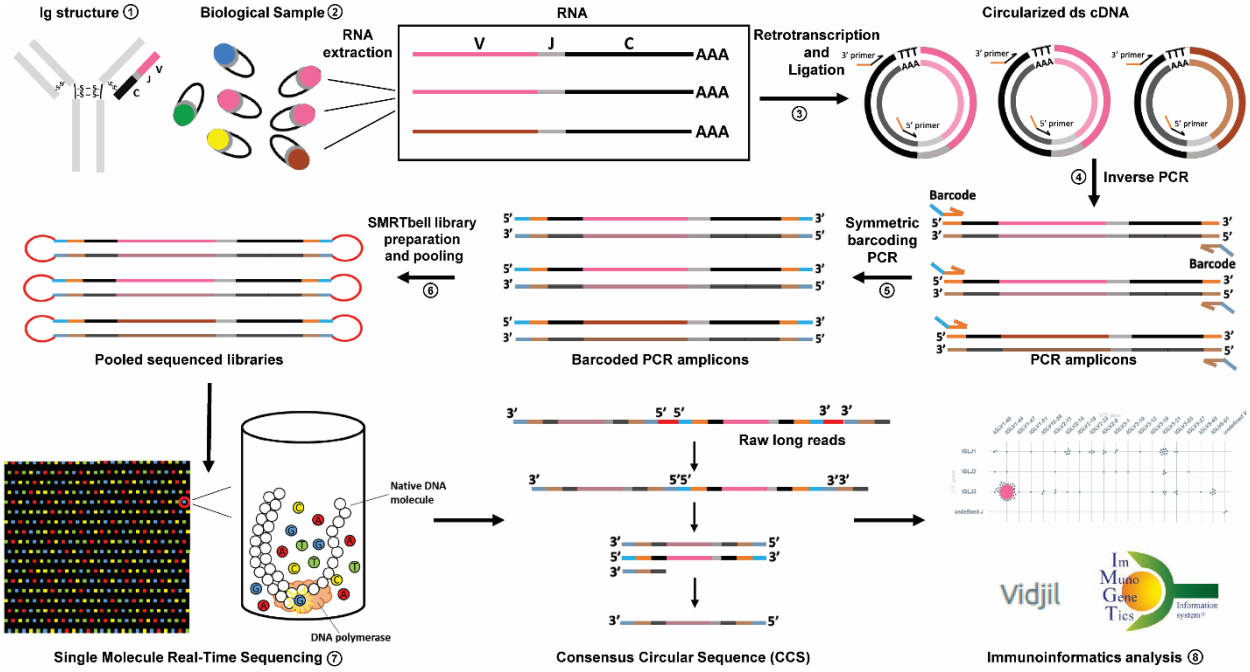

Fig. 1 Single Molecule Real-Time Sequencing of the M protein (SMaRT M-Seq)
Schematic representation of the workflow underlying SMaRT M-Seq. The purpose of the assay is to obtain the full-length sequence of the variable region of immunoglobulin (Ig) light (or heavy) chains (①) and to rank the obtained sequences based on their relative abundance, so as to identify potential dominant (clonal) sequences, if a B cell or plasma cell clone is present in the biological sample (e.g., bone-marrow derived mononuclear cells) (②). Total RNA is extracted from the biological sample, mRNA is retrotranscribed using an anchored oligo-dT and double stranded complementary DNA (ds cDNA) is synthetized and circularized (③). Two primers (in black) annealing to the constant region of the isotype of interest and containing an adaptor sequence (in orange) are used in the context of an inverse PCR using a high-fidelity DNA polymerase to obtain an amplicon comprising the entire variable region (④). Two primers (in orange) annealing to the adaptor sequence and containing sample ID barcodes (in cyan) are used to generate barcoded amplicons (⑤) which are used for library preparation with bell-adaptors (⑥) and subjected to single-molecule real-time sequencing (⑦). Computational methods are employed to analyze raw long reads and to extract circular consensus sequences (CCS). Immunoinformatic analyses, including Vidjil and IMGT/HighV-QUEST, are used to scrutinize repertoires and identify dominant clones (⑧).

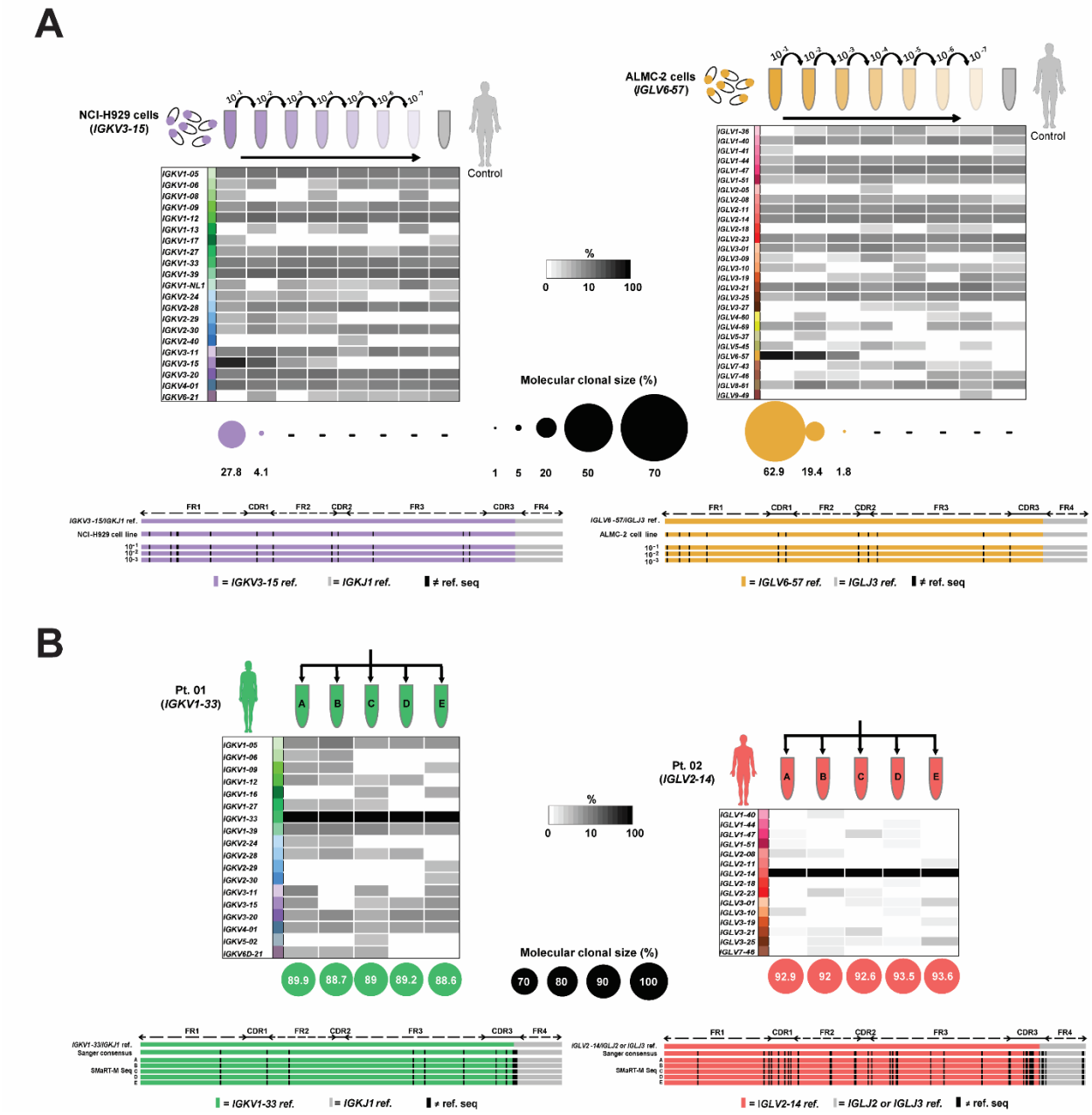

Figure 2: Technical validation of SMaRT M-Seq

(A) Expression levels (in shades of grey) of different *IGKV* (left) and *IGLV* (right) germline genes (each denoted by a distinctive colour) as assessed by SMaRT M-Seq, starting from serial Log_{10} dilutions of RNA from *IGKV3-15*-secreting NCI-H929 cells (left) or *IGLV6-57*-secreting ALMC-2 cells (right) into RNA of the bone marrow from a control subject (unspiked control sample in grey). **(B)** Expression levels of different *IGKV* (left) and *IGLV* (right) germline genes as assessed by SMaRT M-Seq, starting from five replicate bone marrow samples (A to E) from two patients (Pt. 01 and 02) affected by AL amyloidosis, with a plasma cell clone secreting an *IGKV1-33* (left) or an *IGLV2-14* (right) clonal light chain. In both (**A**) and (**B**), scaled pie charts denote the molecular clonal size of the dominant clone identified in each tested sample (the corresponding *IGKV* or *IGLV* germline gene is indicated with the pie chart colour). Minus sign (-) indicate samples where no dominant clone could be identified with Vidjil. At the bottom, sequence alignments of the clonotypic variable region of the light chain secreted by NCI-H929 and ALMC-2 cells (**A**) or of the clonal light chain from patient 01 and patient 02 (**B**), as assessed by cloning and Sanger sequencing (Sanger) or by SMaRT M-Seq (denoted by the corresponding dilution, A, or replicate label, B), with the corresponding *IGKV/IGKJ* or *IGLV/IGLJ* germline genes (ref., with the J gene in grey and the V gene denoted by the

corresponding colour). Black tick denotes sequence mismatches (≠ ref. seq.) in the clonotypic light chain with respect to the corresponding germline genes. FR: framework region; CDR: complementarity determining region; Pt.: patient.

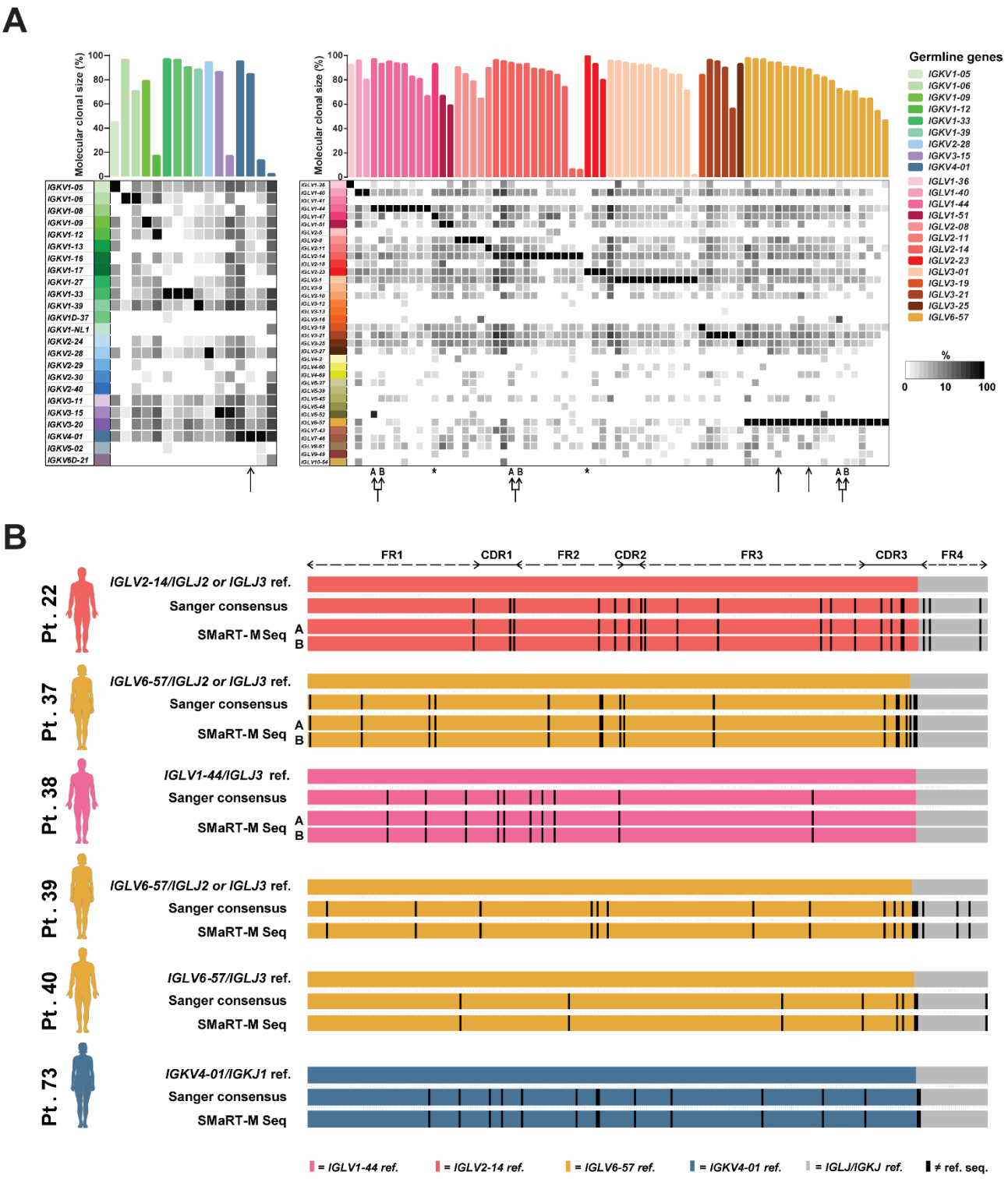

Figure 3: SMaRT M-Seq identifies the full-length variable sequence of clonal light chains in a cohort of AL patients

(A) Expression levels of different *IGKV* (left) and *IGLV* (right) germline genes (each denoted by a distinctive colour) as assessed by SMaRT M-Seq, starting from the bone marrow of 84 affected by AL amyloidosis analyzed in parallel in one sequencing round. Bar graphs indicate the molecular clonal

size of the dominant clone identified by Vidjil analysis in each tested sample (the corresponding germline gene is indicated with the bar colour). In two patients (*) the dominant clone was identified by IMGT/HighV-Quest. Three patients were analyzed in duplicates (arrows). (**B)** Sequence alignments of the clonal light chain from six patients as assessed by cloning and Sanger sequencing (Sanger) or by SMaRT M-Seq (A-B indicate technical duplicates), with the corresponding *IGKV*/*IGKJ* or *IGLV*/*IGLJ* germline genes (ref., with the J gene in grey and the V gene denoted by the corresponding colour). Black tick denotes sequence mismatches (≠ ref. seq.) in the clonotypic light chain with respect to the corresponding germline genes. FR: framework region; CDR: complementarity determining region; Pt.: patient.

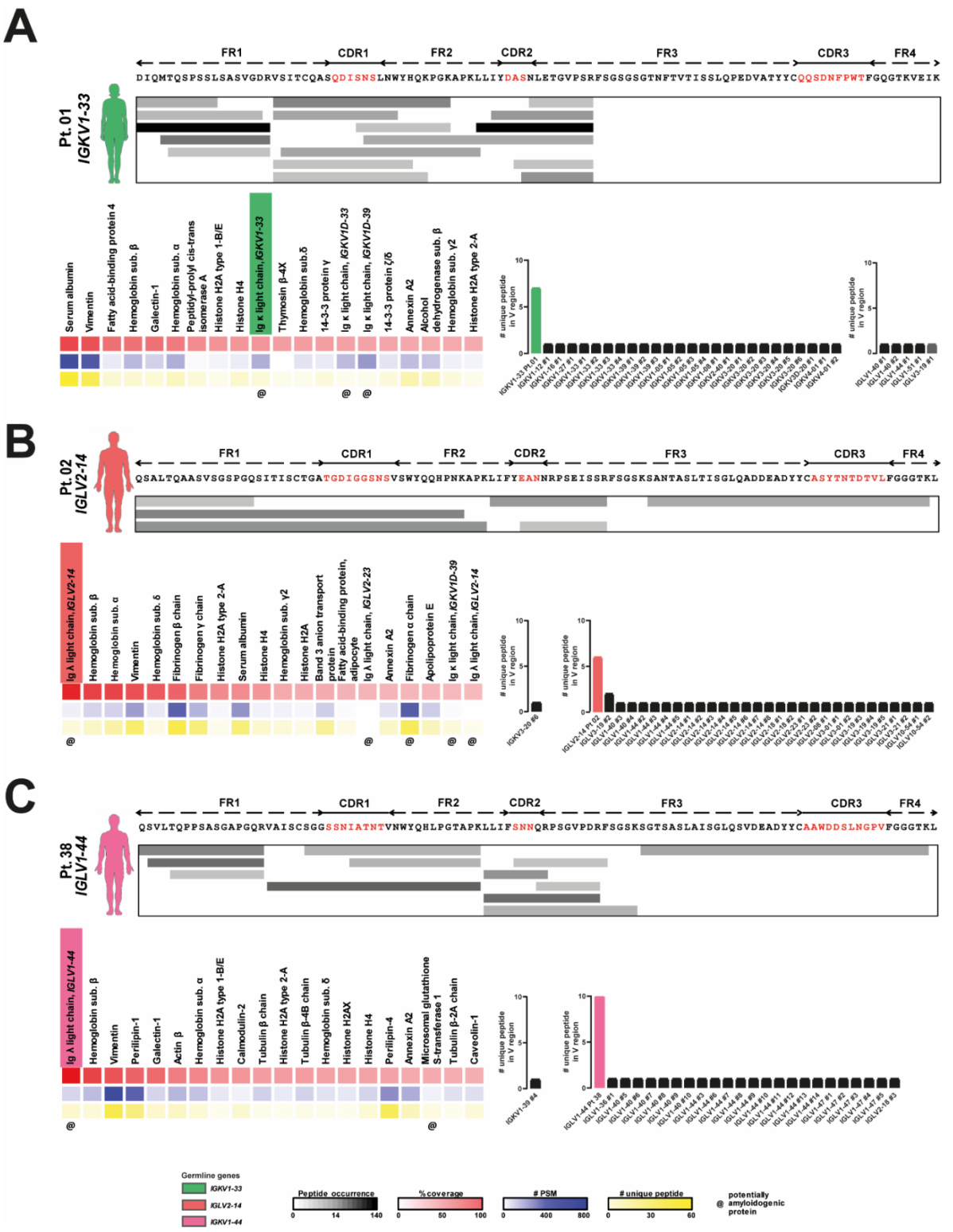

Figure 4: Mass spectrometry-based amyloid typing exploiting full-length variable light chain sequence knowledge

A-C Top: Liquid chromatography and tandem mass spectrometry in fat pad tissue from three AL patients. Peptide ions mapping is performed against an augmented database including the human proteome, known immunoglobulin sequences from public databases and each patient's clonal light chain sequence (protein sequence predicted based on the nucleotide sequence determined through SMaRT M-Seq). Physical distribution and absolute number (in shades of grey) of peptide ions mapping against each patient's clonal light chain sequence. Bottom, left: Heatmaps show the 20

proteins with the highest sequence coverage identified in each patient's fat pad, with their relative coverage (shades of red), absolute number of peptide-spectrum match (PSM, shades of blue) and absolute number of unique peptides (shades of yellow). Bottom, right: Bar graphs indicate the number of unique peptides assigned to κ or λ light chains. Patient's clonal light chain is colored according to the corresponding germline gene. Other light chains are designated with their corresponding germline gene and a progressive number. FR: framework region, CDR: complementarity determining region, Pt.: patient.

Bibliography

1 Merlini, G. & Stone, M. J. Dangerous small B-cell clones. *Blood* **108**, 2520-2530, doi:10.1182/blood-2006-03-001164 (2006).

2 Fermand, J. P. *et al.* Monoclonal gammopathy of clinical significance: a novel concept with therapeutic implications. *Blood* **132**, 1478-1485, doi:10.1182/blood-2018-04-839480 (2018).

3 Merlini, G. & Bellotti, V. Molecular mechanisms of amyloidosis. *N Engl J Med* **349**, 583-596, doi:10.1056/NEJMra023144 (2003).

4 Bellotti, V., Mangione, P. & Merlini, G. Review: immunoglobulin light chain amyloidosis--the archetype of structural and pathogenic variability. *J Struct Biol* **130**, 280-289, doi:10.1006/jsbi.2000.4248 (2000).

5 Chiti, F. & Dobson, C. M. Protein Misfolding, Amyloid Formation, and Human Disease: A Summary of Progress Over the Last Decade. *Annu Rev Biochem* **86**, 27-68, doi:10.1146/annurev-biochem-061516-045115 (2017).

6 Merlini, G. *et al.* Systemic immunoglobulin light chain amyloidosis. *Nat Rev Dis Primers* **4**, 38, doi:10.1038/s41572-018-0034-3 (2018).

7 Kyle, R. A. *et al.* Incidence of AL Amyloidosis in Olmsted County, Minnesota, 1990 through 2015. *Mayo Clin Proc* **94**, 465-471, doi:10.1016/j.mayocp.2018.08.041 (2019).

8 Duhamel, S. *et al.* Incidence and prevalence of light chain amyloidosis: a population-based study. *Blood* **130**, 5577 (2017).

9 Quock, T. P., Yan, T., Chang, E., Guthrie, S. & Broder, M. S. Epidemiology of AL amyloidosis: a real-world study using US claims data. *Blood Adv* **2**, 1046-1053, doi:10.1182/bloodadvances.2018016402 (2018).

10 Gertz, M. A. & Dispenzieri, A. Systemic Amyloidosis Recognition, Prognosis, and Therapy: A Systematic Review. *JAMA* **324**, 79-89, doi:10.1001/jama.2020.5493 (2020).

11 Weiss, B. M., Lund, S. H., Bjorkholm, M., Cohen, A. D., Dember, L., Landgren, O., & Kristinsson, S. Y. Improved survival in AL amyloidosis: a population-based study on 1,430 patients diagnosed in Sweden 1995-2013. *Blood* **128** (2016).

12 Desport, E. *et al.* Al amyloidosis. *Orphanet J Rare Dis* **7**, 54, doi:10.1186/1750-1172-7-54 (2012).

13 Muchtar, E. *et al.* Improved outcomes for newly diagnosed AL amyloidosis between 2000 and 2014: cracking the glass ceiling of early death. *Blood* **129**, 2111-2119, doi:10.1182/blood-2016-11-751628 (2017).

14 Palladini, G. *et al.* Melphalan and dexamethasone with or without bortezomib in newly diagnosed AL amyloidosis: a matched case-control study on 174 patients. *Leukemia* **28**, 2311-2316, doi:10.1038/leu.2014.227 (2014).

15 Palladini, G. *et al.* A European collaborative study of cyclophosphamide, bortezomib, and dexamethasone in upfront treatment of systemic AL amyloidosis. *Blood* **126**, 612-615, doi:10.1182/blood-2015-01-620302 (2015).

16 Kastritis E, L. X., Arnulf B, Zamagni E, Cibeira MT, Kwok F, Mollee P, Hajek R, Moreau P, Jaccard A, Schönland S, Filshie R, Virelizier EN, Augustson B, Mateos MV, Wechalekar A, Hachulla E, Milani P, Dimopoulos MA, Fermand JP, Foli A, Gavriatopoulou M, Palumbo A, Sonneveld P, Johnsen HE, Merlini G, Palladini G A Randomized Phase III Trial of Melphalan and Dexamethasone (MDex) Versus Bortezomib, Melphalan and Dexamethasone (BMDex) for Untreated Patients with AL Amyloidosis. *Blood* **128** (2016).

17 da Silva Filho, M. I. *et al.* Genome-wide association study of immunoglobulin light chain amyloidosis in three patient cohorts: comparison with myeloma. *Leukemia* **31**, 1735-1742, doi:10.1038/leu.2016.387 (2017).

18 Kyle, R. A. Monoclonal gammopathy of undetermined significance. Natural history in 241 cases. *Am J Med* **64**, 814-826, doi:10.1016/0002-9343(78)90522-3 (1978).

19 Kyle, R. A. *et al.* Long-Term Follow-up of Monoclonal Gammopathy of Undetermined Significance. *N Engl J Med* **378**, 241-249, doi:10.1056/NEJMoa1709974 (2018).

20 Kyle, R. A. *et al.* A long-term study of prognosis in monoclonal gammopathy of undetermined significance. *N Engl J Med* **346**, 564-569, doi:10.1056/NEJMoa01133202 (2002).
21 Kourelis, T. V. *et al.* Immunoglobulin light chain amyloidosis is diagnosed late in patients with preexisting plasma cell dyscrasias. *Am J Hematol* **89**, 1051-1054, doi:10.1002/ajh.23827 (2014).
22 Palladini, G. *et al.* Multicentre versus single centre approach to rare diseases: the model of systemic light chain amyloidosis. *Amyloid* **12**, 120-126, doi:10.1080/13506120500107055 (2005).
23 Rutten, K. H. G. *et al.* Haematological response and overall survival in two consecutive Dutch patient cohorts with AL amyloidosis diagnosed between 2008 and 2016. *Amyloid* **25**, 227-233, doi:10.1080/13506129.2018.1536043 (2018).
24 Lousada, I., Comenzo, R. L., Landau, H., Guthrie, S. & Merlini, G. Light Chain Amyloidosis: Patient Experience Survey from the Amyloidosis Research Consortium. *Adv Ther* **32**, 920-928, doi:10.1007/s12325-015-0250-0 (2015).
25 Hester, L. L. *et al.* Diagnostic delay and characterization of the clinical prodrome in AL amyloidosis among 1523 US adults diagnosed between 2001 and 2019. *Eur J Haematol* **107**, 428-435, doi:10.1111/ejh.13679 (2021).
26 Thakral, B. & Kanagal-Shamanna, R. Systemic AL amyloidosis associated with Waldenstrom macroglobulinemia: an unusual presenting complication. *Blood* **127**, 168, doi:10.1182/blood-2015-10-674895 (2016).
27 Jones, C. H., Kanagasundaram, N. S., Coral, A. P., Coyne, J. D. & Will, E. J. Combined Waldenstrom's macroglobulinaemia associated AL and beta-2-microglobulin amyloidosis. *Nephrol Dial Transplant* **12**, 2708-2712, doi:10.1093/ndt/12.12.2708 (1997).
28 Ishiguro, T. *et al.* Waldenstrom's macroglobulinemia accompanying systemic amyloidosis: the usefulness of endobronchial ultrasound-guided transbronchial needle aspiration for detecting amyloid deposits. *Intern Med* **53**, 2789-2793, doi:10.2169/internalmedicine.53.2907 (2014).
29 Gertz, M. A., Kyle, R. A. & Noel, P. Primary systemic amyloidosis: a rare complication of immunoglobulin M monoclonal gammopathies and Waldenstrom's macroglobulinemia. *J Clin Oncol* **11**, 914-920, doi:10.1200/JCO.1993.11.5.914 (1993).
30 Cohen, A. D. *et al.* Systemic AL amyloidosis due to non-Hodgkin's lymphoma: an unusual clinicopathologic association. *Br J Haematol* **124**, 309-314, doi:10.1046/j.1365-2141.2003.04779.x (2004).
31 Telio, D. *et al.* Two distinct syndromes of lymphoma-associated AL amyloidosis: a case series and review of the literature. *Am J Hematol* **85**, 805-808, doi:10.1002/ajh.21814 (2010).
32 Benson, M. D. *et al.* Amyloid nomenclature 2020: update and recommendations by the International Society of Amyloidosis (ISA) nomenclature committee. *Amyloid* **27**, 217-222, doi:10.1080/13506129.2020.1835263 (2020).
33 Basset, M. *et al.* Nonlymphoplasmacytic lymphomas associated with light-chain amyloidosis. *Blood* **135**, 293-296, doi:10.1182/blood.2019002762 (2020).
34 Ikee, R., Kobayashi, S., Hemmi, N., Suzuki, S. & Miura, S. Amyloidosis associated with chronic lymphocytic leukemia. *Amyloid* **12**, 131-134, doi:10.1080/13506120500107261 (2005).
35 Kourelis, T. V. *et al.* Systemic amyloidosis associated with chronic lymphocytic leukemia/small lymphocytic lymphoma. *Am J Hematol* **88**, 375-378, doi:10.1002/ajh.23413 (2013).
36 Adami, F. *et al.* Coexistence of primary AL amyloidosis and POEMS syndrome: efficacy of melphalan-dexamethasone and role of biochemical markers in monitoring the diseases course. *Am J Hematol* **85**, 131-132, doi:10.1002/ajh.21581 (2010).
37 Adams, D. *et al.* [New elements in the diagnosis and the treatment of primary AL amyloid polyneuropathy and neuropathy due to POEMS syndrome]. *Rev Neurol (Paris)* **167**, 57-63, doi:10.1016/j.neurol.2010.07.042 (2011).
38 Sobue, Y. *et al.* Coexistence of amyloidosis and light chain deposition disease in the heart. *Cardiovasc Pathol* **51**, 107315, doi:10.1016/j.carpath.2020.107315 (2021).

39 Faa, G. *et al.* Light chain deposition disease of the liver associated with AL-type amyloidosis and severe cholestasis. *J Hepatol* **12**, 75-82, doi:10.1016/0168-8278(91)90913-v (1991).

40 Said, S. M. *et al.* The characteristics of patients with kidney light chain deposition disease concurrent with light chain amyloidosis. *Kidney Int*, doi:10.1016/j.kint.2021.10.019 (2021).

41 Hofmann-Guilaine, C. *et al.* Association light chain deposition disease (LCDD) and amyloidosis. One case. *Pathol Res Pract* **180**, 214-219, doi:10.1016/S0344-0338(85)80177-1 (1985).

42 Said, S. M. *et al.* The characteristics of patients with kidney light chain deposition disease concurrent with light chain amyloidosis. *Kidney Int*, doi:10.1016/j.kint.2021.10.019 (2021).

43 Muchtar, E. *et al.* A Modern Primer on Light Chain Amyloidosis in 592 Patients With Mass Spectrometry-Verified Typing. *Mayo Clin Proc* **94**, 472-483, doi:10.1016/j.mayocp.2018.08.006 (2019).

44 Kourelis, T. V. *et al.* Coexistent multiple myeloma or increased bone marrow plasma cells define equally high-risk populations in patients with immunoglobulin light chain amyloidosis. *J Clin Oncol* **31**, 4319-4324, doi:10.1200/JCO.2013.50.8499 (2013).

45 Perfetti, V. *et al.* AL amyloidosis. Characterization of amyloidogenic cells by anti-idiotypic monoclonal antibodies. *Lab Invest* **71**, 853-861 (1994).

46 McElroy, E. A., Jr., Witzig, T. E., Gertz, M. A., Greipp, P. R. & Kyle, R. A. Detection of monoclonal plasma cells in the peripheral blood of patients with primary amyloidosis. *Br J Haematol* **100**, 326-327, doi:10.1046/j.1365-2141.1998.00583.x (1998).

47 Perfetti, V. *et al.* Cells with clonal light chains are present in peripheral blood at diagnosis and in apheretic stem cell harvests of primary amyloidosis. *Bone Marrow Transplant* **23**, 323-327, doi:10.1038/sj.bmt.1701590 (1999).

48 Manske, M. K. *et al.* Quantitative analysis of clonal bone marrow CD19+ B cells: use of B cell lineage trees to delineate their role in the pathogenesis of light chain amyloidosis. *Clin Immunol* **120**, 106-120, doi:10.1016/j.clim.2006.01.008 (2006).

49 Perfetti, V. *et al.* Translocation T(4;14)(p16.3;q32) is a recurrent genetic lesion in primary amyloidosis. *Am J Pathol* **158**, 1599-1603, doi:10.1016/S0002-9440(10)64115-6 (2001).

50 Comenzo, R. L. *et al.* Mobilized CD34+ cells selected as autografts in patients with primary light-chain amyloidosis: rationale and application. *Transfusion* **38**, 60-69, doi:10.1046/j.1537-2995.1998.38198141500.x (1998).

51 Pardanani, A. *et al.* Circulating peripheral blood plasma cells as a prognostic indicator in patients with primary systemic amyloidosis. *Blood* **101**, 827-830, doi:10.1182/blood-2002-06-1698 (2003).

52 Sidana, S. *et al.* Prognostic significance of circulating plasma cells by multi-parametric flow cytometry in light chain amyloidosis. *Leukemia* **32**, 1421-1426, doi:10.1038/s41375-018-0063-7 (2018).

53 Solomon, A., Macy, S. D., Wooliver, C., Weiss, D. T. & Westermark, P. Splenic plasma cells can serve as a source of amyloidogenic light chains. *Blood* **113**, 1501-1503, doi:10.1182/blood-2008-04-154484 (2009).

54 Gertz, M. A., Kyle, R. A. & Greipp, P. R. The plasma cell labeling index: a valuable tool in primary systemic amyloidosis. *Blood* **74**, 1108-1111 (1989).

55 Sidiqi, M. H. *et al.* Plasma cell proliferative index predicts outcome in immunoglobulin light chain amyloidosis treated with stem cell transplantation. *Haematologica* **103**, 1229-1234, doi:10.3324/haematol.2018.189985 (2018).

56 Rajkumar, S. V., Gertz, M. A. & Kyle, R. A. Primary systemic amyloidosis with delayed progression to multiple myeloma. *Cancer* **82**, 1501-1505 (1998).

57 Oliva, L. *et al.* The amyloidogenic light chain is a stressor that sensitizes plasma cells to proteasome inhibitor toxicity. *Blood* **129**, 2132-2142, doi:10.1182/blood-2016-08-730978 (2017).

58 Fraser, C., Sanchorawala, V., Sarosiek, K. & Sarosiek, S. Clonal plasma cells in AL amyloidosis are dependent on anti-apoptotic BCL-2 family proteins. *Blood* **132**, 2654 (2018).

59 Arendt, B. K. *et al.* Biologic and genetic characterization of the novel amyloidogenic lambda light chain-secreting human cell lines, ALMC-1 and ALMC-2. *Blood* **112**, 1931-1941, doi:10.1182/blood-2008-03-143040 (2008).

60 Drexler, H. G. & Matsuo, Y. Malignant hematopoietic cell lines: in vitro models for the study of multiple myeloma and plasma cell leukemia. *Leuk Res* **24**, 681-703, doi:10.1016/s0145-2126(99)00195-2 (2000).
61 Sarin, V. *et al.* Evaluating the efficacy of multiple myeloma cell lines as models for patient tumors via transcriptomic correlation analysis. *Leukemia* **34**, 2754-2765, doi:10.1038/s41375-020-0785-1 (2020).
62 Yaccoby, S., Barlogie, B. & Epstein, J. Primary myeloma cells growing in SCID-hu mice: a model for studying the biology and treatment of myeloma and its manifestations. *Blood* **92**, 2908-2913 (1998).
63 Calimeri, T. *et al.* A unique three-dimensional SCID-polymeric scaffold (SCID-synth-hu) model for in vivo expansion of human primary multiple myeloma cells. *Leukemia* **25**, 707-711, doi:10.1038/leu.2010.300 (2011).
64 Das, R. *et al.* Microenvironment-dependent growth of preneoplastic and malignant plasma cells in humanized mice. *Nat Med* **22**, 1351-1357, doi:10.1038/nm.4202 (2016).
65 Hayman, S. R. *et al.* Translocations involving the immunoglobulin heavy-chain locus are possible early genetic events in patients with primary systemic amyloidosis. *Blood* **98**, 2266-2268, doi:10.1182/blood.v98.7.2266 (2001).
66 Fonseca, R., Harrington, D., Oken, M. M., Dewald, G. W., Bailey, R. J., Van Wier, S. A., ... & Greipp, P. R. Prognostic significance of 13q deletions and the t (11; 14)(q13; q32) in myeloma (MM); An interphase FISH study of 351 patients entered into the Eastern Cooperative Oncology Group E9487 clinical trial. *Blood* **96** (2000).
67 Warsame, R. *et al.* Abnormal FISH in patients with immunoglobulin light chain amyloidosis is a risk factor for cardiac involvement and for death. *Blood Cancer J* **5**, e310, doi:10.1038/bcj.2015.34 (2015).
68 Bochtler, T. *et al.* Hyperdiploidy is less frequent in AL amyloidosis compared with monoclonal gammopathy of undetermined significance and inversely associated with translocation t(11;14). *Blood* **117**, 3809-3815, doi:10.1182/blood-2010-02-268987 (2011).
69 Bochtler, T. *et al.* Gain of chromosome 1q21 is an independent adverse prognostic factor in light chain amyloidosis patients treated with melphalan/dexamethasone. *Amyloid: The International Journal of Experimental and Clinical Investigation: The Official Journal of the International Society of Amyloidosis* **21**, 9-17, doi:10.3109/13506129.2013.854766 (2014).
70 Bochtler, T. *et al.* Cytogenetic intraclonal heterogeneity of plasma cell dyscrasia in AL amyloidosis as compared with multiple myeloma. *Blood Adv* **2**, 2607-2618, doi:10.1182/bloodadvances.2018023200 (2018).
71 Bochtler, T. *et al.* Translocation t(11;14) is associated with adverse outcome in patients with newly diagnosed AL amyloidosis when treated with bortezomib-based regimens. *J Clin Oncol* **33**, 1371-1378, doi:10.1200/JCO.2014.57.4947 (2015).
72 Bochtler, T. *et al.* Prognostic impact of cytogenetic aberrations in AL amyloidosis patients after high-dose melphalan: a long-term follow-up study. *Blood* **128**, 594-602, doi:10.1182/blood-2015-10-676361 (2016).
73 Paiva, B. *et al.* Phenotypic, transcriptomic, and genomic features of clonal plasma cells in light-chain amyloidosis. *Blood* **127**, 3035-3039, doi:10.1182/blood-2015-10-673095 (2016).
74 Granzow, M. *et al.* Novel recurrent chromosomal aberrations detected in clonal plasma cells of light chain amyloidosis patients show potential adverse prognostic effect: first results from a genome-wide copy number array analysis. *Haematologica* **102**, 1281-1290, doi:10.3324/haematol.2016.160721 (2017).
75 Chyra, Z. *et al.* Heterogenous mutation spectrum and deregulated cellular pathways in aberrant plasma cells underline molecular pathology of light-chain amyloidosis. *Haematologica* **106**, 601-604, doi:10.3324/haematol.2019.239756 (2021).
76 Boyle E M, A. C., Wardell CP, Rowczenio D, Sachchithanantham S, Wang Y, Johnson S, Bauer M, Weinhold N, Kaiser M, Johnson DC, Jones JR,.. Wechalekar AD. The genomic landscape of plasma cells in systemic light chain amyloidosis. *Blood* **132** (2018).
77 Huang, X. F. *et al.* Genomic profiling in amyloid light-chain amyloidosis reveals mutation profiles associated with overall survival. *Amyloid* **27**, 36-44, doi:10.1080/13506129.2019.1678464 (2020).

78 Cuenca, I. *et al.* Immunogenetic characterization of clonal plasma cells in systemic light-chain amyloidosis. *Leukemia* **35**, 245-249, doi:10.1038/s41375-020-0800-6 (2021).
79 Puig, N. *et al.* Flow cytometry for fast screening and automated risk assessment in systemic light-chain amyloidosis. *Leukemia* **33**, 1256-1267, doi:10.1038/s41375-018-0308-5 (2019).
80 Abraham, R. S. *et al.* Functional gene expression analysis of clonal plasma cells identifies a unique molecular profile for light chain amyloidosis. *Blood* **105**, 794-803, doi:10.1182/blood-2004-04-1424 (2005).
81 Zhou, P. *et al.* Clonal plasma cell pathophysiology and clinical features of disease are linked to clonal plasma cell expression of cyclin D1 in systemic light-chain amyloidosis. *Clin Lymphoma Myeloma Leuk* **12**, 49-58, doi:10.1016/j.clml.2011.09.217 (2012).
82 Alameda, D. *et al.* Tumor cells in light-chain amyloidosis and myeloma show distinct transcriptional rewiring of normal plasma cell development. *Blood* **138**, 1583-1589, doi:10.1182/blood.2020009754 (2021).
83 Perfetti, V. *et al.* Analysis of V(lambda)-J(lambda) expression in plasma cells from primary (AL) amyloidosis and normal bone marrow identifies 3r (lambdaIII) as a new amyloid-associated germline gene segment. *Blood* **100**, 948-953, doi:10.1182/blood-2002-01-0114 (2002).
84 Abraham, R. S. *et al.* Immunoglobulin light chain variable (V) region genes influence clinical presentation and outcome in light chain-associated amyloidosis (AL). *Blood* **101**, 3801-3808, doi:10.1182/blood-2002-09-2707 (2003).
85 Comenzo, R. L., Zhang, Y., Martinez, C., Osman, K. & Herrera, G. A. The tropism of organ involvement in primary systemic amyloidosis: contributions of Ig V(L) germ line gene use and clonal plasma cell burden. *Blood* **98**, 714-720, doi:10.1182/blood.v98.3.714 (2001).
86 Prokaeva, T. *et al.* Soft tissue, joint, and bone manifestations of AL amyloidosis: clinical presentation, molecular features, and survival. *Arthritis Rheum* **56**, 3858-3868, doi:10.1002/art.22959 (2007).
87 Perfetti, V. *et al.* The repertoire of lambda light chains causing predominant amyloid heart involvement and identification of a preferentially involved germline gene, IGLV1-44. *Blood* **119**, 144-150, doi:10.1182/blood-2011-05-355784 (2012).
88 Hurle, M. R., Helms, L. R., Li, L., Chan, W. & Wetzel, R. A role for destabilizing amino acid replacements in light-chain amyloidosis. *Proc Natl Acad Sci U S A* **91**, 5446-5450, doi:10.1073/pnas.91.12.5446 (1994).
89 Helms, L. R. & Wetzel, R. Specificity of abnormal assembly in immunoglobulin light chain deposition disease and amyloidosis. *J Mol Biol* **257**, 77-86, doi:10.1006/jmbi.1996.0148 (1996).
90 Bellotti, V. & Merlini, G. Toward understanding the molecular pathogenesis of monoclonal immunoglobulin light-chain deposition. *Nephrol Dial Transplant* **11**, 1708-1711 (1996).
91 Raffen, R. *et al.* Physicochemical consequences of amino acid variations that contribute to fibril formation by immunoglobulin light chains. *Protein Sci* **8**, 509-517, doi:10.1110/ps.8.3.509 (1999).
92 Myatt, E. A. *et al.* Pathogenic potential of human monoclonal immunoglobulin light chains: relationship of in vitro aggregation to in vivo organ deposition. *Proc Natl Acad Sci U S A* **91**, 3034-3038, doi:10.1073/pnas.91.8.3034 (1994).
93 Baden, E. M., Randles, E. G., Aboagye, A. K., Thompson, J. R. & Ramirez-Alvarado, M. Structural insights into the role of mutations in amyloidogenesis. *J Biol Chem* **283**, 30950-30956, doi:10.1074/jbc.M804822200 (2008).
94 Poshusta, T. L. *et al.* Mutations in specific structural regions of immunoglobulin light chains are associated with free light chain levels in patients with AL amyloidosis. *PLoS One* **4**, e5169, doi:10.1371/journal.pone.0005169 (2009).
95 Garofalo, M. *et al.* Machine learning analyses of antibody somatic mutations predict immunoglobulin light chain toxicity. *Nat Commun* **12**, 3532, doi:10.1038/s41467-021-23880-9 (2021).
96 Rawat, P., Prabakaran, R., Kumar, S. & Gromiha, M. M. Exploring the sequence features determining amyloidosis in human antibody light chains. *Sci Rep* **11**, 13785, doi:10.1038/s41598-021-93019-9 (2021).

97 Weiss, B. M. *et al.* Increased serum free light chains precede the presentation of immunoglobulin light chain amyloidosis. *J Clin Oncol* **32**, 2699-2704, doi:10.1200/JCO.2013.50.0892 (2014).
98 Iadanza, M. G., Jackson, M. P., Hewitt, E. W., Ranson, N. A. & Radford, S. E. A new era for understanding amyloid structures and disease. *Nat Rev Mol Cell Biol* **19**, 755-773, doi:10.1038/s41580-018-0060-8 (2018).
99 Chiti, F. & Dobson, C. M. Amyloid formation by globular proteins under native conditions. *Nat Chem Biol* **5**, 15-22, doi:10.1038/nchembio.131 (2009).
100 Swuec, P. *et al.* Cryo-EM structure of cardiac amyloid fibrils from an immunoglobulin light chain AL amyloidosis patient. *Nat Commun* **10**, 1269, doi:10.1038/s41467-019-09133-w (2019).
101 Radamaker, L. *et al.* Cryo-EM structure of a light chain-derived amyloid fibril from a patient with systemic AL amyloidosis. *Nat Commun* **10**, 1103, doi:10.1038/s41467-019-09032-0 (2019).
102 Radamaker, L. *et al.* Cryo-EM reveals structural breaks in a patient-derived amyloid fibril from systemic AL amyloidosis. *Nat Commun* **12**, 875, doi:10.1038/s41467-021-21126-2 (2021).
103 Radamaker, L. *et al.* Role of mutations and post-translational modifications in systemic AL amyloidosis studied by cryo-EM. *Nat Commun* **12**, 6434, doi:10.1038/s41467-021-26553-9 (2021).
104 Nevone, A., Merlini, G. & Nuvolone, M. Treating Protein Misfolding Diseases: Therapeutic Successes Against Systemic Amyloidoses. *Front Pharmacol* **11**, 1024, doi:10.3389/fphar.2020.01024 (2020).
105 Mikhael, J. Turn off the Tap! The Need for Induction Therapy for AL Amyloidosis Before Transplantation. *Biol Blood Marrow Transplant* **24**, e1-e2, doi:10.1016/j.bbmt.2018.09.019 (2018).
106 Nuvolone, M. & Merlini, G. Redirecting proteoxicity. *Leukemia* **34**, 3109-3110, doi:10.1038/s41375-020-01028-w (2020).
107 Nuvolone, M. & Merlini, G. Systemic amyloidosis: novel therapies and role of biomarkers. *Nephrol Dial Transplant* **32**, 770-780, doi:10.1093/ndt/gfw305 (2017).
108 Minnema, M. C., Oostvogel, R., Raymakers, R. & Jak, M. Differences and similarities in treatment paradigms and goals between AL amyloidosis and multiple myeloma. *Hemato* **2**, 608-691 (2021).
109 Kaufman, G. P. & Cerchione, C. Beyond Andromeda: Improving Therapy for Light Chain Amyloidosis. *Front Oncol* **10**, 624573, doi:10.3389/fonc.2020.624573 (2020).
110 Sanchorawala, V. *et al.* Long-term outcome of patients with AL amyloidosis treated with high-dose melphalan and stem cell transplantation: 20-year experience. *Blood* **126**, 2345-2347, doi:10.1182/blood-2015-08-662726 (2015).
111 Sidiqi, M. H. *et al.* Stem Cell Transplantation for Light Chain Amyloidosis: Decreased Early Mortality Over Time. *J Clin Oncol* **36**, 1323-1329, doi:10.1200/JCO.2017.76.9554 (2018).
112 Sidana, S. *et al.* Fifteen year overall survival rates after autologous stem cell transplantation for AL amyloidosis. *Am J Hematol*, doi:10.1002/ajh.25566 (2019).
113 Hwa, Y. L. *et al.* Induction therapy pre-autologous stem cell transplantation in immunoglobulin light chain amyloidosis: a retrospective evaluation. *Am J Hematol* **91**, 984-988, doi:10.1002/ajh.24453 (2016).
114 Scharman, C. D. *et al.* Autologous Stem Cell Transplant in the Era of Bortezomib-Based Induction for AL Amyloidosis Results in Improved Hematologic Response Rates: a Single Institution 11 Year Experience. *Blood* **130**, 4552-4552 (2017).
115 Palladini, G. *et al.* Circulating amyloidogenic free light chains and serum N-terminal natriuretic peptide type B decrease simultaneously in association with improvement of survival in AL. *Blood* **107**, 3854-3858, doi:10.1182/blood-2005-11-4385 (2006).
116 Kastritis, E. *et al.* Evaluation of minimal residual disease using next-generation flow cytometry in patients with AL amyloidosis. *Blood Cancer J* **8**, 46, doi:10.1038/s41408-018-0086-3 (2018).

117 Palladini, G. *et al.* Minimal residual disease negativity by next-generation flow cytometry is associated with improved organ response in AL amyloidosis. *Blood Cancer J* **11**, 34, doi:10.1038/s41408-021-00428-0 (2021).
118 Mao, Y. Structure, Dynamics and Function of the 26S Proteasome. *Subcell Biochem* **96**, 1-151, doi:10.1007/978-3-030-58971-4_1 (2021).
119 Tanaka, K. The proteasome: overview of structure and functions. *Proc Jpn Acad Ser B Phys Biol Sci* **85**, 12-36, doi:10.2183/pjab.85.12 (2009).
120 Farshi, P. *et al.* Deubiquitinases (DUBs) and DUB inhibitors: a patent review. *Expert Opin Ther Pat* **25**, 1191-1208, doi:10.1517/13543776.2015.1056737 (2015).
121 Sgorbissa, A., Potu, H. & Brancolini, C. Isopeptidases in anticancer therapy: looking for inhibitors. *Am J Transl Res* **2**, 235-247 (2010).
122 Katz, E. J., Isasa, M. & Crosas, B. A new map to understand deubiquitination. *Biochem Soc Trans* **38**, 21-28, doi:10.1042/BST0380021 (2010).
123 Bernassola, F., Ciechanover, A. & Melino, G. The ubiquitin proteasome system and its involvement in cell death pathways. *Cell Death Differ* **17**, 1-3, doi:10.1038/cdd.2009.189 (2010).
124 Collins, G. A. & Goldberg, A. L. The Logic of the 26S Proteasome. *Cell* **169**, 792-806, doi:10.1016/j.cell.2017.04.023 (2017).
125 D'Arcy, P. & Linder, S. Proteasome deubiquitinases as novel targets for cancer therapy. *Int J Biochem Cell Biol* **44**, 1729-1738, doi:10.1016/j.biocel.2012.07.011 (2012).
126 Merlini, G. AL amyloidosis: from molecular mechanisms to targeted therapies. *Hematology Am Soc Hematol Educ Program* **2017**, 1-12, doi:10.1182/asheducation-2017.1.1 (2017).
127 Gertz, M. A. Immunoglobulin Light Chain Amyloidosis: 2022 Update on Diagnosis, Prognosis, and Treatment. *Am J Hematol*, doi:10.1002/ajh.26569 (2022).
128 Reece, D. E. *et al.* Efficacy and safety of once-weekly and twice-weekly bortezomib in patients with relapsed systemic AL amyloidosis: results of a phase 1/2 study. *Blood* **118**, 865-873, doi:10.1182/blood-2011-02-334227 (2011).
129 Mikhael, J. R. *et al.* Cyclophosphamide-bortezomib-dexamethasone (CyBorD) produces rapid and complete hematologic response in patients with AL amyloidosis. *Blood* **119**, 4391-4394, doi:10.1182/blood-2011-11-390930 (2012).
130 Jelinek, T., Kryukova, E., Kufova, Z., Kryukov, F. & Hajek, R. Proteasome inhibitors in AL amyloidosis: focus on mechanism of action and clinical activity. *Hematol Oncol* **35**, 408-419, doi:10.1002/hon.2351 (2017).
131 Kastritis, E. *et al.* Bortezomib, Melphalan, and Dexamethasone for Light-Chain Amyloidosis. *J Clin Oncol* **38**, 3252-3260, doi:10.1200/JCO.20.01285 (2020).
132 Kastritis, E. *et al.* Daratumumab-Based Treatment for Immunoglobulin Light-Chain Amyloidosis. *N Engl J Med* **385**, 46-58, doi:10.1056/NEJMoa2028631 (2021).
133 Dimopoulos, M. A. & Kastritis, E. Bortezomib for AL amyloidosis: moving forward. *Blood* **118**, 827-828, doi:10.1182/blood-2011-05-355115 (2011).
134 Wei, R. *et al.* Deubiquitinases in cancer. *Oncotarget* **6**, 12872-12889, doi:10.18632/oncotarget.3671 (2015).
135 Chauhan, D. *et al.* A small molecule inhibitor of ubiquitin-specific protease-7 induces apoptosis in multiple myeloma cells and overcomes bortezomib resistance. *Cancer Cell* **22**, 345-358, doi:10.1016/j.ccr.2012.08.007 (2012).
136 Tian, Z. *et al.* A novel small molecule inhibitor of deubiquitylating enzyme USP14 and UCHL5 induces apoptosis in multiple myeloma and overcomes bortezomib resistance. *Blood* **123**, 706-716, doi:10.1182/blood-2013-05-500033 (2014).
137 Song, Y. *et al.* Targeting proteasome ubiquitin receptor Rpn13 in multiple myeloma. *Leukemia* **30**, 1877-1886, doi:10.1038/leu.2016.97 (2016).
138 Song, Y. *et al.* Blockade of deubiquitylating enzyme Rpn11 triggers apoptosis in multiple myeloma cells and overcomes bortezomib resistance. *Oncogene* **36**, 5631-5638, doi:10.1038/onc.2017.172 (2017).
139 Hay, S. B., Ferchen, K., Chetal, K., Grimes, H. L. & Salomonis, N. The Human Cell Atlas bone marrow single-cell interactive web portal. *Experimental hematology* **68**, 51-61, doi:10.1016/j.exphem.2018.09.004 (2018).

140 Edgar, R., Domrachev, M. & Lash, A. E. Gene Expression Omnibus: NCBI gene expression and hybridization array data repository. *Nucleic acids research* **30**, 207-210, doi:10.1093/nar/30.1.207 (2002).
141 Clough, E. & Barrett, T. The Gene Expression Omnibus Database. *Methods in molecular biology* **1418**, 93-110, doi:10.1007/978-1-4939-3578-9_5 (2016).
142 Chng, W. J. *et al.* Molecular dissection of hyperdiploid multiple myeloma by gene expression profiling. *Cancer research* **67**, 2982-2989, doi:10.1158/0008-5472.CAN-06-4046 (2007).
143 Gertz, M. A. *et al.* Definition of organ involvement and treatment response in immunoglobulin light chain amyloidosis (AL): a consensus opinion from the 10th International Symposium on Amyloid and Amyloidosis, Tours, France, 18-22 April 2004. *Am J Hematol* **79**, 319-328, doi:10.1002/ajh.20381 (2005).
144 Bradwell, A. R. *et al.* Highly sensitive, automated immunoassay for immunoglobulin free light chains in serum and urine. *Clin Chem* **47**, 673-680 (2001).
145 Katzmann, J. A. *et al.* Serum reference intervals and diagnostic ranges for free kappa and free lambda immunoglobulin light chains: relative sensitivity for detection of monoclonal light chains. *Clin Chem* **48**, 1437-1444 (2002).
146 Westermark, P. Subcutaneous adipose tissue biopsy for amyloid protein studies. *Methods in molecular biology* **849**, 363-371, doi:10.1007/978-1-61779-551-0_24 (2012).
147 Arbustini, E. *et al.* Electron and immuno-electron microscopy of abdominal fat identifies and characterizes amyloid fibrils in suspected cardiac amyloidosis. *Amyloid* **9**, 108-114 (2002).
148 Ohtsuki, T. *et al.* Two human myeloma cell lines, amylase-producing KMS-12-PE and amylase-non-producing KMS-12-BM, were established from a patient, having the same chromosome marker, t(11;14)(q13;q32). *Br J Haematol* **73**, 199-204, doi:10.1111/j.1365-2141.1989.tb00252.x (1989).
149 Nilsson, K., Bennich, H., Johansson, S. G. & Ponten, J. Established immunoglobulin producing myeloma (IgE) and lymphoblastoid (IgG) cell lines from an IgE myeloma patient. *Clinical and experimental immunology* **7**, 477-489 (1970).
150 Perfetti, V. *et al.* Inverse polymerase chain reaction for cloning complete human immunoglobulin variable regions and leaders conserving the original sequence. *Analytical biochemistry* **239**, 107-109, doi:10.1006/abio.1996.0297 (1996).
151 van Dongen, J. J. *et al.* EuroFlow antibody panels for standardized n-dimensional flow cytometric immunophenotyping of normal, reactive and malignant leukocytes. *Leukemia* **26**, 1908-1975, doi:10.1038/leu.2012.120 (2012).
152 Lefever, S., Pattyn, F., Hellemans, J. & Vandesompele, J. Single-nucleotide polymorphisms and other mismatches reduce performance of quantitative PCR assays. *Clin Chem* **59**, 1470-1480, doi:10.1373/clinchem.2013.203653 (2013).
153 Vandesompele, J. *et al.* Accurate normalization of real-time quantitative RT-PCR data by geometric averaging of multiple internal control genes. *Genome biology* **3**, RESEARCH0034, doi:10.1186/gb-2002-3-7-research0034 (2002).
154 Dominici, M. *et al.* Minimal criteria for defining multipotent mesenchymal stromal cells. The International Society for Cellular Therapy position statement. *Cytotherapy* **8**, 315-317, doi:10.1080/14653240600855905 (2006).
155 Crouch, S. P., Kozlowski, R., Slater, K. J. & Fletcher, J. The use of ATP bioluminescence as a measure of cell proliferation and cytotoxicity. *J Immunol Methods* **160**, 81-88, doi:10.1016/0022-1759(93)90011-u (1993).
156 Strober, W. Trypan blue exclusion test of cell viability. *Curr Protoc Immunol* **Appendix 3**, Appendix 3B, doi:10.1002/0471142735.ima03bs21 (2001).
157 Chauhan, D., Hideshima, T. & Anderson, K. C. Proteasome inhibition in multiple myeloma: therapeutic implication. *Annu Rev Pharmacol Toxicol* **45**, 465-476, doi:10.1146/annurev.pharmtox.45.120403.100037 (2005).
158 Muchtar, E. *et al.* Interphase fluorescence in situ hybridization in untreated AL amyloidosis has an independent prognostic impact by abnormality type and treatment category. *Leukemia* **31**, 1562-1569, doi:10.1038/leu.2016.369 (2017).

159 Bochtler, T. *et al.* Translocation t(11;14) is associated with adverse outcome in patients with newly diagnosed AL amyloidosis when treated with bortezomib-based regimens. *J. Clin. Oncol.* **33**, 1371-1378, doi:10.1200/JCO.2014.57.4947 (2015).
160 Bodin, K. *et al.* Antibodies to human serum amyloid P component eliminate visceral amyloid deposits. *Nature* **468**, 93-97, doi:10.1038/nature09494 (2010).
161 Richards, D. B. *et al.* Therapeutic Clearance of Amyloid by Antibodies to Serum Amyloid P Component. *N Engl J Med* **373**, 1106-1114, doi:10.1056/NEJMoa1504942 (2015).
162 Richards, D. B. *et al.* Repeat doses of antibody to serum amyloid P component clear amyloid deposits in patients with systemic amyloidosis. *Sci Transl Med* **10**, doi:10.1126/scitranslmed.aan3128 (2018).
163 Popkova, T., Hajek, R. & Jelinek, T. Monoclonal antibodies in the treatment of AL amyloidosis: co-targetting the plasma cell clone and amyloid deposits. *Br J Haematol* **189**, 228-238, doi:10.1111/bjh.16436 (2020).
164 Godara, A. *et al.* Dual Monoclonal Antibody Therapy in Patients With Systemic AL Amyloidosis and Cardiac Involvement. *Clin Lymphoma Myeloma Leuk* **20**, 184-189, doi:10.1016/j.clml.2019.10.019 (2020).
165 Gertz, M. A. *et al.* First-in-Human Phase I/II Study of NEOD001 in Patients With Light Chain Amyloidosis and Persistent Organ Dysfunction. *J Clin Oncol* **34**, 1097-1103, doi:10.1200/JCO.2015.63.6530 (2016).
166 Edwards, C. V. *et al.* Phase 1a/b Study of Monoclonal Antibody CAEL-101 (11-1F4) in Patients with AL Amyloidosis. *Blood*, doi:10.1182/blood.2020009039 (2021).
167 Sitia, R., Palladini, G. & Merlini, G. Bortezomib in the treatment of AL amyloidosis: targeted therapy? *Haematologica* **92**, 1302-1307, doi:10.3324/haematol.12136 (2007).
168 Feng, X., Holmlund, T., Zheng, C. & Fadeel, B. Proapoptotic effects of the novel proteasome inhibitor b-AP15 on multiple myeloma cells and natural killer cells. *Experimental hematology* **42**, 172-182, doi:10.1016/j.exphem.2013.11.010 (2014).
169 Jiang, L. *et al.* Proteasomal cysteine deubiquitinase inhibitor b-AP15 suppresses migration and induces apoptosis in diffuse large B cell lymphoma. *J Exp Clin Cancer Res* **38**, 453, doi:10.1186/s13046-019-1446-y (2019).
170 Ma, Y. S. *et al.* Inhibition of USP14 and UCH37 deubiquitinating activity by b-AP15 as a potential therapy for tumors with p53 deficiency. *Signal Transduct Target Ther* **5**, 30, doi:10.1038/s41392-020-0143-9 (2020).
171 Chitta, K. *et al.* Targeted inhibition of the deubiquitinating enzymes, USP14 and UCHL5, induces proteotoxic stress and apoptosis in Waldenstrom macroglobulinaemia tumour cells. *Br J Haematol* **169**, 377-390, doi:10.1111/bjh.13304 (2015).
172 Liu, D., Song, Z., Wang, X. & Ouyang, L. Ubiquitin C-Terminal Hydrolase L5 (UCHL5) Accelerates the Growth of Endometrial Cancer via Activating the Wnt/beta-Catenin Signaling Pathway. *Front Oncol* **10**, 865, doi:10.3389/fonc.2020.00865 (2020).
173 Fang, Y. *et al.* Ubiquitin C-terminal Hydrolase 37, a novel predictor for hepatocellular carcinoma recurrence, promotes cell migration and invasion via interacting and deubiquitinating PRP19. *Biochim Biophys Acta* **1833**, 559-572, doi:10.1016/j.bbamcr.2012.11.020 (2013).
174 Didier, R. *et al.* Targeting the Proteasome-Associated Deubiquitinating Enzyme USP14 Impairs Melanoma Cell Survival and Overcomes Resistance to MAPK-Targeting Therapies. *Mol Cancer Ther* **17**, 1416-1429, doi:10.1158/1535-7163.MCT-17-0919 (2018).
175 Xie, W. & Xu, L. Ubiquitin-specific protease 14 promotes radio-resistance and suppresses autophagy in oral squamous cell carcinoma. *Exp Cell Res* **398**, 112385, doi:10.1016/j.yexcr.2020.112385 (2021).
176 Geng, L., Chen, X., Zhang, M. & Luo, Z. Ubiquitin-specific protease 14 promotes prostate cancer progression through deubiquitinating the transcriptional factor ATF2. *Biochem Biophys Res Commun* **524**, 16-21, doi:10.1016/j.bbrc.2019.12.128 (2020).
177 Han, K. H. *et al.* USP14 Inhibition Regulates Tumorigenesis by Inducing Autophagy in Lung Cancer In Vitro. *Int J Mol Sci* **20**, doi:10.3390/ijms20215300 (2019).

178 Zhang, B., Li, M., Huang, P., Guan, X. Y. & Zhu, Y. H. Overexpression of ubiquitin specific peptidase 14 predicts unfavorable prognosis in esophageal squamous cell carcinoma. *Thorac Cancer* **8**, 344-349, doi:10.1111/1759-7714.12453 (2017).
179 Xu, X. *et al.* The role of ubiquitin-specific protease 14 (USP14) in cell adhesion-mediated drug resistance (CAM-DR) of multiple myeloma cells. *Eur J Haematol* **98**, 4-12, doi:10.1111/ejh.12729 (2017).
180 Fejzo, M. S. *et al.* Amplification Target ADRM1: Role as an Oncogene and Therapeutic Target for Ovarian Cancer. *Int J Mol Sci* **14**, 3094-3109, doi:10.3390/ijms14023094 (2013).
181 Fejzo, M. S. *et al.* ADRM1-amplified metastasis gene in gastric cancer. *Genes Chromosomes Cancer* **54**, 506-515, doi:10.1002/gcc.22262 (2015).
182 Jiang, R. T. *et al.* Early and consistent overexpression of ADRM1 in ovarian high-grade serous carcinoma. *J Ovarian Res* **10**, 53, doi:10.1186/s13048-017-0347-y (2017).
183 Wu, W. *et al.* Prognostic and Therapeutic Significance of Adhesion-regulating Molecule 1 in Estrogen Receptor-positive Breast Cancer. *Clin Breast Cancer* **20**, 131-144 e133, doi:10.1016/j.clbc.2019.07.009 (2020).
184 Sun, T., Liu, Z., Bi, F. & Yang, Q. Deubiquitinase PSMD14 promotes ovarian cancer progression by decreasing enzymatic activity of PKM2. *Mol Oncol*, doi:10.1002/1878-0261.13076 (2021).
185 Seo, D. *et al.* The deubiquitinating enzyme PSMD14 facilitates tumor growth and chemoresistance through stabilizing the ALK2 receptor in the initiation of BMP6 signaling pathway. *EBioMedicine* **49**, 55-71, doi:10.1016/j.ebiom.2019.10.039 (2019).
186 Yokoyama, S. *et al.* Targeting PSMD14 inhibits melanoma growth through SMAD3 stabilization. *Sci Rep* **10**, 19214, doi:10.1038/s41598-020-76373-y (2020).
187 Zhu, R. *et al.* Deubiquitinating enzyme PSMD14 promotes tumor metastasis through stabilizing SNAIL in human esophageal squamous cell carcinoma. *Cancer Lett* **418**, 125-134, doi:10.1016/j.canlet.2018.01.025 (2018).
188 Das, D. S. *et al.* Blockade of Deubiquitylating Enzyme USP1 Inhibits DNA Repair and Triggers Apoptosis in Multiple Myeloma Cells. *Clin Cancer Res* **23**, 4280-4289, doi:10.1158/1078-0432.CCR-16-2692 (2017).
189 Liao, Y. *et al.* USP1-dependent RPS16 protein stability drives growth and metastasis of human hepatocellular carcinoma cells. *J Exp Clin Cancer Res* **40**, 201, doi:10.1186/s13046-021-02008-3 (2021).
190 Liao, Y. *et al.* A new role of GRP75-USP1-SIX1 protein complex in driving prostate cancer progression and castration resistance. *Oncogene* **40**, 4291-4306, doi:10.1038/s41388-021-01851-0 (2021).
191 Niu, Z. *et al.* The deubiquitinating enzyme USP1 modulates ERalpha and modulates breast cancer progression. *J Cancer* **11**, 6992-7000, doi:10.7150/jca.50477 (2020).
192 Li, Y. *et al.* USP1 Maintains the Survival of Liver Circulating Tumor Cells by Deubiquitinating and Stabilizing TBLR1. *Front Oncol* **10**, 554809, doi:10.3389/fonc.2020.554809 (2020).
193 Goncalves, J. M., Cordeiro, M. M. R. & Rivero, E. R. C. The Role of the Complex USP1/WDR48 in Differentiation and Proliferation Processes in Cancer Stem Cells. *Curr Stem Cell Res Ther* **12**, 416-422, doi:10.2174/1574888X12666170315104013 (2017).
194 Ye, M. *et al.* USP7 promotes hepatoblastoma progression through activation of PI3K/AKT signaling pathway. *Cancer Biomark* **31**, 107-117, doi:10.3233/CBM-200052 (2021).
195 Jiang, S. *et al.* Suppression of USP7 induces BCR-ABL degradation and chronic myelogenous leukemia cell apoptosis. *Cell Death Dis* **12**, 456, doi:10.1038/s41419-021-03732-6 (2021).
196 Chen, H. *et al.* Ubiquitin-specific protease 7 is a druggable target that is essential for pancreatic cancer growth and chemoresistance. *Invest New Drugs* **38**, 1707-1716, doi:10.1007/s10637-020-00951-0 (2020).
197 Xie, P. *et al.* USP7 promotes proliferation of papillary thyroid carcinoma cells through TBX3-mediated p57(KIP2) repression. *Mol Cell Endocrinol* **518**, 111037, doi:10.1016/j.mce.2020.111037 (2020).

198 Sha, B. *et al.* Deubiquitylatinase inhibitor b-AP15 induces c-Myc-Noxa-mediated apoptosis in esophageal squamous cell carcinoma. *Apoptosis* **24**, 826-836, doi:10.1007/s10495-019-01561-9 (2019).
199 Yu, Y. *et al.* Inhibition of Ubiquitin-Specific Protease 14 Suppresses Cell Proliferation and Synergizes with Chemotherapeutic Agents in Neuroblastoma. *Mol Cancer Ther* **18**, 1045-1056, doi:10.1158/1535-7163.MCT-18-0146 (2019).
200 Yu, G. Y. *et al.* RA190, a Proteasome Subunit ADRM1 Inhibitor, Suppresses Intrahepatic Cholangiocarcinoma by Inducing NF-KB-Mediated Cell Apoptosis. *Cell Physiol Biochem* **47**, 1152-1166, doi:10.1159/000490210 (2018).
201 Soong, R. S. *et al.* RPN13/ADRM1 inhibitor reverses immunosuppression by myeloid-derived suppressor cells. *Oncotarget* **7**, 68489-68502, doi:10.18632/oncotarget.12095 (2016).
202 Liang, Y. C. *et al.* ADRM1 as a therapeutic target in hepatocellular carcinoma. *Kaohsiung J Med Sci* **37**, 47-54, doi:10.1002/kjm2.12298 (2021).
203 Kuang, X. *et al.* Inhibition of USP1 induces apoptosis via ID1/AKT pathway in B-cell acute lymphoblastic leukemia cells. *Int J Med Sci* **18**, 245-255, doi:10.7150/ijms.47597 (2021).
204 Wang, M. *et al.* The USP7 Inhibitor P5091 Induces Cell Death in Ovarian Cancers with Different P53 Status. *Cell Physiol Biochem* **43**, 1755-1766, doi:10.1159/000484062 (2017).
205 Fu, C., Zhu, X., Xu, P. & Li, Y. Pharmacological inhibition of USP7 promotes antitumor immunity and contributes to colon cancer therapy. *Onco Targets Ther* **12**, 609-617, doi:10.2147/OTT.S182806 (2019).
206 An, T. *et al.* USP7 inhibitor P5091 inhibits Wnt signaling and colorectal tumor growth. *Biochem Pharmacol* **131**, 29-39, doi:10.1016/j.bcp.2017.02.011 (2017).
207 Bustin, S. A. *et al.* The MIQE guidelines: minimum information for publication of quantitative real-time PCR experiments. *Clin Chem* **55**, 611-622, doi:10.1373/clinchem.2008.112797 (2009).
208 Bustin, S. A. *et al.* Primer sequence disclosure: a clarification of the MIQE guidelines. *Clin Chem* **57**, 919-921, doi:10.1373/clinchem.2011.162958 (2011).
209 Nevone, A., Cascino, P., Bozzola, M., Palladini, G., & Nuvolone, M. Identificazione di geni di normalizzazione per studi trascrizionali con Polymerase Chain Reaction quantitativa. *Biochimica Clinica* (2019).
210 Cai, J. *et al.* A novel deubiquitinase inhibitor b-AP15 triggers apoptosis in both androgen receptor-dependent and -independent prostate cancers. *Oncotarget* **8**, 63232-63246, doi:10.18632/oncotarget.18774 (2017).
211 Xia, X. *et al.* Targeting proteasome-associated deubiquitinases as a novel strategy for the treatment of estrogen receptor-positive breast cancer. *Oncogenesis* **7**, 75, doi:10.1038/s41389-018-0086-y (2018).
212 Hillert, E. K. *et al.* Proteasome inhibitor b-AP15 induces enhanced proteotoxicity by inhibiting cytoprotective aggresome formation. *Cancer Lett* **448**, 70-83, doi:10.1016/j.canlet.2019.02.003 (2019).
213 Wang, X. *et al.* The 19S Deubiquitinase inhibitor b-AP15 is enriched in cells and elicits rapid commitment to cell death. *Mol Pharmacol* **85**, 932-945, doi:10.1124/mol.113.091322 (2014).
214 Shukla, N. *et al.* Proteasome Addiction Defined in Ewing Sarcoma Is Effectively Targeted by a Novel Class of 19S Proteasome Inhibitors. *Cancer research* **76**, 4525-4534, doi:10.1158/0008-5472.CAN-16-1040 (2016).
215 Zhang, X. *et al.* The deubiquitinase inhibitor b-AP15 induces strong proteotoxic stress and mitochondrial damage. *Biochem Pharmacol* **156**, 291-301, doi:10.1016/j.bcp.2018.08.039 (2018).
216 Zhang, X. *et al.* Oxidative Stress Induced by the Deubiquitinase Inhibitor b-AP15 Is Associated with Mitochondrial Impairment. *Oxid Med Cell Longev* **2019**, 1659468, doi:10.1155/2019/1659468 (2019).
217 Vogel, R. I. *et al.* Simultaneous inhibition of deubiquitinating enzymes (DUBs) and autophagy synergistically kills breast cancer cells. *Oncotarget* **6**, 4159-4170, doi:10.18632/oncotarget.2904 (2015).

218 Brnjic, S. *et al.* Induction of tumor cell apoptosis by a proteasome deubiquitinase inhibitor is associated with oxidative stress. *Antioxid Redox Signal* **21**, 2271-2285, doi:10.1089/ars.2013.5322 (2014).
219 Wang, X. *et al.* Synthesis and evaluation of derivatives of the proteasome deubiquitinase inhibitor b-AP15. *Chem Biol Drug Des* **86**, 1036-1048, doi:10.1111/cbdd.12571 (2015).
220 American Type Culture Collection Standards Development Organization Workgroup, A. S. N. Cell line misidentification: the beginning of the end. *Nat Rev Cancer* **10**, 441-448, doi:10.1038/nrc2852 (2010).
221 Masters, J. R. Cell-line authentication: End the scandal of false cell lines. *Nature* **492**, 186, doi:10.1038/492186a (2012).
222 Garderet, L. *et al.* Mesenchymal stem cell abnormalities in patients with multiple myeloma. *Leuk Lymphoma* **48**, 2032-2041, doi:10.1080/10428190701593644 (2007).
223 Arnulf, B. *et al.* Phenotypic and functional characterization of bone marrow mesenchymal stem cells derived from patients with multiple myeloma. *Leukemia* **21**, 158-163, doi:10.1038/sj.leu.2404466 (2007).
224 Valsecchi C, C. S., Maltese A, Montagna L, Lenta E, Nevone A, Girelli M, Milani P, Bosoni T, Massa M, Abbà C, Campanelli R, Ripepi J, De Silvestri A, Carolei A, Palladini G, Zecca M, Nuvolone M, Avanzini MA. . Bone Marrow Microenvironment in Light-Chain Amyloidosis: In Vitro Expansion and Characterization of Mesenchymal Stromal Cells. *Biomedicines*, doi:https://doi.org/10.3390/biomedicines9111523 (2021).
225 Braham, M. V. J. *et al.* Cellular immunotherapy on primary multiple myeloma expanded in a 3D bone marrow niche model. *Oncoimmunology* **7**, e1434465, doi:10.1080/2162402X.2018.1434465 (2018).
226 Braham, M. V. *et al.* Liposomal drug delivery in an in vitro 3D bone marrow model for multiple myeloma. *Int J Nanomedicine* **13**, 8105-8118, doi:10.2147/IJN.S184262 (2018).
227 Wang, X. *et al.* Corrigendum: The proteasome deubiquitinase inhibitor VLX1570 shows selectivity for ubiquitin-specific protease-14 and induces apoptosis of multiple myeloma cells. *Sci Rep* **6**, 30667, doi:10.1038/srep30667 (2016).
228 Rowinsky, E. K. *et al.* Phase 1 study of the protein deubiquitinase inhibitor VLX1570 in patients with relapsed and/or refractory multiple myeloma. *Invest New Drugs* **38**, 1448-1453, doi:10.1007/s10637-020-00915-4 (2020).
229 Song, Y. *et al.* Development and preclinical validation of a novel covalent ubiquitin receptor Rpn13 degrader in multiple myeloma. *Leukemia* **33**, 2685-2694, doi:10.1038/s41375-019-0467-z (2019).
230 Sarhan, D. *et al.* A novel inhibitor of proteasome deubiquitinating activity renders tumor cells sensitive to TRAIL-mediated apoptosis by natural killer cells and T cells. *Cancer Immunol Immunother* **62**, 1359-1368, doi:10.1007/s00262-013-1439-1 (2013).
231 D'Arcy, P. *et al.* Inhibition of proteasome deubiquitinating activity as a new cancer therapy. *Nat Med* **17**, 1636-1640, doi:10.1038/nm.2536 (2011).
232 Soong, R. S. *et al.* Bis-benzylidine Piperidone RA190 treatment of hepatocellular carcinoma via binding RPN13 and inhibiting NF-kappaB signaling. *BMC Cancer* **20**, 386, doi:10.1186/s12885-020-06896-0 (2020).
233 Anchoori, R. K. *et al.* A bis-benzylidine piperidone targeting proteasome ubiquitin receptor RPN13/ADRM1 as a therapy for cancer. *Cancer Cell* **24**, 791-805, doi:10.1016/j.ccr.2013.11.001 (2013).